

Photoplethysmography Signal Processing and Synthesis

Elisa Mejía-Mejía, John Allen, Karthik Budidha, Chadi El-Hajj, Panayiotis A. Kyriacou and Peter H. Charlton*

* Corresponding author

Affiliations

E. Mejía-Mejía, K. Budidha, C. El-Hajj and P.A. Kyriacou are with the Research Centre for Biomedical Engineering, City, University of London, London, EC1V 0HB, UK. e-mails: elisa.mejia-mejia@city.ac.uk, karthik.budidha@city.ac.uk, chadi.el-hajj@city.ac.uk, and p.kyriacou@city.ac.uk. ORCiDs: E. Mejía Mejía - [0000-0002-5357-4329](https://orcid.org/0000-0002-5357-4329); K. Budidha - [0000-0002-6329-8399](https://orcid.org/0000-0002-6329-8399); P. Kyriacou - [0000-0002-2868-485X](https://orcid.org/0000-0002-2868-485X)

J. Allen is with: (i) the Research Centre for Intelligent Healthcare, Coventry University, Coventry, CV1 5RW, UK; and (ii) the Faculty of Medical Sciences, Newcastle University, Newcastle upon Tyne, NE2 4HH, UK. e-mail: ad5325@coventry.ac.uk. ORCID: [0000-0002-7263-0533](https://orcid.org/0000-0002-7263-0533)

P. H. Charlton is with: (i) the Department of Public Health and Primary Care, University of Cambridge, Cambridge, CB1 8RN, UK; and (ii) the Research Centre for Biomedical Engineering, City, University of London, London, EC1V 0HB, UK. e-mail: pc657@medschl.cam.ac.uk. ORCID: [0000-0003-3836-8655](https://orcid.org/0000-0003-3836-8655)

NON-PRINT ITEMS

Abstract

This chapter presents the fundamental signal processing techniques used to analyse the PPG signal. The chapter starts by providing an overview of the PPG signal, covering its physiological origins, presentation, and acquisition. Fundamental signal processing techniques are then presented, covering: pre-processing techniques; analysis in the time domain; analysis in the frequency domain; the application of machine learning; and methods to estimate physiological parameters from PPG signals. Finally, the chapter provides a review of methods to synthesise PPG signals.

Index Terms

Blood volume pulse, cardiovascular, digital volume pulse, photoplethysmogram, pulse wave, signal processing

Citation

This is the pre-copy edited version of a book chapter submitted for publication in *Photoplethysmography*. The chapter can be cited as:

Mejía-Mejía E., Allen J., Budidha K., El-Hajj C., Kyriacou P.A. and Charlton P.H., **Photoplethysmography Signal Processing and Synthesis**. In *Photoplethysmography*; Kyriacou, P.A., Allen, J., Eds.; Elsevier, 2021.

CONTENTS

1	Introduction	3
2	The Photoplethysmogram Signal	4
2.1	Physiological origins	4
2.2	Presentation of the photoplethysmogram signal	4
2.3	Signal acquisition	5
2.3.1	Sensor types	5
2.3.2	Sensor configurations	6
2.3.3	Simultaneous signal acquisition	7
3	Photoplethysmogram Signal Processing	8
3.1	Pre-processing	8
3.1.1	Digital filtering	8
3.1.2	Motion artefact removal	11
3.1.3	Signal quality and its assessment	11
3.1.4	Calculating derivatives	15
3.1.5	Empirical mode decomposition	15
3.2	Time domain analysis	16
3.2.1	Identifying individual pulse waves	16
3.2.2	Identifying fiducial points	17
3.2.3	Calculating pulse wave features	19
3.2.4	Obtaining representative measurements from a recording	22
3.2.5	Identifying abnormal pulse waves	22
3.2.6	Analysing simultaneous signals	22
3.3	Frequency domain analysis	23
3.3.1	Spectral analysis	23
3.3.2	Time-frequency analysis	25
3.4	Machine learning	26
3.4.1	Linear regression	26
3.4.2	Tree-based algorithms	27
3.4.3	Support vector machines	28
3.4.4	Neural networks and deep learning	29
3.5	Nonlinear analysis in phase space	29
3.6	Estimating physiological parameters	29
3.6.1	Heart rate	29
3.6.2	Inter-beat-intervals	30
3.6.3	Detecting atrial fibrillation	31
3.6.4	Pulse rate variability	32
3.6.5	Respiratory rate	33
3.6.6	Blood pressure	35
3.6.7	Arterial stiffness	36
3.6.8	Left ventricular ejection time	37
4	Photoplethysmogram Signal Synthesis	39
4.1	Simulating photoplethysmogram pulse waves	39
4.1.1	Mathematical models	39
4.1.2	Physical models	40
4.2	Simulating photoplethysmogram signals	40
4.2.1	Simulating different heart rhythms	40
4.2.2	Adding motion artefact and noise	41
5	Conclusion	42
	References	43

1. INTRODUCTION

The photoplethysmogram (PPG) signal is widely used in clinical and consumer devices due to its non-invasive nature and cost-effectiveness [1]. Traditionally, it has been primarily used to measure blood oxygen saturation and to monitor heart rate in patients at rest. Despite its use in clinical settings for several decades, PPG signal processing has now emerged as a large and growing field of research. This research has been prompted by the widespread use of PPG sensors in consumer wearables. This setting poses several challenges to the design of signal processing algorithms, not least that of handling motion artifact. In addition, the PPG signal contains valuable information on the cardiovascular, respiratory and autonomic nervous systems which is not yet routinely exploited. Together, these factors give opportunity to use the PPG to provide detailed health information, unobtrusively, in daily life. A key step in realising this opportunity is the development of robust PPG signal processing algorithms.

This chapter provides a comprehensive overview of photoplethysmography signal processing and synthesis. It is intended to give the reader a broad introduction to the subject, equipping them with the fundamentals necessary to engage with the wide body of literature on each individual topic. The chapter consists of three main sections:

The photoplethysmogram signal

The chapter starts by providing an overview of the PPG signal, covering its physiological origins, presentation, and acquisition. This section provides the reader with an understanding of the physiological, technical, and environmental factors which can influence the PPG signal. The intended application of a PPG-based device determines which of these factors should be taken into account when designing PPG signal processing algorithms for the device.

Photoplethysmography signal processing

This section presents the fundamental PPG signal processing techniques. The topics covered include: pre-processing techniques; analysis in the time domain; analysis in the frequency domain; the application of machine learning; and methods to estimate physiological parameters from PPG signals. The broad approaches to signal processing taken at each stage of an algorithm are outlined, equipping the reader with the necessary knowledge to explore the literature on any individual approach.

Photoplethysmography signal synthesis

Finally, the chapter provides a review of methods for generating synthetic PPG signals. This section outlines the different approaches taken to simulate individual PPG pulse waves, and to subsequently simulate a PPG signal consisting of a train of pulse waves.

This chapter focuses primarily on the analysis and synthesis of single PPG signals. Its scope does not extend to oxygen saturation monitoring (see [Chapter 5](#)). Furthermore, it focuses on PPG signals acquired through tissue contact, rather than non-contact ('imaging') photoplethysmography.

2. THE PHOTOPLETHYSMOGRAM SIGNAL

This section provides an overview of the photoplethysmogram (PPG) signal, introducing its physiological origins, presentation, and acquisition.

2.1. Physiological origins

Photoplethysmography measures changes in the blood volume of a vascular tissue bed [1], [2]. Optical radiation is used to illuminate peripheral tissue, where it is scattered and absorbed as it travels through different tissue layers before being transmitted through or reflected from the tissue surface. This attenuated light intensity is detected by an optical sensor and is recorded as a voltage signal known as the photoplethysmogram (PPG). A raw PPG waveform reflects the variations in attenuation of incident optical radiation by different tissue components within the tissue volume, as illustrated in Figure 1 [3]. High frequency variations (the ‘AC’ part) are caused by changes in arterial blood volume with each heartbeat, and lower frequency variations (the ‘DC’ part) are caused by changes in other tissue components such as venous and capillary blood, bloodless tissue, etc. As described in Chapter 2, the attenuation of light in tissue can be described as a function of the optical pathlength and the attenuation coefficient of the medium, based on the modified Beer-Lambert law [4]. The origins of the PPG waveform have also been attributed to red blood cell orientation, the mechanical movement of cellular components, and a combination of factors [5]–[7].

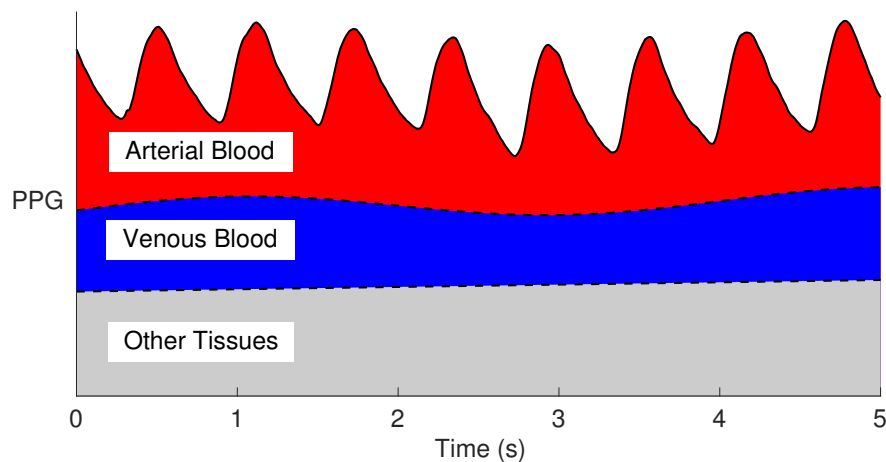


Fig. 1. The simplified origins of the photoplethysmogram (PPG) signal: The PPG is primarily influenced by changes in the volumes of arterial blood, venous blood and other tissues.

Source: [8] under CC BY 4.0.

2.2. Presentation of the photoplethysmogram signal

The PPG signal exhibits a quasi-periodic pattern consisting of an arterial pulse wave for each heartbeat. The pulse wave resembles an arterial blood pressure pulse wave, although there are important differences in the waveform contour [9], [10]. Each PPG pulse wave consists of two distinct phases, as shown in Figure 2: the anacrotic and catacrotic phases, corresponding to the rising and falling limbs respectively [10]. The morphology of the PPG pulse wave is influenced by: the heart (characteristics of cardiac ejection including heart rate, heart rhythm, and stroke volume); the circulation (including cardiovascular properties such as arterial stiffness and blood pressure); additional physiological processes including respiration and the autonomic nervous system (which can be affected by stress); and disease [1], [10]–[12]. Figure 3 shows the changes in PPG pulse wave shape which occur in healthy ageing, for example.

There are several challenges to PPG signal analysis, rendering the extraction of reliable information from the PPG a complex task [17]. The PPG signal exhibits several physiological variations, only one or some of which are relevant to any particular analysis. It is also susceptible to several types of noise as illustrated in Figure 4. These include motion artefact and probe-tissue interface disturbance [1], powerline interference [10], low- and high-frequency noise. In addition, technical aspects such as the type of sensor used and the location of the measurement site affect the waveform (see Chapter 12) [10], [17]. The range of influences on the PPG adds complexity to its analysis.

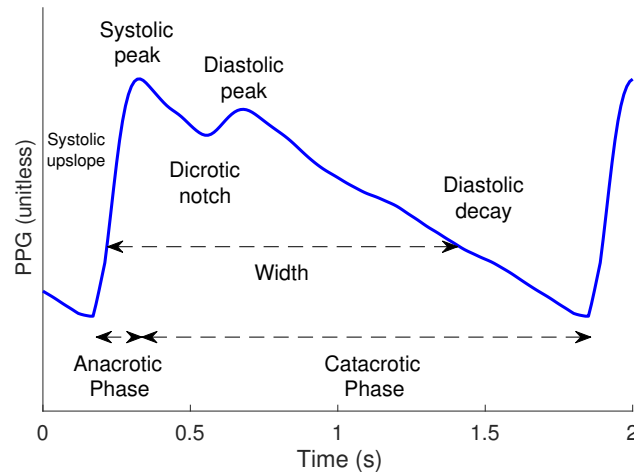


Fig. 2. A typical photoplethysmogram (PPG) pulse wave: The waveform can be separated into anacrotic and catacrotic phases, which are dominated by systolic ejection and wave reflections from the periphery respectively [1]. The systolic rising edge in the anacrotic phase is caused by the expansion of the arterial system due to inflow of blood. The rate of expansion is linked to the contractility of the heart, and the amplitude of the systolic peak is linked to the stroke volume. The diastolic notch and diastolic peak are caused by wave reflections, with their location and timing influenced by arterial stiffness [13]. The diastolic decay is determined by the exponential contraction of the arterial system due to the outflow of blood, and is influenced by the vascular resistance and compliance.

Source: [14] under [CC BY 4.0](#).

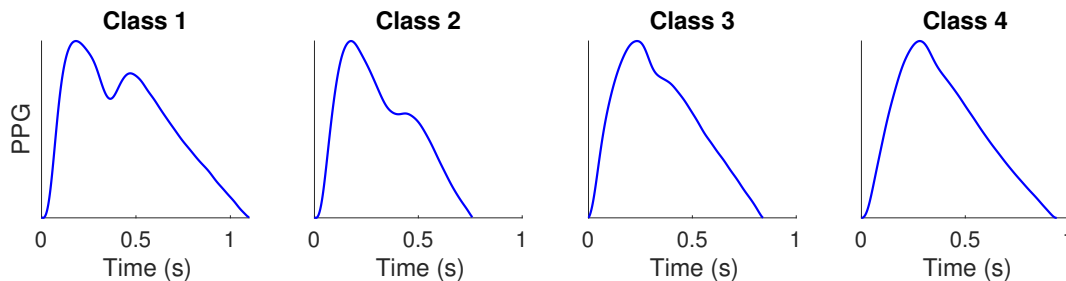


Fig. 3. Classes of photoplethysmogram (PPG) pulse wave shape: The PPG pulse wave often exhibits a diastolic peak in young subjects (class 1) which diminishes with age (higher classes), as described in [15].

Source: [16] under [CC BY 4.0](#).

2.3. Signal acquisition

This section describes the aspects of PPG sensor design required to ensure high-quality PPG signals. The interested reader is referred to [Chapter 3](#) for details of the optical and electronic building blocks that make up a PPG system, as well as their high and low-level design architecture and theory of operation.

2.3.1. Sensor types

Photoplethysmography is usually performed by tissue contact sensing configured in either transmission (‘trans-illumination’) or reflection (‘adjacent’) mode [1]. A conventional PPG sensor consists of a light emitter and a highly sensitive photodetector mounted inside a reusable spring-loaded clip. The most commonly used light sources are light-emitting diodes (LEDs). The photodetector is usually a silicon photodiode, but other detectors such as photocells and phototransistors are also used.

The arrangement of the LED and the photodiode inside the sensor defines the configuration of the probe and its possible measurement site application. In transmission probes, the LED and photodiode are mounted on opposite sides of a clip, and the light transmitted by the LED passes through the tissue sample to the photodiode (see [Figure 5\(a\)](#)). Transmission probes are the most widely used probes in healthcare settings, used to measure arterial oxygen saturation [18]. Their use is limited to peripheral sites to which a clip can be attached, such as the finger, earlobe, or toe. In reflectance probes, the LED and photodiode are mounted side-by-side, typically millimetres apart, so that

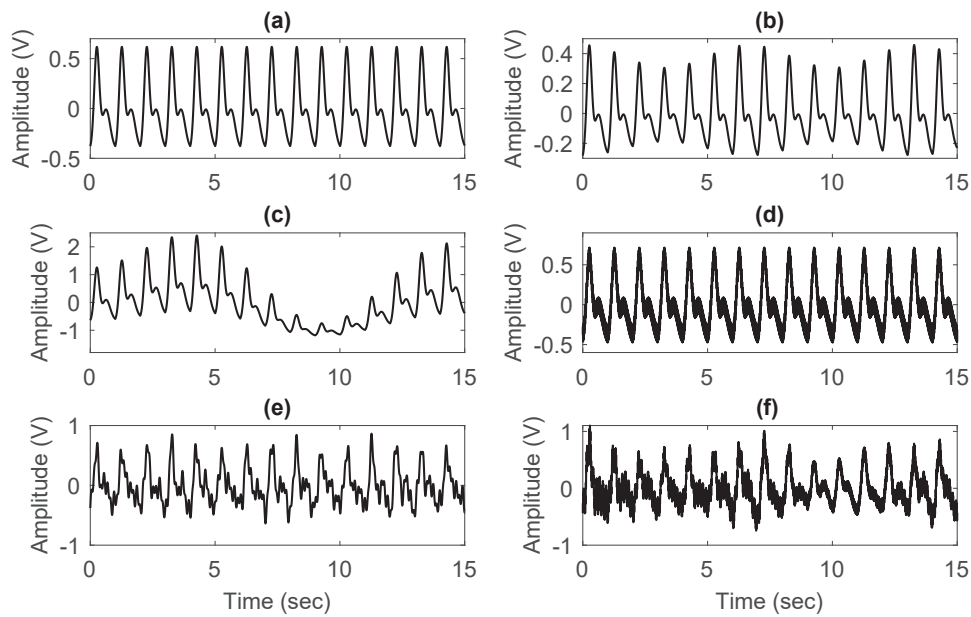


Fig. 4. Idealised examples of clean and noise-corrupted PPG signals: (a) clean, (b) respiratory modulated, (c) baseline modulated, (d) power-line affected, (e) motion affected; (f) affected by all of the above.

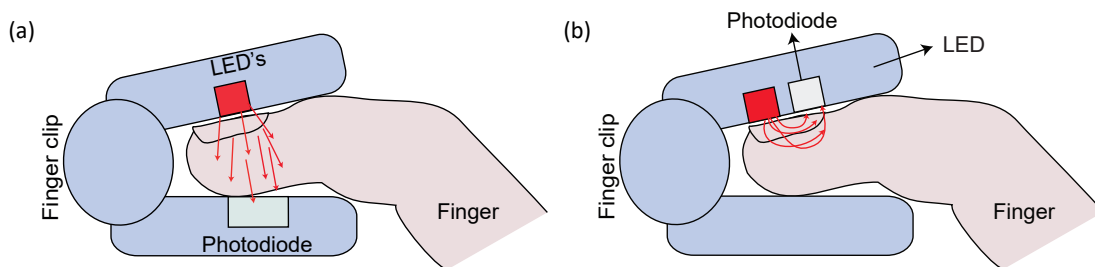


Fig. 5. The two modes of contact photoplethysmography: (a) transmission mode, and (b) reflectance mode. Note the relative positions of the light sources (LEDs) and photodetectors (photodiodes).

the light produced by the LED transilluminates the tissue and the photodiode detects the backscattered light (see Figure 5(b)). Reflection probes can be used at virtually any vascular tissue site since the LED and photodiode are mounted next to each other [19], and consequently are widely used in consumer wearables. The PPG signal can also be acquired by non-contact methods, *i.e.*, ‘imaging PPG’ (‘iPPG’) [20], but this approach is beyond the scope of this chapter and the interested reader is referred to [Chapter 13](#).

The optoelectronics of the PPG sensor and their tissue attachment mechanism are fundamental building blocks in a PPG measurement system. Their design will impact on signal quality, subsequent pulse wave analysis techniques, and the need for skilful denoising. There are a number of other considerations to be made in the design and choice of PPG sensor, including: whether reflection mode or transmission mode is best suited to the intended application; how potential artefacts from external ambient lighting can be minimised including daylight filtering considerations; the position of the digital interfacing relative to the sensor itself; safety; and, aesthetics. Probe-tissue interface pressure should be sufficient so that the PPG probe is held securely in place to minimise probe-tissue movement artefact and the associated signal noise, but not so high as to distort the main features of the pulse wave (see [Chapter: 6](#)) [21].

2.3.2. Sensor configurations

The quality of a PPG signal is determined by both the instrumentation and the sensor setup. Given optimal PPG instrumentation (as described in [Chapter 3](#)) capable of collecting high-quality PPG signals with minimum

noise, the sensor design must be optimised for parameters such as operating wavelength and intensity, sampling rate, and geometric settings such as source-detector separation and sensor geometry, as these determine the quality and appearance of the PPG waveform [5]. The configuration of these sensor parameters depends on the intended application. This is now demonstrated in two example applications: measuring heart rate at the wrist, and blood pressure estimation at the finger.

Firstly, consider acquiring the PPG waveform at the wrist to measure heart rate, as is commonly performed by consumer wearables. The anatomical site determines that reflectance mode will be used. Only the systolic peak is of importance for heart rate monitoring, hence: a relatively low sampling rate can be used (*e.g.*, < 40 Hz as per the Nyquist sampling theorem since the cardiac bandwidth is < 5 Hz); a shorter wavelength can be used (*e.g.*, green or red) to acquire the PPG signal from transcutaneous tissue since the deeper penetration provided by longer wavelengths (*e.g.*, infrared) is not required; a small source-detector separation (SDS) should be used, ideally $\text{SDS} < 3$ mm, as light does not penetrate deeply at the shorter visible wavelengths. Finally, a short recording time can be used (≈ 10 seconds), which is sufficient to measure heart rate accurately using both time and frequency domain methods [3].

Secondly, consider acquiring the PPG waveform at the finger to assess autonomic variations or changes in blood pressure. Transmission mode will be used to ensure that the PPG is influenced by the major arteries of the finger. The morphological features of individual PPG pulse waves will be analysed, hence: a relatively high sampling rate is required (*e.g.*, > 500 Hz to assess pulse wave timing [22]); a longer wavelength should be used (*e.g.*, infrared, $\lambda \approx 940$ nm) to penetrate more deeply and ensure the PPG signal reflects arterial blood volume changes; a longer SDS will be required to accommodate the finger (*e.g.*, $\text{SDS} \approx 5$ mm). Finally, the recording time should be relatively long (≈ 5 -20 mins) so that the effect of physiological changes can be seen in the recorded PPG signals.

There are additional considerations in applications where different wavelength LEDs are used. Such applications include: pulse oximetry (*e.g.*, 660 nm and 940 nm); pulse CO-oximetry (5 to 12 wavelengths, range: 420 nm to 980 nm); and near infrared spectroscopy (*e.g.*, 770 nm, 810nm, 900 nm). In these applications it is often preferable to acquire PPG signals at a higher sampling rate (> 500 Hz). The SDS is determined by the range of wavelengths used: a shorter SDS ($\text{SDS} \approx 2$ mm) is desirable for shorter wavelength ranges (430 nm to 590 nm), and a slightly longer SDS ($\text{SDS} \approx 4$ -5 mm) is desirable for longer wavelength ranges [5].

2.3.3. Simultaneous signal acquisition

The PPG waveform provides a wealth of information about cardiovascular haemodynamics and can be used to obtain several vital parameters such as heart rate, respiration rate, arterial oxygen saturation, and blood pressure. However, the true potential of the PPG is realised when other physiological signals such as the electrocardiogram (ECG), accelerometry, and galvanic skin response (GSR - electrodermal activity) signals are recorded and analysed concurrently.

Simultaneous acquisition of multiple PPG signals at different body sites facilitates measurement of pulse transit time (PTT), the time taken for the pulse wave to propagate along an arterial path. PTT is related to blood pressure [23], and can be used to calculate pulse wave velocity (PWV), a marker of cardiovascular risk [24].

Simultaneous acquisition of the ECG can serve as a cardiac timing reference for PPG signals. Pulse arrival time (PAT) can be calculated from simultaneous PPG and ECG signals, which can be used for blood pressure assessment (similarly to PTT), and to assess cardiovascular risk factors such as arterial stiffness and hypertension [25].

The GSR signal correlates with sympathetic nervous system activity and is a valuable instrument for measuring arousal and certain facets of autonomic control. This information complements related information derived from pulse rate variability analysis of the PPG signal [26]. Hence, combined acquisition and analysis of these signals offers opportunity for deeper mental stress assessment, along with cardiovascular haemodynamics.

The accelerometry signal can be used to remove motion interference from PPG signals, which is a particularly important issue when using portable devices. The simultaneous reference motion measurements provided by accelerometers can be used to remove such interference [27]. However, accelerometers do not differentiate between acceleration due to movement and acceleration due to gravity. Hence, it has been suggested that gyroscopes could be used for better removal of motion interference from PPG signals [28], [29].

3. PHOTOPLETHYSMOGRAM SIGNAL PROCESSING

PPG signal processing is now a vast area of research [10], [17], [30], motivated by the widespread use of PPG sensors in both clinical and consumer devices. The availability of several publicly available datasets containing PPG signals alongside reference parameters ensures that the field is accessible to all. This section provides an overview of the fundamental techniques of PPG signal processing. It includes: pre-processing techniques (Section 3.1); analysis in the time domain (Section 3.2); analysis in the frequency domain (Section 3.3); the application of machine learning (Section 3.4); and methods to estimate physiological parameters from PPG signals (Section 3.6).

3.1. Pre-processing

3.1.1. Digital filtering

Digital filtering is an important step to minimise the impact of noise on PPG signal analysis. The attenuation of noise from PPG signals is a crucial step in extracting valuable information from it. Digital filtering can be used to attenuate noise within specific frequency ranges (*e.g.*, low- and high-frequency noise), although additional processes are required to attenuate noise which occurs within the frequency range of interest (*e.g.*, motion artefact due to walking, where the frequency of steps can be similar to the heart rate).

Digital filtering consists of convolving the input signal with filter coefficients to produce a filtered signal. The transfer function of a filter can be expressed in the z -domain as:

$$H(z) = \frac{Y(z)}{X(z)} = \frac{\sum_{k=0}^K b[k] z^{-k}}{\sum_{l=0}^L a[l] z^{-l}} \quad (1)$$

where $b[k]$ and $a[l]$ are the coefficients of the numerator and denominator respectively. The coefficients are determined in the design process according to the type of filter and the cut-off frequencies required [31]. This transfer function can also be expressed as a difference equation, which can be easily applied to the original signal in the time domain, in order to obtain the filtered signal, y . The difference equation can be expressed as:

$$y[n] = \sum_{k=0}^{K-1} b[k] x[n-k] - \sum_{l=1}^L a[l] y[n-l] \quad (2)$$

The design process of a digital filter consists simply on finding the $b[k]$ and $a[l]$ coefficients that give the desired response of the filter [31]. It is important to design digital filters with the end application in mind, as they can have a marked input on PPG signal morphology [32].

There are two main families of digital filters which differ according to their transfer function: Finite Impulse Response (FIR) and Infinite Impulse Response (IIR) filters. The difference between these families of filters can be explained using Eqn. 2. In FIR filters, all $a[l]$ coefficients, with $l > 0$, are equal to zero. Consequently, the filtered signal, y , is solely dependent on the input signal, x , and is not influenced by the behaviour of the filter with previous samples of the signal [31]. Furthermore, it is only dependent on a finite number of input signal samples. In contrast, in IIR filters the $a[l]$ coefficients are not all equal to zero, and so the filtered signal, y , is dependent on both y and the input signal, x . Infinite Impulse Response (IIR) filters are so called because each sample can affect the output for an infinite period of time.

Three characteristics determine the response of a filter. Filters have an order, a cut-off frequency, and are of a particular type: a low-pass (LPF), high-pass (HPF), band-pass (BPF) or band-stop (BSF) filter [31]. Figure 6 shows an example of the frequency-domain representation of each type of filter. The order determines the behaviour of the slope of transitions between the pass bands and the reject bands, or *vice versa*. Higher order filters have steeper transitions (see Figure 6), but also require a longer duration of input signal and generate a higher delay in the filtered signal [31]. The cut-off frequency determines the frequency at which the gain of the resulting signal is around 70% the original amplitude. Low-pass and high-pass filters each have one transition and therefore one cut-off frequency, whereas band-pass and band-stop filters each have two transition bands, and therefore two distinct cut-off frequencies.

The most commonly used FIR filter in the field of biomedical signal processing, including pre-processing the PPG signal, is the Moving Average (MA) filter, in which all $b[k]$ coefficients have the same value [17]. Other commonly used FIR filters are the median filter, in which instead of using the mean value of n samples, the result of the filter is determined by the median value of the last n samples; and FIR filters based on the use of Hanning or Hamming windows, which can be designed for any desired filter type.

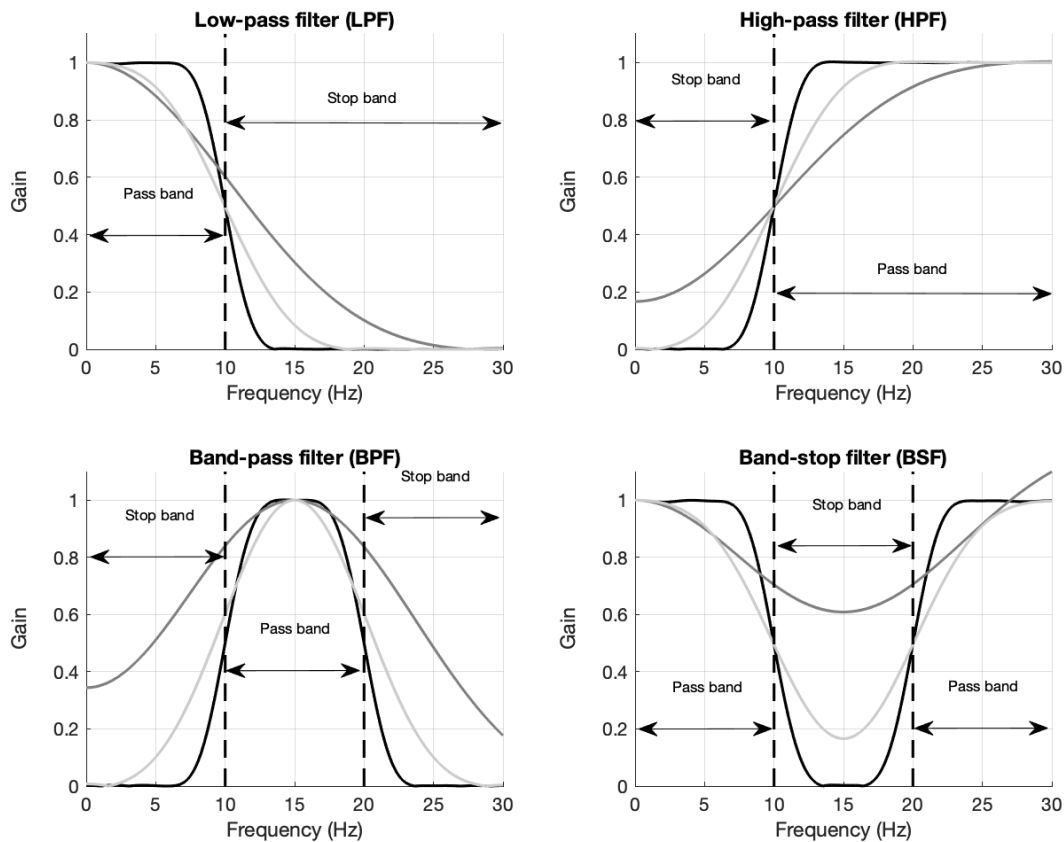


Fig. 6. Frequency-domain behaviour of four types of filter: A low-pass filter (LPF), a high-pass filter (HPF), a band-pass filter (BPF), and a band-stop filter (BSF). In this example, FIR filters with orders $n = 100$ (dark grey line), $n = 200$ (light grey line) and $n = 500$ (black line) were designed. The cut-off frequencies (dashed line) were set at 10 Hz for the LPF and the HPF, and at 10 and 20 Hz for the BPF and BSF.

IIR filters were initially designed using tools developed for analogue filters [31]. The most common IIR filters are the Butterworth filter, the type I and II Chebyshev filters, and the Elliptic filter [17]. The main difference between the design methods can be seen in the frequency response of the filters. Elliptic and Chebyshev filters tend to have a steeper slope than Butterworth filters, but they feature pass and stop bands without ripple, which is usually desired in biomedical signal analysis [31]. The frequency response of these filters is illustrated in Figure 7. Although there are no standards for PPG signal filtering, Liang et al. have suggested that fourth-order Chebyshev type II filters are more effective in improving PPG signal quality [32]. Other advanced techniques have been proposed as filtering solutions, such as de-noising using the Wavelet transform [31], [32]. More information about the Wavelet transform and its applications in PPG signal analysis can be found in Section 3.3.2.

One of the inherent aspects of filtering is the delay it imposes in the resulting signal. This delay can be corrected when filtering the signal *offline*, so the entire signal is available and the filter can be applied both in forward and reverse directions. However, zero-phase filtering in real-time is not possible [31]. Hence, real-time filtering always imposes some delay on the signal. This delay increases with the order of the filter. Since FIR filters have higher orders to achieve similar responses, they tend to impose longer delays. Nonetheless, FIR filters may be preferred rather than IIR filters in some real-time applications that can deal with longer delays. Furthermore, FIR filters are linear-phase filters, so the delay is always linear and of a known value, unlike IIR filters which usually have non-linear phase [31]. Figure 8 illustrates a PPG signal filtered in real-time using different FIR and IIR filters.

Standards have not been developed to determine cut-off frequencies for PPG filters. Most of the frequency content of the PPG signal is below 15 Hz, but the selection of cut-off frequencies for PPG signal analysis is highly dependent

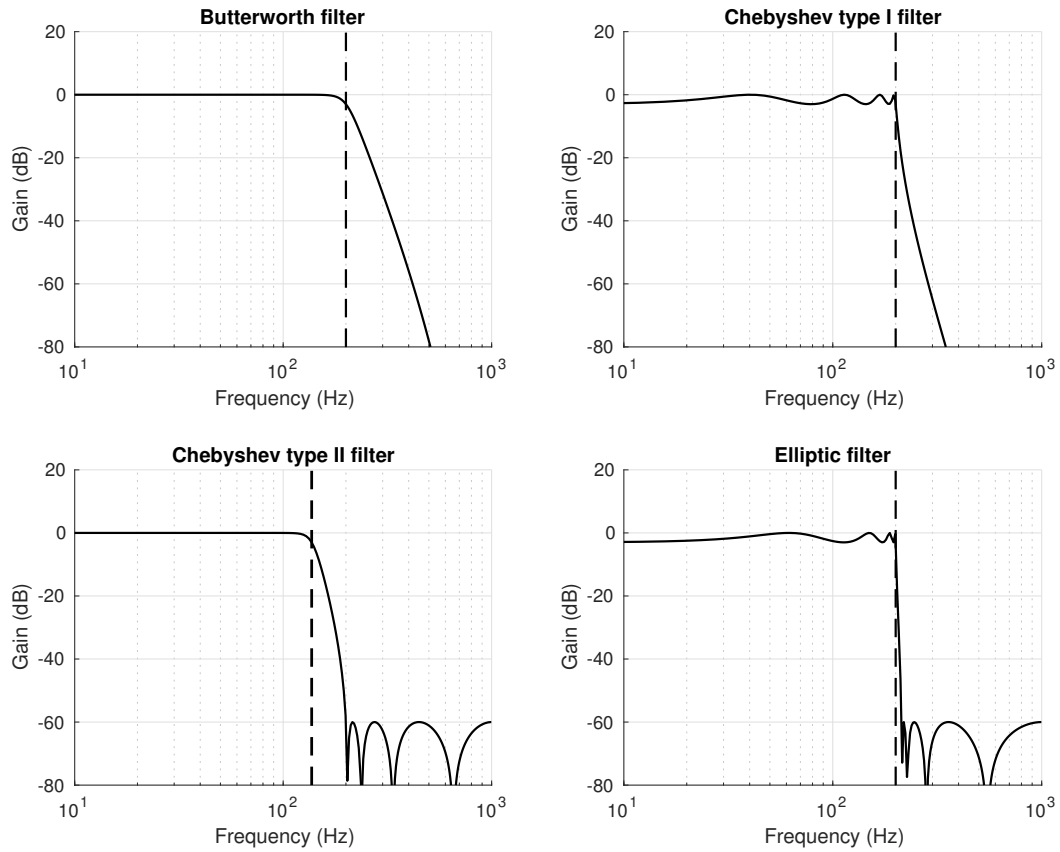


Fig. 7. Frequency response of filters: (a) a Butterworth filter, (b) a Chebyshev type I filter, (c) a Chebyshev type II filter, and (d) an Elliptic filter.

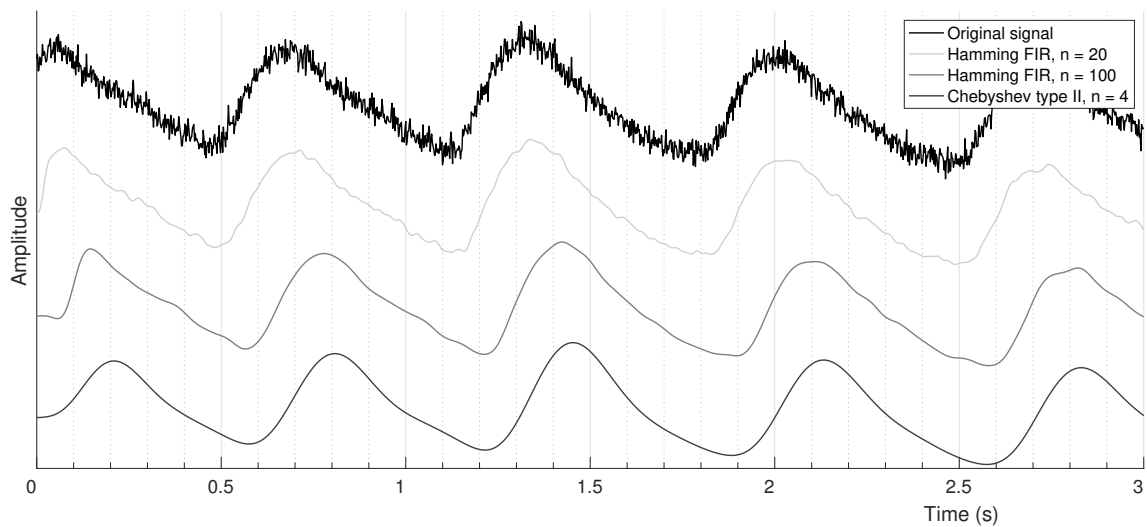


Fig. 8. Filtering in real-time: Effects of order (n) and family of filters in the delay generated after filtering a PPG signal in real time.

on the application. The selection of cut-off frequencies is often a design compromise [1]: a lower low-pass cut-off frequency helps make individual pulse waves more recognisable but distorts their shape.

3.1.2. Motion artefact removal

Subject and PPG probe movements are likely to result in episodes of significant alterations to the PPG waveform, with resultant timing, amplitude and/or shape measures affected across a number of heart beats. Furthermore, sudden breathing changes - a cough, even talking - can also impact on the PPG signal. The goal should be to try to reduce noise in the first place by collecting signals of high quality and to a well-considered protocol whereby a subject is at rest and their body movements minimised. However, in the real world this is not always possible, especially in applications involving wearable sensors and ambulatory measurements. Robust signal processing algorithms are thus required to reduce the impact of artefacts on PPG measurements, and to cover a range of clinical applications for the technology. However, the removal of movement artefact can be very challenging, particularly as such noise can initially appear quite similar to that of normal physiological variation, for example, such as the PPG response to a deep inspiratory gasp manoeuvre (see Figure 9(d)). Algorithms are thus unlikely to be perfect at removing movement noise from a signal whilst conserving the full spectrum of normal signal variation. The extent of noise reduction required depends on the intended clinical application. For instance, signal quality is particularly important in applications requiring the morphological analysis of the pulse shape [33].

A number of de-noising techniques have been proposed. These include: manual identification and labelling for exclusion of noisy pulses [34], [35]; cluster technique approaches to extract the most consistent presentations of pulse shapes in a recording [36]; independent component analysis such as in SpO₂ pulse oximetry by exploiting the quasi-periodicity of the PPG signal and the independence between the PPG and the motion artefact signals, by combining independent component analysis and block interleaving with low pass filtering to reduce motion artefacts under the condition of general dual-wavelength measurement [37]; signal decomposition and reconstruction, for example using iterative motion artefact removal based on a singular spectral analysis algorithm to obtain accurate heart rate and SpO₂ values from a pulse oximeter [38], and the general framework TROIKA (signal decomposiTiOn for denoising, sparse signal RecOnstruction for hIgh resolution for spectrum estimation, and spectral peaK tracking with verification) for accurate heart rate tracking under motion [39]; periodic moving average filtering [40]; and wavelet denoising as a pre-processing stage for robust heart rate detection [41], [42]. In addition, methods requiring a reference motion signal have been proposed, including: adaptive filtering with least square based active noise cancellation [43]; incorporating signals indicative of motion as an algorithm enhancement, *e.g.*, 3D accelerometry data from the wrist [27], [44]; and using gyroscope data to obtain improved noise cancellation performance compared to accelerometry measurements [29].

3.1.3. Signal quality and its assessment

The noise related to probe-tissue movement artefact is considered the nemesis of PPG signal processing [30], [45]. Signal quality is expected to be high in measurements acquired at rest, but reduces with movement [33], [46]. PPG signals are acquired by consumer wearables in a range of activities, such as walking, running, working, or cycling. Noise hinders the extraction of reliable information from the PPG signal in these activities. In this section, signal quality assessment methods are discussed. These methods can be used to identify noise-corrupted signal segments and eliminate them from analyses, allowing parameters such as heart rate or oxygen saturation to be measured with confidence from high quality signal segments [30]. This approach is in contrast to that of motion artefact removal, in which low quality signal segments are improved and included in analyses.

a) Defining PPG signal quality

Signal quality assessment is usually performed by producing measures of PPG signal quality. There are different concepts as to what can be considered as a high-quality PPG signal. For example, PPG signals can be classified according to the capability of obtaining pulse rate reliably. Tang *et al.* proposed three classes of PPG pulse waves: (i) excellent PPG featuring salient systolic and diastolic waves; (ii) acceptable PPG in which systolic and diastolic waves cannot be distinguished but from which heart rate can be estimated; and (iii) unfit PPG in which systolic and diastolic waves cannot be distinguished and heart rate cannot be estimated [47]. Examples of excellent, acceptable, and unfit PPG signals are shown in Figure 10. Similarly, PPG signals have been classified as basic quality, in which pulse peaks are identifiable, and diagnostic quality, in which both systolic and diastolic sections are identifiable [30].

The level of PPG signal quality required is dependent on the application. Only limited research has attempted to define a high quality PPG signal in relation to pulse wave shape. Normal physiological variability is inherent in PPG

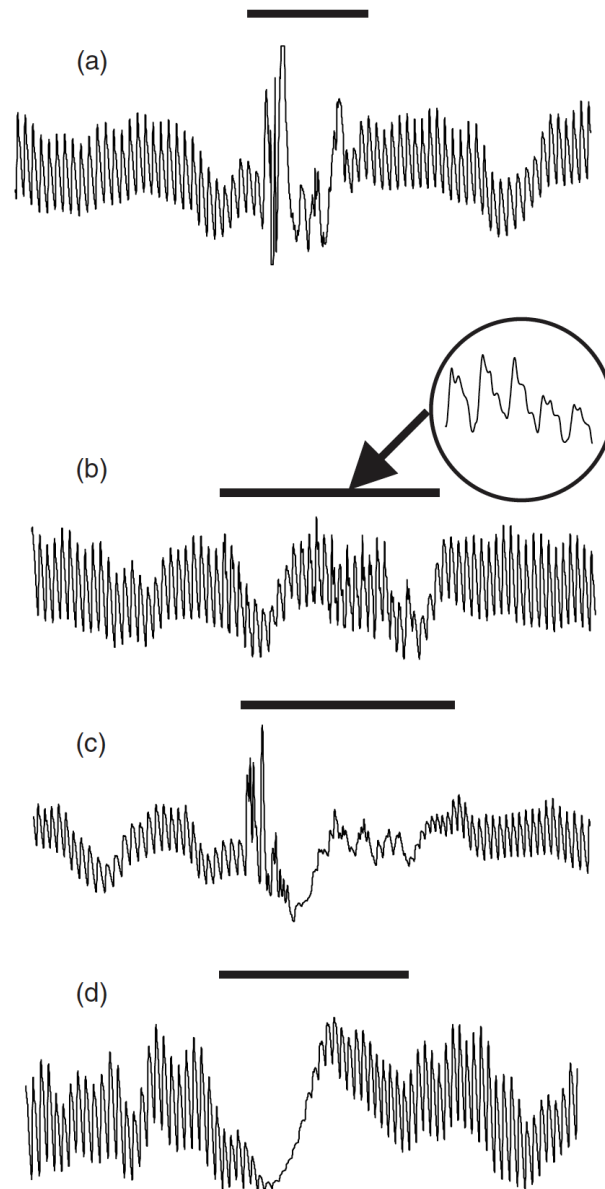


Fig. 9. Artefact and physiological variation in the PPG: Each recording is from the index finger site over a period of 1 minute. The artefact/physiological events are marked. (a) An episode of gross movement artefact or PPG probe cable tugging lasting approximately 15 s. (b) Hand or finger tremor, (c) a bout of coughing, and (d) marked changes in the breathing pattern (a deep gasp or yawn, for example). These types of artefact and physiological variation must be considered within the measurement protocol and for the subsequent algorithm development work and pulse wave analysis.

Source: [1], © Institute of Physics and Engineering in Medicine. Reproduced by permission of IOP Publishing. All rights reserved.

signals, and with differences between body sites and subjects [34], it is challenging to establish such standards. By asking experts in the field, Huthart *et al.* aimed to determine for resting subjects the minimum recording length, the minimum number of diagnostic quality pulses required, and the threshold proportion of noisy beats needed for the PPG recording to be considered of high quality [33]. For morphological analysis of PPG signals obtained from the finger and toe sites, a minimum recording time of 2 minutes was recommended, with 86-95% of a PPG recording being of diagnostic quality. Also, experts suggested that recordings in which 26-50% of beats exhibit artefact should be rejected. More research is needed in this area to establish standards and guidelines for the acquisition of PPG signals, and the analysis of changes in pulse wave shape [1], [33].

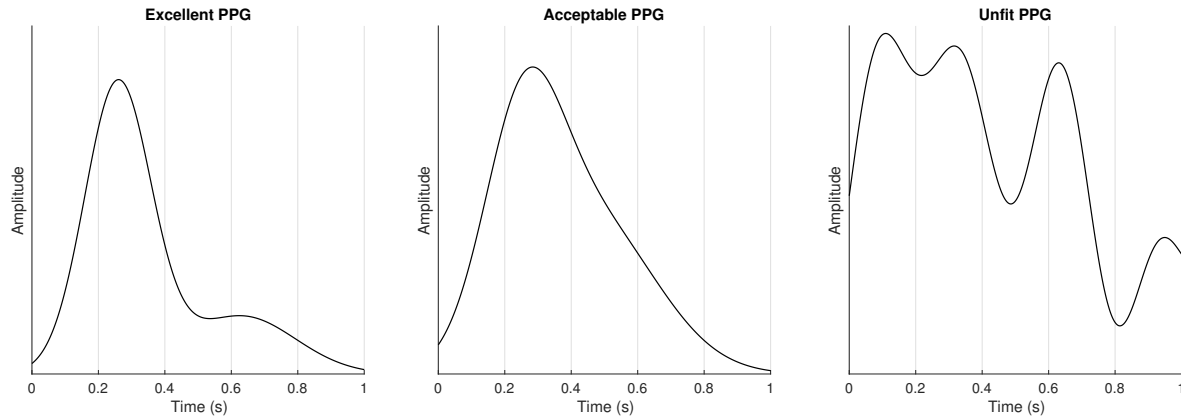


Fig. 10. **Classes of PPG signal quality:** Examples of excellent, acceptable and unfit PPG pulse waves, as defined in [47].

b) Assessing PPG signal quality

Several methods have been proposed to assess PPG signal quality. Most methods begin with the identification of clearly poor-quality segments using checks of physiological plausibility, and then apply more sophisticated techniques to identify the remaining, less evident poor-quality segments [30]. Most methods extract morphological, spectral, or trend-based characteristics from a single PPG pulse wave, and then a pulse wave is classified as high or low quality based on heuristic, empirically determined or machine learning-derived thresholds [30]. These characteristics are usually extracted in the time domain, such as amplitude [48], [49] or timing characteristics. Some studies have also used frequency-domain indices [30].

A wide range of pulse wave characteristics have been used to assess signal quality. Amplitude characteristics include: pulse wave amplitude [49], [50], and the Perfusion Index (PI, which measures the ratio of the ‘AC’ to ‘DC’ component of the signal) [51]. Timing characteristics include the systolic phase duration, the ratio of systolic to diastolic phase duration, inter-beat-intervals [52], the average pulse rate. Shape characteristics include: the number of diastolic peaks; the number of times the signal changes from positive to negative, or vice versa, also called the zero-crossing rate; the signal-to-noise ratio (SNR); and the comparison of the accuracy of different systolic wave detectors for isolating events (*e.g.*, beats or noise artefacts) [51]. Higher order statistics, such as skewness and kurtosis, give an indication of the distribution of the data, therefore serve as an indication of how the pulse wave is distributed over time [30], [51]. These measurements are especially good at identifying PPG pulses with outliers generated by noise [30]. Shannon entropy has been proposed as another measurement of the presence of ‘disorder’ in a PPG pulse wave, since it is a measure of uncertainty in a system, which increases in noisy PPG signals [51], [53].

In addition, some algorithms assess the similarities between successive pulse waves, such as the variation in pulse wave duration, systolic phase duration, and pulse wave amplitude, the trough depth differences between successive troughs and the relation between the pulse wave amplitude and the diastolic wave amplitude [50], [54]. Additionally, some morphological features can be used to detect portions of the PPG signal that do not include any pulses, as explained in [55]. Recently, an algorithm was proposed in which the autocorrelation function of PPG segments was used to identify artefacts, which can result in different shapes of this function [55]. The first zero crossing point, the maximum peak and the lag value of the maximum peak were extracted as features to characterise the autocorrelation function.

Template-matching techniques are popular measures of regularity in PPG segments, since pulse waves are expected to have similar morphologies in high quality signal segments [30]. Several variants of template-matching have been proposed, such as the comparison between each pulse wave and an average representation of these pulse waves (*i.e.*, the template) measuring the Euclidean distance and the ratio of amplitudes [50]; by obtaining the mean value of the correlation coefficients between each cycle and the extracted template [52]; or by modifying the width of each pulse when comparing it to the template, using advanced techniques as Dynamic Time Warping (DWT) [48], [54]. Template extraction can be performed using different approaches too. For instance, Karlen *et al.* compared the PPG pulse against a previously formed reference pulse set, which included only those pulses that were previously determined as high quality pulse waves, according to the correlation coefficient [56]; and Li & Clifford proposed a

template-matching algorithm in which an average template cycle was obtained from all pulses in the PPG segment, and then corrected using only the average of the pulses with correlation coefficients higher than 0.8 with respect to the original template [48].

Most signal quality assessment algorithms rely on automatic pulse wave detection algorithms, whose results might be largely affected by signal quality and by the algorithm used to detect pulse waves [30]. Further studies are needed to establish a universally accepted, noise-robust approach for the detection of individual pulse waves.

Frequency-domain analysis has also been used to identify low-quality PPG signals. Elgendi proposed the measurement of a relative power of the frequency spectrum, by comparing the energy concentrated within a 1 to 2.25 Hz band with respect to the overall signal energy, concentrated within 0 and 8 Hz [51]. Krishnan *et al.* proposed the measurement of the kurtosis of the distribution of the Fourier spectrum of a PPG segment and the extraction of features from the PPG signal bi-spectrum, such as the Quadratic Phase Coupling (QPC), for assessing the presence of noise [57].

Figure 11 exemplifies the behaviour of some time- and frequency-domain indices when extracted from high- and low-quality PPG segments.

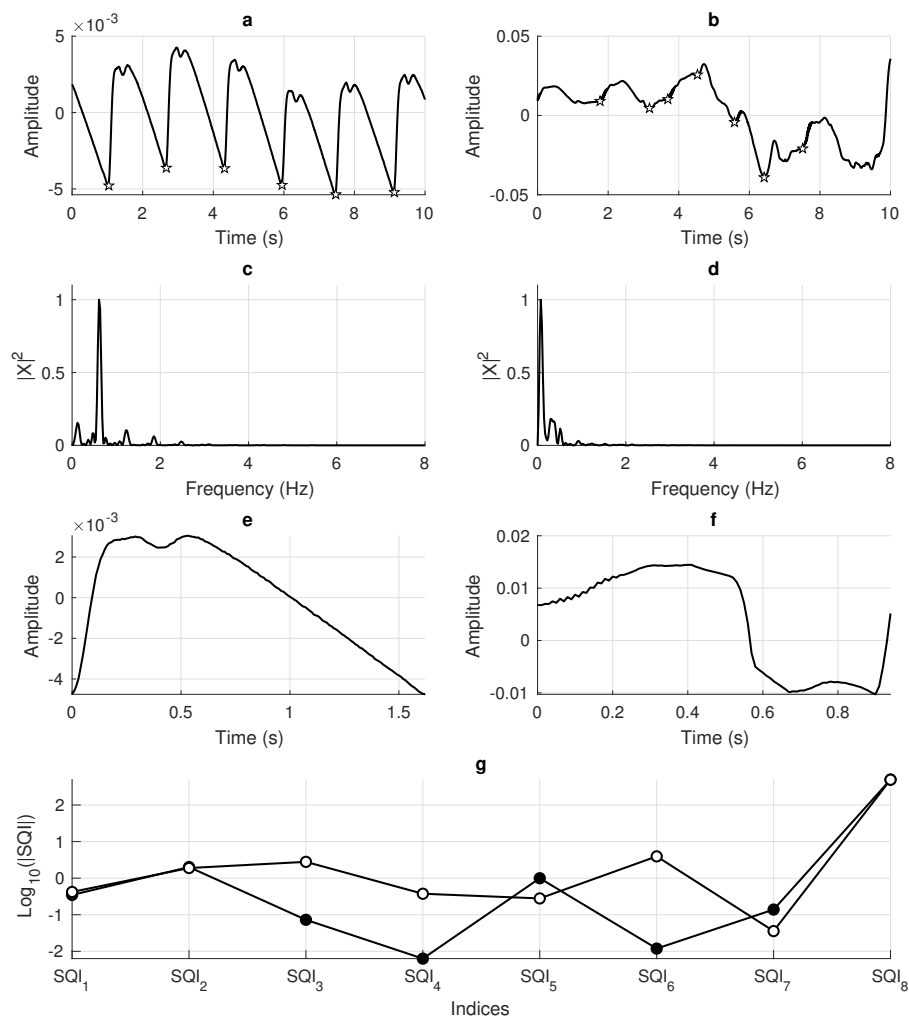


Fig. 11. Signal quality indices (SQIs) extracted from high- and low-quality PPG segments: (a) a high-quality PPG segment; (b) a low-quality PPG segment; (c) and (d) frequency-domain representation of the high- and low-quality segments; (e) and (f) template pulse waves extracted from the high- and low-quality segments; (g) trend-based and frequency-domain SQIs extracted from the high-quality (black dots) and low-quality (white dots) segments. Values for signal quality indices are presented on a log scale for visualisation purposes. SQI_1 : Skewness in time domain; SQI_2 : Kurtosis in time domain; SQI_3 : Shannon entropy; SQI_4 : Maximum autocorrelation; SQI_5 : Mean Pearson's correlation coefficient between the template and each cycle; SQI_6 : Mean Euclidean distance between the template and each cycle; SQI_7 : Ratio between the power between 1 and 2.25 Hz, and the power between 0 and 8 Hz; SQI_8 : Kurtosis in frequency domain.

Once signal quality indices have been extracted, the question that arises is how to determine the values of the indices that are related to high- and low-quality PPG signals. Decision rules are then established to determine the labelling of the PPG signal. There are two main approaches for the decision rules: physiological thresholds and heuristics, and data fusion [30]. In the first case, thresholds are usually established using physiological knowledge or empirical evidence, and in most cases the systems for assessing signal quality use combinations of rules based on multiple features [30]. In the case of data fusion, different extracted features are combined to produce robust decisions. Probabilistic strategies, such as the Kalman filter, have been applied to determine PPG signal quality [48], [54], while machine learning techniques have also been proposed for the automatic identification of decision rules based on extracted indices [48], [58], [59]. With the advances in physiological data analysis and the increased availability of databases, the application of machine learning techniques for PPG signal quality assessment is expected to grow, not only as a means for combining different indices and generating automatic decision rules, but also as alternatives for the identification of poor-quality segments in the PPG. Such an approach has already been investigated by Pereira *et al.*, who successfully applied deep learning algorithms to automatically identify poor-quality PPG segments without the extraction of signal quality indices [60].

3.1.4. Calculating derivatives

The calculation of derivatives of the PPG signal is often a key step in pulse wave analysis. For instance, several indices of vascular ageing can be extracted from the second derivative of the pulse wave [61]. Several approaches have been proposed to calculate the derivative of a PPG signal [62]. For instance, the simplest approach to calculate a derivative is to use the single-sided difference quotient, in which the derivative, x' , of a signal, x , is calculated from the difference between adjacent points ($x'[n] = (x[n+1] - x[n])/T$, where $x[n]$ is the signal, and T is the time interval). However, this approach is highly susceptible to high frequency noise because it only uses two points on the signal. Whilst the symmetric difference quotient ($x'[n] = (x[n+1] - x[n-1])/T$) can provide a more accurate estimate for the derivative, it is similarly susceptible to noise. Broadly, there are two approaches to reducing susceptibility to noise: low-pass filtering the signal (such as below 7 Hz [63]) prior to differentiation, or using more signal points in the calculation. More signal points can be included by using differential quadrature methods, in which the derivative is calculated as the weighted sum of multiple points on the signal. One example is Savitzky-Golay filters [64], [65], which incorporate smoothing, thus reducing the impact of high frequency noise on calculated derivatives.

3.1.5. Empirical mode decomposition

In the late nineties, Huang *et al.* proposed a novel method for analysing nonlinear and non-stationary data, which they called Empirical Mode Decomposition (EMD) [66]. This has proven to be a useful tool for analysing physiological data, such as the PPG, since it can be used to decompose any complicated data set into a finite number of Intrinsic Mode Functions (IMFs), which represent the energy associated with various intrinsic time scales and allows for the localisation of any event both in time and frequency domains [66].

The main advantage of EMD is that it is data-driven and locally adaptive, differentiating it from other time-frequency analysis techniques [67]. The goal of EMD is to obtain IMFs from a signal. IMFs satisfy two conditions: (1) in the whole data set, the number of extrema and the number of zero crossings must be equal or differ at most by one; and (2) at any point, the mean value of the envelope defined by the local maxima and the envelope defined by the local minima is zero [66]. Therefore, the EMD process consists of finding all functions that classify as IMFs when extracted from the original signal. This process is also known as sifting, and a deeper explanation of it can be found elsewhere [66], [68], [69]. Figure 12 shows an example of the extraction of IMFs from a PPG signal exhibiting a rapid change in baseline.

One disadvantage of EMD is that it is sensitive to the presence of noise in the recorded signal. More recently, an improved version of the EMD, called Ensemble Empirical Mode Decomposition (EEMD), has been proposed, in which IMFs are identified as the mean of an ensemble of trials, and each trial consists of the signal with the addition of white noise [70]. This process effectively reduces the effects of noise on the resulting decomposition.

EMD and EEMD have been widely used in PPG signal analysis. Most applications have focused on the extraction of respiratory information from the PPG signal [71]–[75], the measurement of pulse rate [76]–[79], removal of motion artefacts [80]–[83], and the diagnosis of diseases, such as hypertension [84], [85], diabetes [86], ventricular fibrillation [87] and arterial stiffness [88]–[90].

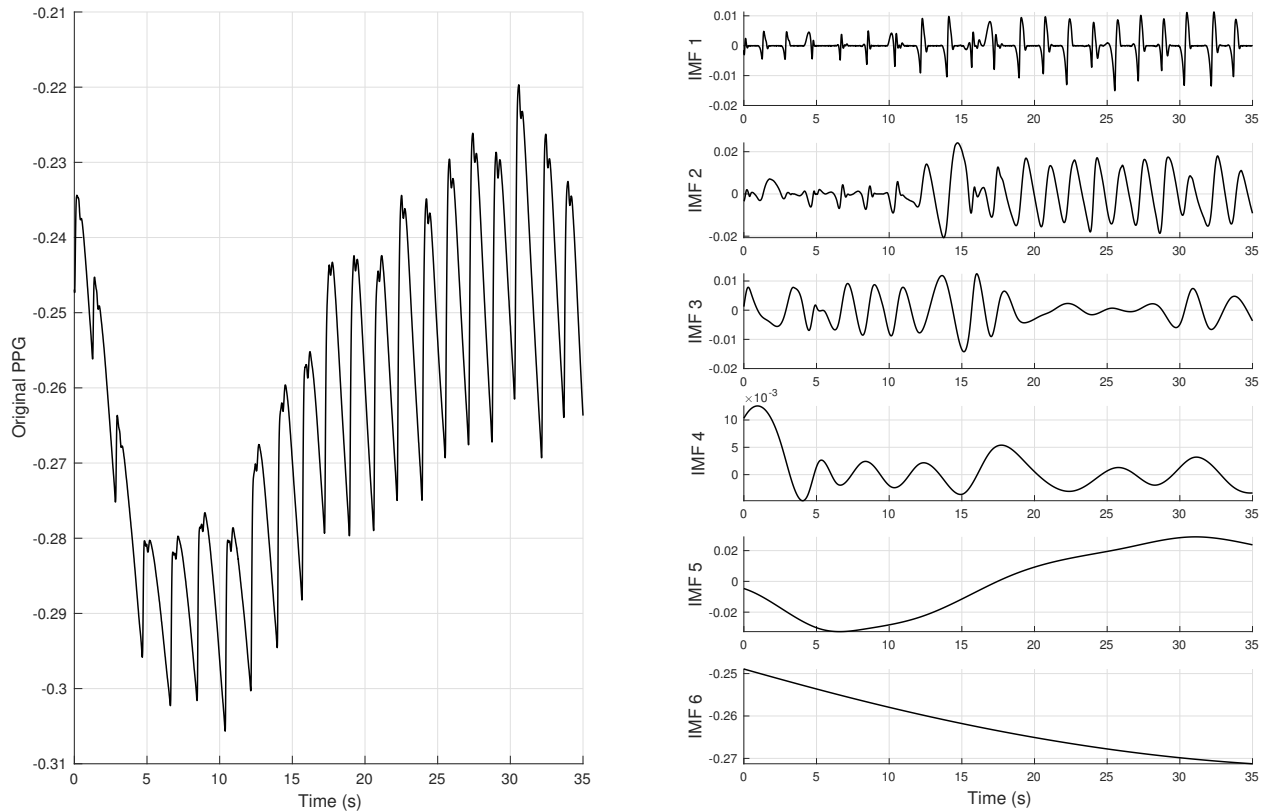


Fig. 12. Empirical mode decomposition: Application of empirical mode decomposition to a PPG signal exhibiting a rapid change in baseline (left) to extract intrinsic mode functions (IMFs, right).

3.2. Time domain analysis

There is great scope to analyse the PPG signal in the time domain as individual pulse waves can be characterised by a number of features. Features can be expressed in terms of amplitude, timing, and shape, as well as the variability of these features [1], [10], [17], [91]. Having pre-processed the PPG as described in Section 3.1, it can be analysed in the time-domain as follows:

- 1) **Identify individual pulse waves** for analysis.
- 2) **Identify fiducial points** on each pulse wave and its derivatives from which pulse wave features can be calculated.
- 3) **Calculate pulse wave features** in order to quantify the amplitude, timing, and shape of each pulse wave.
- 4) **Obtain representative feature measurements** from a recording by averaging features derived from each pulse wave.
- 5) **Identify abnormal pulse waves** in order to remove or replace feature measurements derived from them.

These steps are now discussed in turn, followed by an overview of techniques to analyse simultaneous signals in Section 3.2.6.

3.2.1. Identifying individual pulse waves

The first step in time-domain analysis of the PPG is to identify individual pulse waves for analysis. This task is challenging because: (i) individual pulse waves can exhibit two distinct peaks, particularly in young healthy subjects (see Figure 2); and (ii) noise and low frequency physiological variations can create disturbances in the signal (see Figure 4) [92], [93]. Several methods have been proposed to identify individual pulse waves. Most methods are based on the identification of the systolic peak, since it tends to be the most salient feature [94]. Methods usually consist of four steps: (1) filtering the signal to emphasise the desired components of the PPG; (2) extraction of candidate pulses; (3) identifying peaks or onsets; and (4) correction of these peaks or onsets [95].

As discussed in [96], three of the most common peak detection algorithms are: (i) the detection of peaks using thresholds [97]; (ii) the identification of peaks as zero-crossing points on the first derivative, in conjunction with an

adaptive thresholding scheme [98]; and (iii) the identification of peaks using the slope sum function in conjunction with adaptive thresholding [99]. Other methods include: (i) identifying maxima and minima points of the PPG signal [93]; (ii) identifying points on the first- [94], [96] and second-derivative of the PPG [96]; (iii) identifying upslopes in the PPG [92], [96]; and using more advanced techniques, such as the Wavelet transform [100], [101] and the local maxima scalogram [102]. Table I summarises some of these algorithms. Further information about this topic can be found in [95].

3.2.2. Identifying fiducial points

The second step in time-domain analysis is to identify points of interest on each pulse wave. These points, usually known as fiducial points, are distinct points that can be identified on either the pulse wave or its derivatives. Figure 13 illustrates commonly used fiducial points.

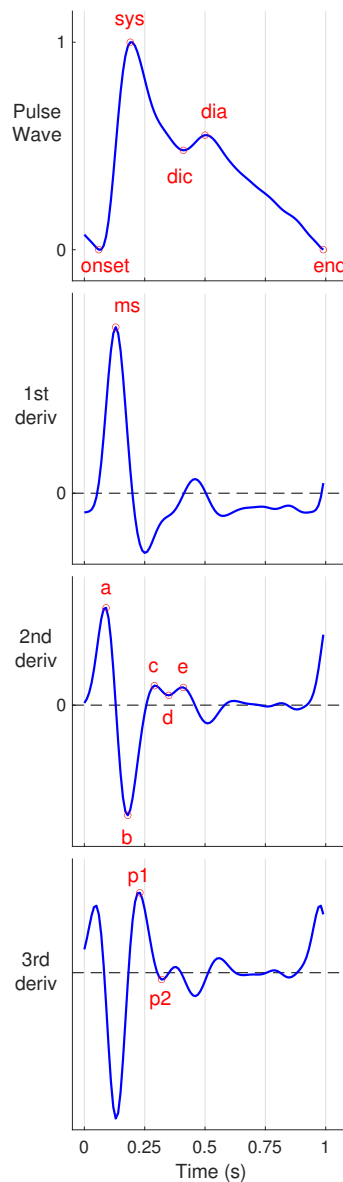


Fig. 13. Fiducial points on the PPG signal and its derivatives: Fiducial points that can be identified on: (a) the PPG pulse wave; (b) its first derivative, PPG'; (c) its second derivative, PPG''; and (d) its third derivative, PPG'''. In (a), the pulse onset (*onset*), systolic peak (*sys*), dicrotic notch (*dic*), diastolic peak (*dia*), and pulse end (*end*) are shown. In (b), the maximum slope point is shown (*ms*). In (c), the *a*-, *b*-, *c*-, *d*- and *e*-waves are shown. In (d), the p_1 and p_2 points are shown.

Source: [103] under CC BY 4.0.

TABLE I
ALGORITHMS TO IDENTIFY INDIVIDUAL PULSE WAVES IN THE PPG SIGNAL.

Methodology	Algorithm	Reference
Detection of maxima from the PPG	<p>Name: HeartPy</p> <p>Description: The algorithm can pre-process the signal using different FIR filters and outlier detection schemes. Then, peaks are detected using an adaptive threshold based on a moving average and the determination of regions of interest (ROIs). The threshold is adapted according to the instantaneous heart rate and the standard deviation of peak-to-peak intervals. Then, detected peaks are corrected based on outlier detection and rejection.</p> <p>Performance: Outperforms other usually used algorithms, such as the Pan-Tompkins algorithm.</p> <p>Advantages: Robustness against signal clipping, low-computational load.</p>	[93]
Identification of maxima from the 2nd derivative of the PPG	<p>Description: The method consists of a pre-processing stage, in which the signal is bandpass filtered and squared, a feature extraction stage, which generates potential locations of the peaks using two moving averages, and a classification stage, based on thresholding. This method takes advantage of the different frequency components of the PPG signal, and applies two different moving average filters, which were selected to emphasise the systolic peak area and the beat area to be used as a threshold for the first moving average</p> <p>Performance: Outperforms other algorithms [97]–[99] during exercise.</p> <p>Advantages: Robustness to movement artefacts.</p>	[96]
Detection of systolic upslopes from the PPG	<p>Description: The method detects systolic upslopes, which is a constant feature of the PPG morphology regardless of the subject from which the signal is acquired, or the body-site. In order to make this approach more robust to noisy segments of the signal, the authors propose a simple approach based on counting how long the upslope is, and rejecting upslopes shorter than expected, which could be related to noise or the diastolic peak.</p> <p>Performance: Good performance when applied in two different PPG data sets.</p> <p>Advantages: Simple algorithm, which could be applied in real-time applications. Robustness to PPG measurement site.</p>	[92]
Detection of maximum upslopes using the first derivative	<p>Description: First, all the peaks from the PPG signal are detected. Then, three bandpass filters are applied to the signal in the pre-processing stage and, using non-linear filters based on ranks for peak detection and decision logic, the peaks from the first derivative of the PPG are detected, which in turn correspond to the points of maximum slope. These peaks are corrected according to the interbeat intervals. Using a nearest neighbour decision logic, the peaks from the PPG signal are filtered by selecting the closest peak to each of the maximum slope points.</p> <p>Performance: Performed well when compared to annotations made by experts.</p> <p>Advantages: Robustness against noise. Good performance in PPG signals with low sampling rate.</p>	[94]
Identification of pulse onsets using Wavelet transform	<p>Description: Applying a fifth-scale quadratic spline Wavelet to the PPG, distinct peaks appear at the start of each beat. Using this peak, a threshold is generated for identifying the valid range for the PPG onset. Then, using FIR filters, the third derivative of the PPG is obtained, and the first zero-crossing of this signal within the valid range is assigned as the onset of each pulse.</p> <p>Performance: Has a comparable performance when compared to other algorithms published in the literature.</p> <p>Advantages: Robustness to noise due to the Wavelet transform. Good temporal accuracy. High performance for the identification of the PPG onsets.</p>	[100]

The key fiducial points on the original PPG pulse wave, referring to Figure 13 (a), are the pulse onset, the systolic and diastolic peaks, and the dicrotic notch. The maximum point on the first derivative is shown in Figure 13 (b), indicating the point of maximum slope in the original signal. On the second derivative, four distinct points occurring in systole can be identified, known as the *a*-, *b*-, *c*- and *d*-waves (see Figure 13 (c)). The *e*-wave can be used to determine the location of the dicrotic notch [10], [104]. p_1 and p_2 points can be identified on the third derivative (see Figure 13 (d)).

a) Original pulse wave

On the original pulse wave, the systolic peak is usually identified as the maximum point [11], and the pulse onset as the minimum (although several more advanced methods have been proposed to identify the timing of pulse onsets [105]–[107]). When the dicrotic notch is present, it can be identified from the timing of the *e*-wave on the second derivative. The diastolic peak can then be determined as the maximum point after the location of the dicrotic notch [11]. When the diastolic peak is not present (such as in older subjects), the corresponding location of this point can be estimated as the first local maxima in the second derivative after the *e*- wave [11] or from the first derivative as proposed by [108].

b) First derivative

On the first derivative, the point of maximum upslope can be easily obtained as the location of the maximum value of the first derivative [11].

c) Second derivative

An algorithm to detect *a*-waves in the second derivative (PPG'') was proposed in [62], based on the squaring PPG'', followed by the generation of blocks of interest and a prior-knowledge-based thresholding approach, and the subsequent identification of the *b*-wave. To identify the remaining fiducial points on PPG'', a similar approach has been proposed [104] in which *a*- and *b*-waves are removed, and then *c*-, *d*- and *e*-waves are identified. These two algorithms showed an improved accuracy for the detection of fiducial points from the SDPPG than other algorithms available in the literature.

d) Third derivative

More recently, methods have been proposed to detect fiducial points on the third derivative of the PPG. These points relate to the early and late systolic components, and are denoted as p_1 and p_2 [11]. p_1 can be identified by searching for the first local maximum of the third derivative after the occurrence of the *b*-wave in the SDPPG, while a candidate p_2 can be identified as the last local minimum of the third derivative before the *d*-wave, or as the local maximum of the original PPG between this candidate and the appearance of the dicrotic notch [11].

3.2.3. Calculating pulse wave features

Pulse wave analysis (PWA) refers to the study of the morphology of the PPG signal through features extracted from the pulse waveform along with its derivatives. Numerous morphological features have been investigated in the literature, which are mainly derived from the amplitude and width of the PPG wave contour. These features quantify pulse wave characteristics in order to obtain information on cardiovascular state. Commonly encountered features of the PPG waveform and its derivatives are defined in Table II, and Figure 14 illustrates some of these features.

On the original pulse wave, the systolic amplitude, that is, the height of the PPG from the baseline to its peak, has been correlated with stroke volume [91], and also suggested as an indicator for blood pressure [115]. Potential indicators of total peripheral resistance include the width at half the amplitude of the PPG [120] and the ratio of pulse area (as described in Table II) [116]. The crest time (CT) has been used to discriminate cardiovascular diseases [121]. Diastolic time, CT, and pulse width from both systolic and diastolic portions of the pulse wave, and their ratios, have been proposed as indicators of blood pressure [12], [111], [122], [123]. The reflection index has been proposed as a correlate of brachial-ankle pulse wave velocity [124]. The large artery stiffness index has been found to correlate with mean arterial blood pressure and age [108].

On the second derivative, the amplitude ratios of the *b*, *c*, *d*, and *e*-waves with respect to the *a*-wave are frequently used for pulse wave analysis. Several features calculated from the second derivative have been found useful indicators for assessing cardiovascular health. For instance, decreases in c/a , d/a , and e/a indices, and an increase in b/a , are thought to reflect increased arterial stiffness, and hence these indices decrease with age [61], [117]. Furthermore, the b/a and c/a ratios have been found useful for discriminating between hypertensive subjects and healthy controls

TABLE II

A LIST OF FEATURES WHICH CAN BE EXTRACTED FROM THE PPG PULSE WAVE AND ITS DERIVATIVES. DEFINITIONS: t - TIME SINCE PULSE ONSET (BEGINNING OF SYSTOLIC UPSLOPE); x , x' , x'' , x''' - PPG SIGNAL AND DERIVATIVES; T - DURATION OF CARDIAC CYCLE (SECS). ADAPTED UNDER [CC BY 3.0](#) FROM [11] (DOI: [10.1088/1361-6579/AABE6A](#)).

Signal	Approach	Feature	Formula	Ref
PPG, x	Timings	ΔT	time delay between systolic and diastolic peaks, $t(dia) - t(sys)$	[109]
		SI	large artery stiffness index, $h/(t(dia) - t(sys))$, where h is the subject's height.	[108]
		CT	crest time (or risetime), the time from pulse onset to systolic peak, $t(sys) - t(0)$.	[110]
		$DW\#\#$	diastolic width, $t(x = \#\#) - t(sys)$, where $t(x = \#\#)$ is time at which $x = \#\#$ on the falling limb, and $\#\#$ is a percentage of amp .	[111]
		$SW\#\#$	systolic width, $t(sys) - t(x = \#\#)$, where $t(x = \#\#)$ is time at which $x = \#\#$ on the rising limb, and $\#\#$ is a percentage of amp .	[111]
		$W\#\#$	total width of pulse wave at $\#\#$ % of its amplitude.	[111]
		$DW\#\#/SW\#\#$	ratio of diastolic to systolic widths at $\#\#$ % of pulse wave amplitude.	[111]
		t_{sys}	time to dicrotic notch, $t(dic) - t(0)$	[112]
		t_{dia}	time from dicrotic notch to pulse end, $T - t(dic)$	[112]
		t_{ratio}	ratio of crest time to time to dicrotic notch, $t(sys)/t(dic)$	[112]
		t_{p1-dia}	time delay calculated using $p1$, $t(dia) - t(p1)$	[113]
		t_{p2-dia}	time delay calculated using $p2$, $t(dia) - t(p2)$	[113]
		IPR	instantaneous pulse rate, $60/T$	[114]
	Amplitudes	amp	pulse wave amplitude, $(x(sys) - x(0))$	[115]
		AI	augmentation index, $(x(p2) - x(p1))/(x(sys) - x(0))$	[61]
		RI	reflection index, $(x(dia) - x(0))/(x(sys) - x(0))$	[109]
		RI_{p1}	reflection index (calculated using $p1$), $(x(dia) - x(0))/(x(p1) - x(0))$	[113]
		RI_{p2}	reflection index (calculated using $p2$), $(x(dia) - x(0))/(x(p2) - x(0))$	[113]
		$ratio_{p2-p1}$	ratio of $p2$ to $p1$, $(x(p2) - x(0))/(x(p1) - x(0))$	[113]
Areas	$A1$	area bounded by times of pulse onset ($t(0)$) and dicrotic notch ($t(dic)$)	[112]	
	$A2$	area bounded by times of dicrotic notch ($t(dic)$) and pulse end (T)	[112]	
	IPA	inflection point area, $A2/A1$	[116]	
PPG', x'	Amplitudes	ms	maximum slope, $x'(ms)/(x(sys) - x(0))$	[110]
PPG'', x''	Amplitudes	b/a	b/a ratio, $x''(b)/x''(a)$	[61]
		c/a	c/a ratio, $x''(c)/x''(a)$	[61]
		d/a	d/a ratio, $x''(d)/x''(a)$	[61]
		e/a	e/a ratio, $x''(e)/x''(a)$	[61]
		AGI	aging index, $(x''(b) - x''(c) - x''(d) - x''(e))/x''(a)$	[61]
	AGI_{inf}	informal aging index (used when c and d cannot be detected), $(x''(b) - x''(e))/x''(a)$	[117]	
	AGI_{mod}	modified aging index, $(x''(b) - x''(c) - x''(d))/x''(a)$	[118]	
	Timings	t_{b-c}	time delay between b and c , $t(c) - t(b)$	[112]
		t_{b-d}	time delay between b and d , $t(d) - t(b)$	[112]
	Slopes	$slope_{b-c}$	d/dt of straight line between b and c , normalised by a	[112]
$slope_{b-d}$		d/dt of straight line between b and d , normalised by a	[112]	
Combined	multiple	$IPAD$	inflection point area plus d-peak, $(A2/A1) + d/a$	[112]
	Amplitudes	k	spring constant, $x''(s)/((x(sys) - x(ms))/(x(sys) - x(0)))$	[119]

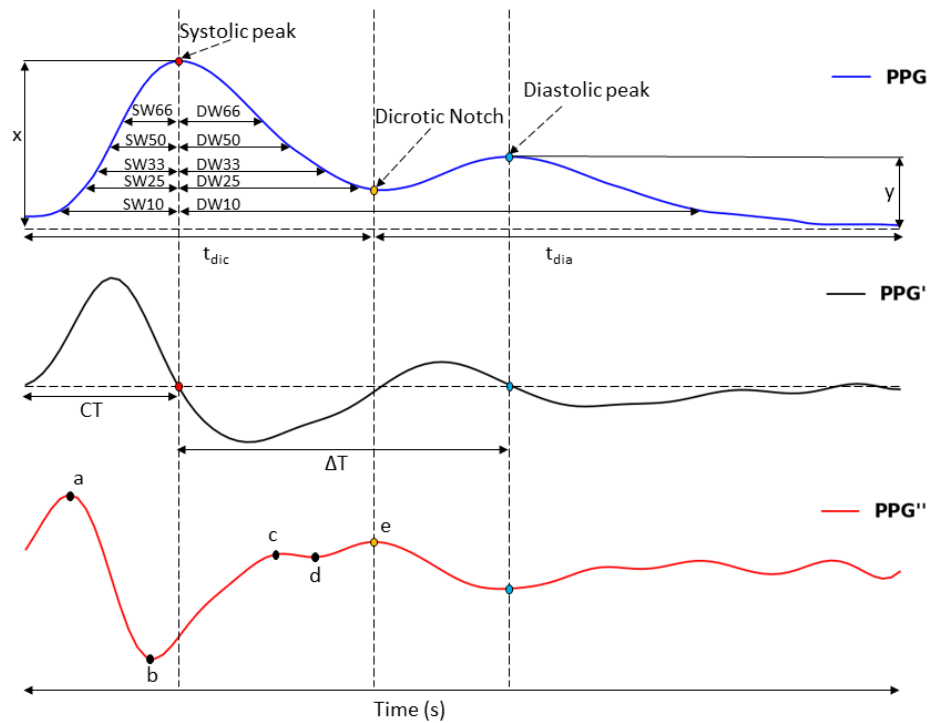


Fig. 14. Extracting features from the PPG and its derivatives: A typical PPG waveform, its first derivative (PPG') and second derivative (PPG'') with key fiducial points and commonly extracted features shown.

[125]. Additionally, b/a has been suggested as a useful index of altered arterial distensibility and atherosclerosis [126]. Other features derived from the second derivative have been proposed, such as the aging index proposed by [61] as $(b - c - d - e)/a$. [117] proposed an alternative aging index as $(b - e)/a$ when the c and d -waves are not visible.

a) Pulse decomposition analysis

The PPG pulse wave can be decomposed into an incident wave and reflected waves - a process known as 'pulse decomposition analysis'. This allows features to be derived from the individual waves which make up the overall pulse wave. Firstly, an incident wave is extracted by assuming that the systolic upslope is predominantly caused by this incident wave. The systolic upslope is flipped horizontally to produce a symmetrical wave, which is either assumed to be the incident wave [127], or to which a Gaussian is fitted to model the incident wave [128]–[130]. This incident wave is then subtracted from the original pulse wave to leave a residual, dominated by one or more reflected waves. These reflected waves are then extracted, by modelling them as either symmetrical waves (determined from the upslope of the running residual) or Gaussian curves. Pulse wave features can then be derived from the timings and amplitudes of the peaks of the individual waves, the widths of the individual waves, and the time delays between their peaks [127].

b) Quantifying features

Timing features (*e.g.*, pulse arrival time and pulse risetime) are straightforward to quantify (in seconds or milliseconds). Pulse amplitude can be quantified in a number of ways, for example in Volts, or normalised to the gain setting of the PPG amplifier. The complex shape profile of a PPG pulse shape can be expressed in a number of ways, including normalised height and width features [1]. Normalisation by pulse width is designed to reduce the impact of heart rate on shape characteristics, although the approach is not always perfect, such as at low heart rates (which can impact pulse risetime) [131].

3.2.4. Obtaining representative measurements from a recording

It is well accepted that there is physiological variability in the PPG at different measurement sites across the body in healthy subjects [1]. The degree of variability has been quantified for amplitude and timing measurements [1], [132]. As a result of this variability, features derived from pulse waves should be averaged over multiple pulse waves to obtain representative measurements. The variability is compounded in the presence of noise, such as during artefact due to movement between the sensor and tissue. A high proportion of noise in a recording can impact the validity of a measurement. Depending on the application noisy pulse waves might need to be excluded, and in the case of gross noise the measurement might need to be repeated. There is no global standardisation for the number of beats needed to obtain representative pulse wave features, although suggestions have been made, *e.g.*, 60 high quality beats [133]. The proportion of noise needed to reject a recording is also not well-defined although a 50% threshold has been proposed [33], [134]. Simple statistical measures can be used to quantify PPG features and their variability over multiple pulse waves, for example using simple mean and standard deviation values calculated, or perhaps median and inter-quartile range values. A range of shape related measures can also be extracted from average pulse waves (an ‘ensemble average’ of multiple pulse waves). There are only a limited number of publications on measurement repeatability and reproducibility across the various measurement sites of the body in health and in vascular disease (examples covering repeatability include [35], [135]).

3.2.5. Identifying abnormal pulse waves

Abnormal pulse waves, caused by ectopic beats and inaccurate pulse wave identifications, are often deemed unsuitable for analysis. They can have quite different characteristics from the remainder of the pulse waves, producing outlying feature measurements. Consequently, features extracted from them are often removed (or replaced) prior to further analysis. Ectopic beats originate from regions of the heart other than the sinoatrial node (which usually triggers heart beats), and consequently their timing can differ substantially from that of normal beats. Pulse waves corresponding to an ectopic beat and its neighbours are often markedly different from normal pulse waves. In addition, if a pulse wave is inaccurately identified (either missed or identified falsely - a false negative or a false positive), then the identified pulse wave will differ greatly from the true pulse wave. Consequently, it is often helpful to identify ectopic beats and inaccurately identified pulse waves (herein termed ‘abnormal’ pulse waves) in order to exclude them from analyses. This is particularly important when performing spectral analysis of a time series of features. For instance, when calculating frequency-domain measures of pulse rate variability, inter-beat-intervals caused by abnormal beats should be excluded and appropriately replaced in order to obtain a representative power spectrum [136], [137]. Methods for identifying abnormal pulse waves are now described.

Abnormal pulse waves are often identified through analysis of inter-beat-intervals. Mateo and Laguna proposed an approach for identifying abnormal beats in the ECG [136], which has since been applied to the PPG [138], [139]. The approach consists of calculating an acceptable variation in instantaneous inter-beat-intervals, above which a beat is considered abnormal (due to an ectopic or inaccurate beat identification). The acceptable variation, in terms of the timing of each heartbeat, t , is defined as:

$$|\hat{r}'_k| = 2 \left| \frac{t_{k-1} - 2t_k + t_{k+1}}{(t_{k-1} - t_k)(t_{k-1} - t_{k+1})(t_k - t_{k+1})} \right| < U \quad , \quad (3)$$

where U is the threshold acceptable variation given by $U = \min\{\xi\sigma_{\hat{r}'_k}, 0.5\}$, $\xi = 4.3$ is an empirical threshold, and $\sigma_{\hat{r}'_k}$ is the (potentially time-varying) standard deviation of $|\hat{r}'_k|$ calculated over a window of at least 5 minutes. This approach is also expected to reject periods of arrhythmia. It is a helpful approach for identifying pulse waves which are deemed suitable for inclusion in analyses because they have similar durations to those expected in a sinus rhythm.

3.2.6. Analysing simultaneous signals

The acquisition of the PPG signal alongside another simultaneous signal provides opportunity to derive additional information relating to pulse wave propagation, differences on either side of the body (bilateral differences), and phase differences. Several clinical and consumer devices can acquire multiple signals simultaneously, as described in Section 2.3.3. Techniques to analyse simultaneous signals are now described.

a) Pulse transit time and pulse arrival time

The speed of arterial pulse wave propagation is principally related to blood pressure and the properties of the arteries through which the pulse wave propagates (arterial stiffness and diameter) [23]. The speed of pulse wave propagation (pulse wave velocity, PWV) along a specific arterial path can be calculated as the path length divided

by the time taken for the pulse wave to propagate along the path (pulse transit time, PTT). PWV can be estimated from signals measured along a specific arterial path, such as wrist and finger signals [140]. In this case the PTT between the signals provides information on pulse wave propagation from the wrist to finger. Alternatively, PWV can be estimated from signals measured on two separate paths, such as finger and toe signals [141]. In this case, the PTT between the signals may be indicative of aortic PTT if the PTTs are similar between the aortic arch and finger, and between the aortic bifurcation and toe. PTT can be measured between two PPG pulse waves [141], or between a PPG pulse wave and a pulse wave identified in an alternative signal (such as a ballistocardiography, seismocardiography, impedance plethysmography, or strain gauge signal [140], [142]). Several different fiducial points on the PPG pulse wave have been used to assess its timing, with the choice of point having a large impact on the utility of PTT estimates [141].

Pulse wave propagation can also be assessed from pulse arrival time (PAT) which can be estimated from simultaneous ECG and PPG signals. PAT is the time between the R-wave of the ECG (indicative of ventricular depolarisation) and the arrival of the subsequent PPG pulse wave. It consists of two components: the pre-ejection period and the PTT from the heart to the PPG measurement site [23]. PAT has been widely studied as a marker of blood pressure [142]. However, the pre-ejection period varies both within and between subjects, meaning that PAT cannot be considered a direct surrogate for PTT [143], and blood pressure estimates calculated from PAT have been found to be less accurate than those calculated from PTT [144].

b) Assessing bilateral differences

Bilateral PPG signals (recorded from opposite limbs) can be compared to assess the degree of bilateral similarity between pulse wave morphology and timing. Cross correlation (CC) analysis has been used to compare bilateral PPG signals acquired at ear, finger and toe sites. Healthy subjects tend to exhibit high bilateral CC values [34], whereas there are greater differences between bilateral PATs in peripheral arterial disease [145], and greater levels of variability over time [146]. The peak CC value at zero phase lag is generally close to one in healthy controls but can be reduced in PAD patients where there is clear bilateral asymmetry in pulse between the right and left great toes. In addition, low frequency variations in bilateral PPGs have been compared using CC analysis. [147] studied diabetic patients with neuropathy and quantified the degree of right to left side similarity in the low frequency variability in pulse amplitudes at bilateral finger and toes sites; a similar approach was used by [148] to study patients with the connective tissue disease known as systemic sclerosis (see Figure 18).

c) Phase differences

The cross-correlation approach can also be used to study autonomic function and cardiovascular control. CC analysis has been used to estimate the phase delay between PAT and inter-beat intervals on a beat-to-beat basis under slow paced breathing in healthy subjects [149]. CC techniques have also been used to study the effect of respiration on PPG signals across the body by studying the phase differences for changes in pulse amplitudes and pulse arrival times between sites under slow paced breathing [22] (see [Chapter 8](#)).

With CC, careful pre-processing of the pair of signals should be performed, such as detrending (*e.g.*, removing the mean of each signal segment), normalising the amplitude, and using filtering to isolate a main frequency range of interest (*e.g.*, the breathing frequency range or very low frequencies). ECG and PPG signals can be studied on a beat-to-beat basis or using resampling (often at 4 Hz) to give a regularly spaced time series [22]. There are also a number of ways the output of a cross-correlation algorithm can be scaled. A correlation lag / lead value at the point of the CC peak can be extracted as can the correlation value at the zero-lag point.

3.3. Frequency domain analysis

Alongside time-domain analysis, the frequency-domain behaviour of the PPG provides valuable information on cardiovascular dynamics and allows for extraction of features for diagnosis and monitoring of various pathological conditions. Indeed, frequency-domain analysis can provide more valuable information than its time-domain counterpart [31]. There are different approaches to assess the frequency content of a signal, which can be broadly classified into two groups: (i) classical methods based on the Fourier transform; and (ii) modern methods based on models of the source of the signal [31]. Both approaches have been applied to PPG signals, with relatively similar performance [150].

3.3.1. Spectral analysis

Frequency spectra of PPG signals are commonly calculated using the Fourier transform. The Fourier transform uses sinusoidal waves to map the contents of the signal to the frequency domain [31]. Sine waves can be expressed

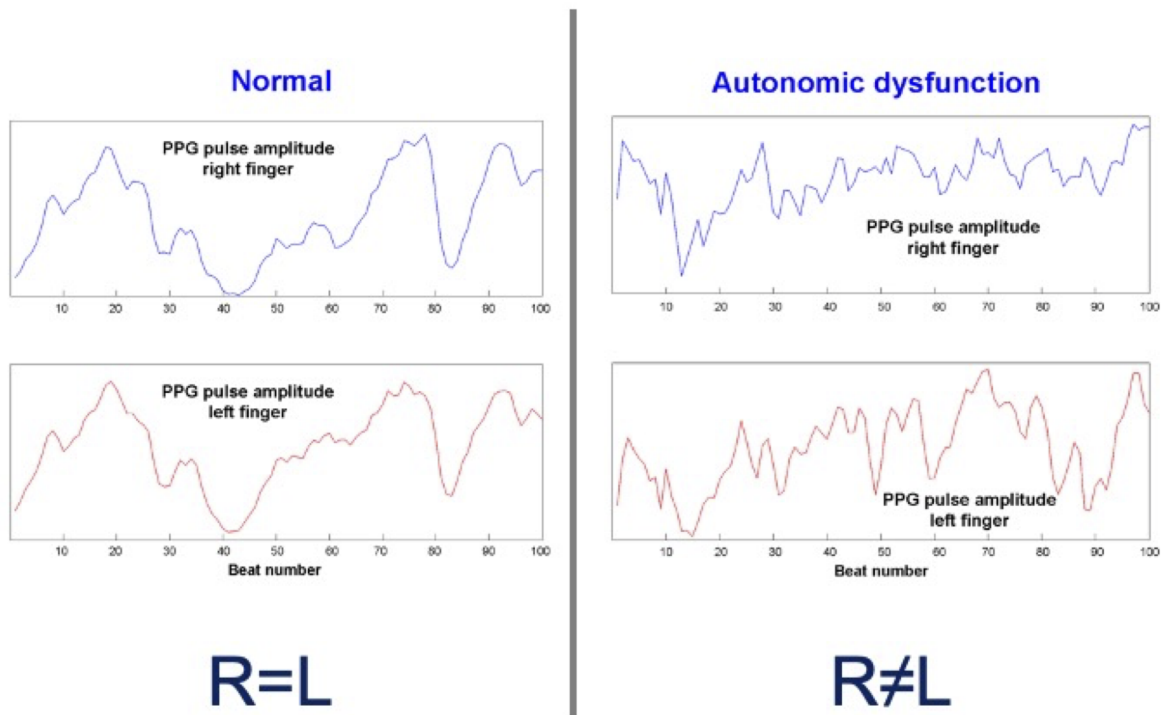


Fig. 15. Low frequency variation in the PPG: Low frequency variability over 100 heart beats for Right (R) and left (L) index finger PPG pulse amplitude for a normal healthy subject, showing the clear bilateral similarity (cross correlation function at zero lag point would be close to 1). In contrast, the PPG pulse amplitude dynamics for a patient with systemic sclerosis shows a clear asynchrony for the right and left side toe PPG amplitude variability (cross correlation function would be below the normal range), as attributed to autonomic dysfunction for this case.

in terms of their amplitude, frequency and phase. Consequently, they can be used to obtain the magnitude and the phase components of a spectrum. Figure 16 illustrates these components for a clean PPG signal. These were obtained using the fast Fourier transform (FFT) algorithm, which was developed for the discrete implementation of the Fourier transform with less computational cost [31]. Most of the information contained in the PPG is below 15 Hz, and the spectrum features a large peak around 1 Hz corresponding to the heart rate.

The sampling frequency and duration of a PPG recording have an impact on spectral analyses. Firstly, the sampling frequency (f_s) determines the maximum frequency available in the frequency spectrum frequency-domain spectrum: ($f_s/2$). Therefore, the sampling frequency should be more than twice the maximum frequency of interest. Secondly, the duration of the recording influences the resolution of the resulting frequency spectrum: the resolution is a function of f_s and the number of data points used to calculate the spectrum. In cases where a higher resolution is needed (*e.g.*, assessing autonomic nervous system activity, which usually occurs in very low frequency bands from 0.04 to 0.4 Hz, approximately [151]), the number of data points can be increased by zero-padding the signal [31].

Additional techniques can be used to obtain the frequency spectrum if only the magnitude component is required. The power spectral density (PSD, or power spectrum) and Welch's periodogram method are commonly used. The PSD is based on the computation of the power of the Fourier transform. Welch's periodogram is based on segmenting the PPG signal, obtaining a PSD for each segment, and then averaging the spectra to produce a final spectrum [31].

Modern approaches to obtain spectral information aim to reduce the effect of noise on the resulting spectrum, making them useful in certain applications in which the behaviour of the signal is well known [31]. Some methods are based on autoregressive models (AR), moving average models (MA) or a combination of both (ARMA). Different approaches have been proposed to estimate the power spectrum using AR models, such as the Yule-Walker, Burg, covariance, and modified covariance methods [31]. Other non-parametric modern approaches for spectral analysis are based on eigenanalysis frequency estimation, in which the signal is separated into correlated and uncorrelated

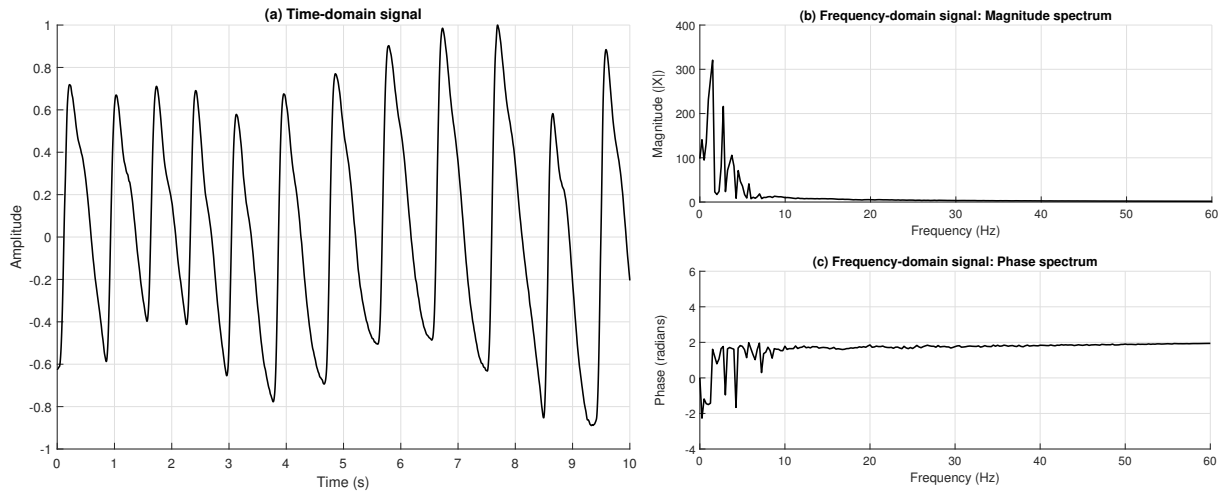


Fig. 16. Time- and frequency-domain representation of a photoplethysmographic signal: (a) Time-domain signal. (b) Magnitude component of the frequency spectrum. (c) Phase component of the frequency spectrum.

signal components using singular value decomposition (SVD) [31]. An example is the multiple signal classification (MUSIC) algorithm [31]. Figure 17 illustrates the behaviour of some of the different classical and modern methods. The methods and parameters used to obtain a frequency spectrum should be chosen based on the application, the available signals and the information to be extracted from the spectra.

3.3.2. Time-frequency analysis

Time-frequency analysis, that is, the study of a signal simultaneously in both time and frequency domains, can be performed using several methods. Time-frequency analysis allows one to investigate how spectral features evolve over time, even in signals of short duration [152]. The short-time Fourier transform (STFT) method is commonly used, as are more advanced techniques such as wavelet techniques. Wavelet transforms (WT) have a number of advantages over traditional methods, including the tailoring of both time and frequency resolutions without one being traded off against the other, and they can identify transients in non-stationary signals. Wavelet analysis can offer time-localised filtering and can help determine discontinuities and other events not readily visible in the raw data. Wavelets can also provide a sparse representation of the data and are useful for denoising or compressing data while preserving important features.

There are various forms of wavelet analysis. The Continuous Wavelet Transform (CWT) is commonly used to analyse 1-D data such as a single PPG signal. In the CWT, the analysing function is a wavelet i.e., Ψ . From [153], the CWT compares the signal ($f(t)$) to shifted and compressed or stretched versions of a wavelet. Stretching or compressing a function is collectively referred to as dilation or scaling and corresponds to the physical notion of scale. By comparing the signal to the wavelet at various scales and positions, a function of two variables is obtained. If the wavelet is complex-valued, the CWT is a complex-valued function of scale or position. If the wavelet is real-valued, the CWT is a real valued function of scale and position. For a scale parameter, $a > 0$, and position, b , the CWT of the time domain signal ($f(t)$) is defined in Equation 4 by:

$$CWT(a, b; f(t), \Psi(t)) = \int_{-\infty}^{\infty} f(t)(1/a)\Psi * ((t - b)/a) dt \quad , \quad (4)$$

where $*$ denotes the complex conjugate. The Discrete Wavelet Transform (DWT) performs scaling and shifting in discrete steps of 2, which is very useful for computer implementation of the algorithm. The DWT can be faster than the CWT, and can be implemented on hardware more easily [153]. There are many different types of wavelet to choose from, including Daubechies, Analytic Morlet (Gabor), Haar, Morse, and Bump. The Morlet wavelet can be a popular starting choice.

Figure 18 shows a CWT time-frequency plot for the example of tracking finger PPG dynamics during a reactive hyperaemia flush following a pressure cuff occlusion challenge to the arm (5 minutes). For this example, wavelet analysis was performed using MATLAB (The MathWorks Inc.), using the *cwt* function with the Morse wavelet

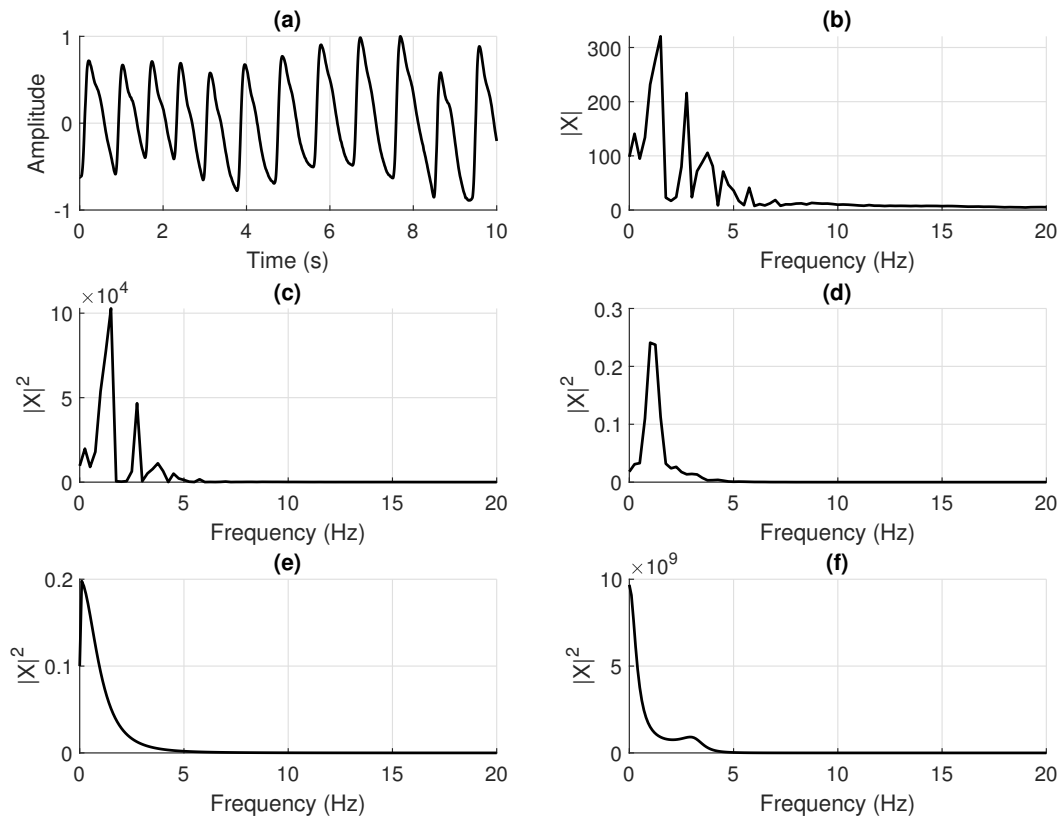


Fig. 17. Spectral analysis: Examples of spectra obtained from a photoplethysmogram (PPG) signal using classical and modern spectral analysis techniques: (a) Time-domain PPG signal; (b) Fast Fourier transform; (c) Power spectrum (PS); (d) PS using Welch's method; (e) Yule-Walker algorithm; (f) Multiple signal classification algorithm.

selected. This clinical application is covered in [Chapter 6](#), where normative responses are contrasted with patient examples.

3.4. Machine learning

Driven by the advances in data processing, computational powers and wearable technologies, there has been an increased interest in applying machine learning to the PPG. Machine learning techniques are typically used for either: (i) classification, in which a class label is allocated; or (ii) parameter estimation, in which a target parameter is estimated. PPG-based machine learning algorithms have been developed to classify patients according to whether they have coronary artery disease [154]–[157] and atrial fibrillation [158]–[163]. Machine learning has also been used to estimate parameters from a PPG signal, including: blood pressure [12], [111], [122], [123], [164], [165], haemoglobin levels [166]–[169], blood glucose [170]–[174], blood oxygen saturation [175]–[177], stress levels [178]–[182], and respiratory rate [71], [183]–[185]. Machine learning has also been used to develop signal quality assessment algorithms [55], [59], [60], [169], [186], [187]. The most popular machine learning techniques used are now described.

3.4.1. Linear regression

Linear regression is one of the most common approaches for parameter estimation. In its simplest form, univariate linear regression models the relationship between an independent (input) variable X and a dependent (output) variable Y :

$$Y = \beta_0 + \beta_1 x_1 + \varepsilon \quad (5)$$

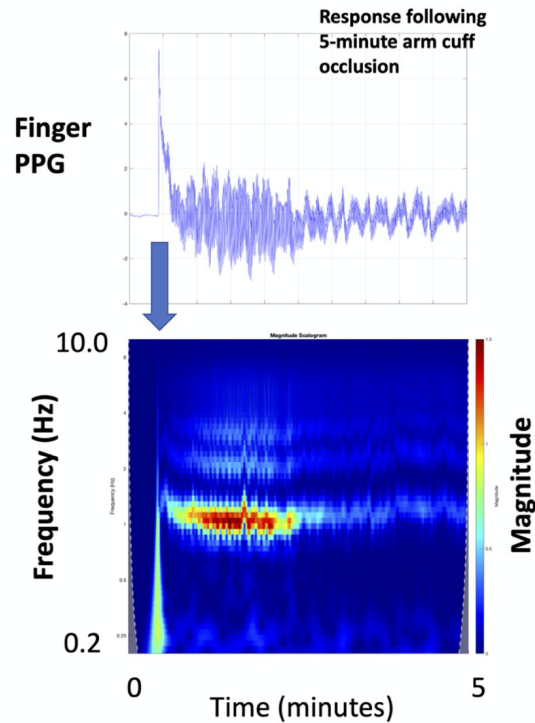


Fig. 18. Time-frequency analysis: Continuous wavelet transform (CWT) finger PPG time-frequency characteristics during a reactive hyperaemia flush following a 5-minute arm cuff occlusion challenge. The intensity of the flush response appears maintained for a few minutes following cuff release for this healthy control subject. The harmonics of the PPG signal can also be studied. The frequency axis is a log10 scale with a dominant signal frequency close to 1 Hz.

where β_0 and β_1 are regression coefficients, and epsilon (ε) is a random error. For multiple linear regression models the relationship between multiple independent variables (X_1, X_2, \dots, X_n) and a single dependent variable Y . Y as a linear combination of the input variables:

$$Y = \beta_0 + \beta_1 x_1 + \beta_2 x_2 + \dots + \beta_n x_n + \varepsilon \quad (6)$$

where $(\beta_1, \beta_2, \dots, \beta_n)$ are regression coefficients. The coefficients are initialised with random values, and then optimised during training by iteratively minimising the error between the estimated and ground truth values for Y using a cost function such as the mean squared error. The random error E represents the difference between the predicted and ground truth values. Training completes when the algorithm reaches a global minimum (*i.e.*, lowest error).

The simplicity of linear regression makes it appealing for modelling non-complex relationships between variables. This makes the model perform well on smaller datasets. However, its performance degrades as the complexity and nonlinearity of the input and target variables increases. Linear regression has been applied in several PPG analysis studies [122], [165], [188], [189].

3.4.2. Tree-based algorithms

Tree-based machine learning algorithms can be used for both classification and parameter estimation. The algorithms take a branching structure similar to that of a tree, with a conditional statement at each branch. For example, at a first branch, a PPG signal could be placed into one of two groups according to whether the derived heart rate is above a threshold. At a second branch, the signal could be placed into one of two subgroups according

to the level of heart rate variability. This splitting process continues until reaching the end of the branching structure, at which point either a class label is provided (such as atrial fibrillation or not), or a parameter estimate is provided (such as systolic blood pressure). Decision trees are used for classification, and regression trees are used for parameter estimation. Such algorithms can perform well when there is increased complexity and non-linearity between dependent and independent variables.

The random forest is the most popular tree-based learning algorithm, introduced in [190]. A random forest is an ensemble of trees (either decision or regression trees), thus can be used for classification and regression tasks. In a random forest, multiple trees are involved in the decision-making process, as opposed to using a single tree as described above. In a classification task, each decision tree returns a categorical value, and the final category is selected based on a voting criterion, *e.g.*, the category with the highest number of votes. In a regression task, the final output is an average of the outputs of the constituent trees. Random forests can perform better than linear models and can handle large datasets with input vectors of high dimensions. They can also model highly nonlinear relationships and achieve a comparable performance with a multilayer perceptron neural network. In addition, the influence of each input feature on the output can be assessed. However, random forests are prone to overfitting and are more computationally complex than single tree-based algorithms. Tree based algorithms, utilising the PPG, have been applied in numerous tasks such as estimating blood pressure [165], [188], blood glucose [174], oxygen saturation levels [177], stress levels [181], and atrial fibrillation detection [162].

3.4.3. Support vector machines

The support vector machine (SVM) is a popular non-parametric machine learning algorithm that can be used for classification and regression. The objective of an SVM is to find the decision boundary that maximizes the distance between the data points and the hyperplane. The boundaries are set by finding the soft margins that maximize the margin between the hyperplane and the closest points to it, known as support vectors (see Figure 19(a)). This is performed by penalising points that are closest to the hyperplane most heavily. SVMs can be used for linear classification tasks, as illustrated in Figure 19(a). For non-linear tasks, a kernel function can be used to transform the data into higher dimensions so that a linear separation can be found [191]. When used for regression, the approach is known as Support Vector Regression (SVR), and the objective is to fit data points that fall outside the margin (further from the hyperplane) such that the error is minimised (see Figure 19(b)). The disadvantages of the SVM are that it does not work well on very large datasets, is prone to noise in the data, and the kernel application increases computational complexity. Nonetheless, it is still widely used to analyse PPG signals [123], [154]–[156], [159], [173], [179].

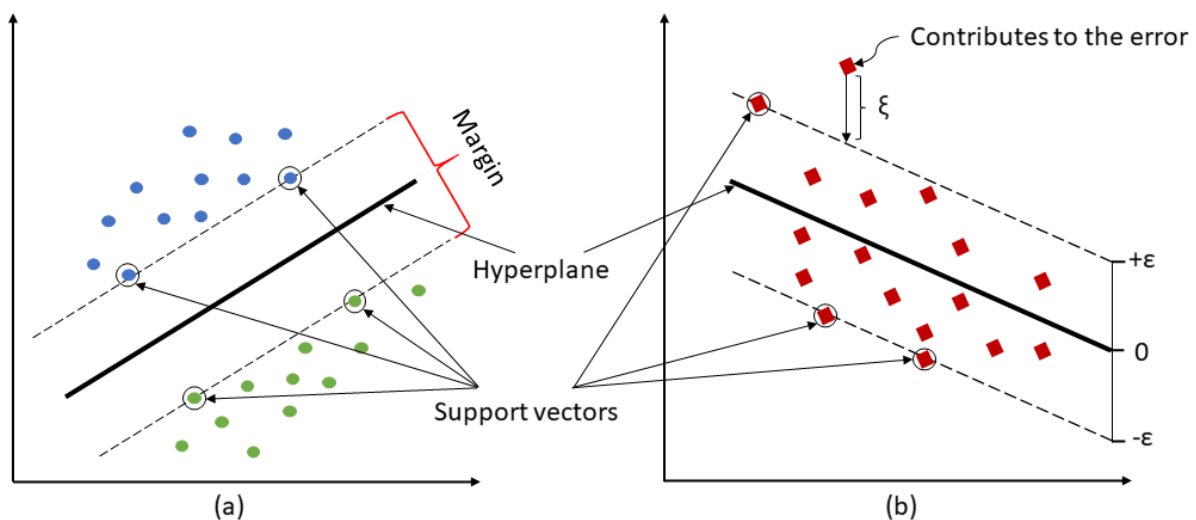


Fig. 19. Support vector machines (SVMs): Illustrations of the use of SVMs for (a) classification; and (b) regression.

3.4.4. Neural networks and deep learning

Neural networks are a type of machine learning algorithm that consists of multiple layers of artificial neurons between the input and the output. The neurons in the first layer each calculate an output as a function of the inputs. The outputs from each layer are passed as inputs to the next layer, until reaching the output layer (and more complex architectures can be used). The simplest form of a neural network consists of one input layer, one hidden layer and one output layer. When more hidden layers are added to the network, the architecture becomes known as Deep Neural Network (DNN). Deep learning refers to training a neural network that consists of more than two intermediate layers between the input and output layers. Neurons in the hidden layers are nonlinear processing units, also known as activation functions. Different architectures of neural networks are designed to handle different tasks, the most popular ones are Feedforward, Convolutional, ResNet, Long Short-Term Memory (LSTM), Gated Recurrent Units (GRU), Encoder-Decoder, and Autoencoders. Neural networks can model highly complex relationships in the data by learning new feature representations through their deep hidden layer units more effectively than classical machine learning techniques. Additionally, due to their complex architectures, neural networks are able to better scale on larger datasets than classical machine learning models. This however comes at the expense of added computational complexity. Neural networks and deep learning are becoming increasingly popular in research [111], [164], [189] for blood pressure estimation, by [171], [172], [174] for predicting blood glucose levels, as well as stress levels [178], atrial fibrillation [158], [161], [163], and PPG quality assessment [60], [169].

3.5. Nonlinear analysis in phase space

The PPG signal can be analysed nonlinearly by transforming it into phase space. It can be transformed into phase space using time-delay embedding, in which points on the signal separated by a specified time delay are plotted against each other [192]. This approach allows for visualisation and analysis of pulse wave morphology and variability [193]. Unlike time-domain analysis, this approach has the potential advantage that it does not require the identification of individual pulse waves. The process of transforming the signal into phase space for analysis is shown in Figure 20, and is now described.

Firstly, the PPG signal (Figure 20(a)) is transformed into phase space (Figure 20(b)) using Takens' Embedding Theorem [195]. This process consists of transforming the PPG signal into m new co-ordinates of $(x(t), x(t - 1\tau), \dots, x(t - (m - 1)\tau))$, where $x(t)$ is the PPG signal, m is the embedding dimension, and τ is the time delay. The resulting representation of the signal is termed an 'attractor'. The choice of embedding dimension affects the resulting attractor, with 2 [26], 3 [196], and 4 [197], [198] dimensions used previously. The time delay also affects the attractor, with delays of one sample [26], a fixed number of samples [26], [198], and $1/m^{\text{th}}$ of the pulse wave duration [193], [196], [197] used previously. The attractor can be used immediately for analysis [192], or it can be transformed further into a 2D attractor using symmetric projection attractor reconstruction as shown in Figure 20(c) [193], [196], [199]. This involves projecting the attractor on to the 2-dimensional plane orthogonal to the vector (1,1,1) [199]. This has the advantage of reducing the influence of baseline drift, and facilitating analysis in two dimensions. Some analyses make use of a density plot of the 2D attractor, as shown in 20(d), to assess variability in pulse wave timing and morphology, with potential applications in identifying illnesses such as sepsis which affect autonomic nervous system functionality [200]. The interested reader is directed to [192], [193], [199] for further details of the methodology, and also to [201] for an example of using recurrence plots for nonlinear PPG analysis.

3.6. Estimating physiological parameters

Despite its simple appearance, the PPG pulse wave contains far more information in its shape, height, and timing than just pulse rate. PPG pulse waves are considered to be a composite of the haemodynamic output of the entire cardiovascular system [202]. Much research has focused on developing algorithms to estimate physiological parameters from the PPG. Some algorithms are widely used, such as heart rate estimation algorithms, whilst others are still in development and not yet widely implemented. The interested reader is referred to [Chapter 12](#) for information on parameters provided by consumer wearables.

3.6.1. Heart rate

The PPG signal is dominated by pulse waves generated by each heartbeat; hence, heart rate or pulse rate can be estimated by simply identifying peaks corresponding to heartbeats. Assuming that the PPG signal is free of noise and other artefacts, the traditional methods employ a peak detection algorithm that detects systolic peaks, counts the

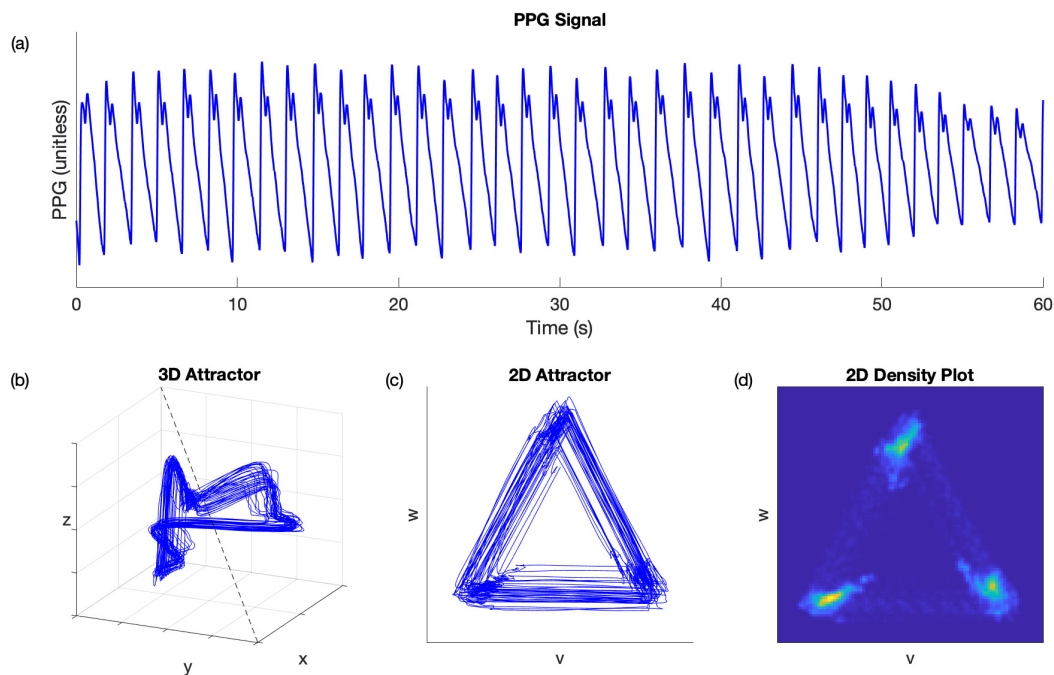


Fig. 20. Nonlinear analysis in phase space: The PPG signal in (a) is shown: (b) transformed into a 3D attractor in phase space; and (c) transformed into a 2D attractor using symmetric projection attractor reconstruction, with (d) showing the corresponding density plot of this 2D attractor.

Source: [194] under [CC BY 4.0](#).

peaks in a fixed time window (usually > 10 seconds), and then extrapolates to calculate the heart rate in beats per minute. In cases where the PPG signal is noisy, digital filtering techniques [17], [29], [203] are used in conjunction with the peak detection algorithm. However, these are strongly dependent on the filter's cut-off frequency. To address this, frequency-domain methods are used, particularly when PPG signals are affected by motion artefact [204]. Spectral analysis techniques (such as Welch's averaged periodogram) can be used to identify the heart rate as the frequency corresponding to the maximum spectral power [204]. However, in some cases the highest magnitude component is not the cardiac component, so other advanced signal decomposition-based spectral techniques can be used [204]. The wavelet transform [205], Hilbert transform [206], and empirical mode decomposition [78] are examples of these techniques, which divide the PPG signal into different frequency components. The cardiac component can then be analysed with a peak detection algorithm used to estimate the heart rate. However, signal decomposition-based algorithms are very hard to embed into everyday devices due to their high signal processing power requirements.

3.6.2. Inter-beat-intervals

Inter-beat-intervals, the intervals between consecutive heartbeats, are used for several applications including arrhythmia identification (see Section 3.6.3) and pulse rate variability assessment (see Section 3.6.4). Inter-beat intervals (IBIs) are extracted by measuring the time delay between occurrences of a particular fiducial point on consecutive pulse waves. This results in a time series of IBIs, sampled once per beat, as shown in Figure 21. Although IBIs can be measured using any fiducial point, their reliability has been found to be greater when measured using the pulse onset rather than the systolic peak. The best-performing algorithm to identify pulse onsets has been found to be based on identifying the intersection point of tangent lines to the apex point of the first derivative of the PPG signal, and to the foot of the PPG pulse [60], [105], [106]. It is often important to exclude outlying IBIs from analyses (see Section 3.2.5), since they can have a profound impact on the results.

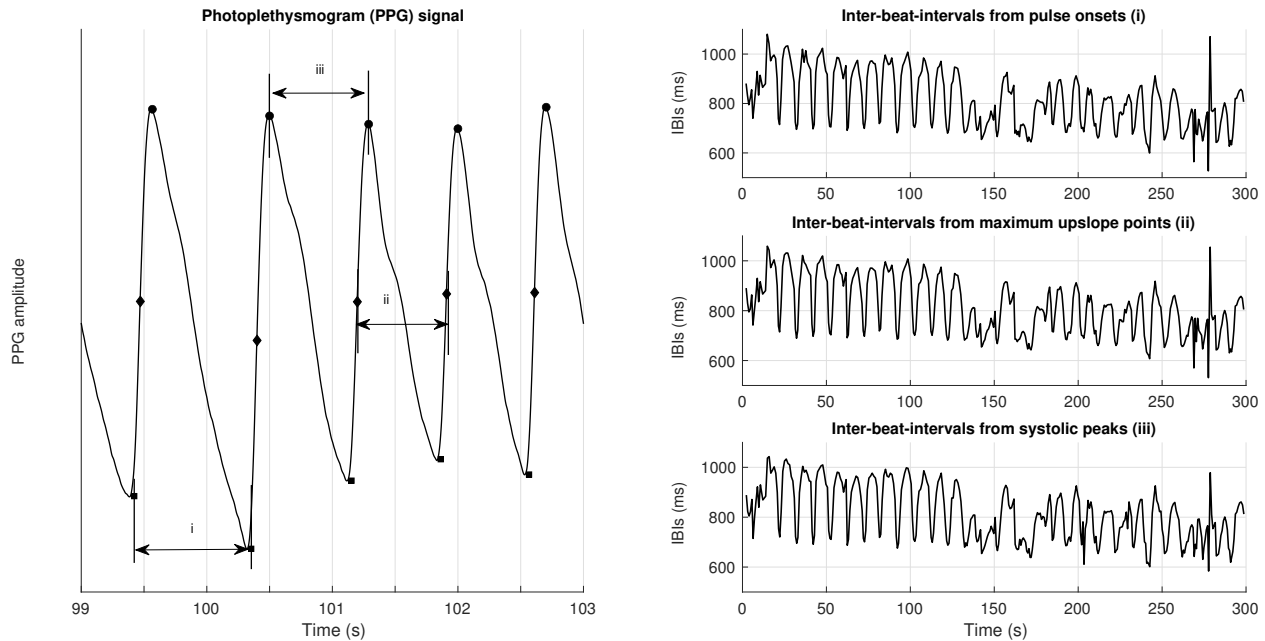


Fig. 21. Extracting inter-beat intervals (IBIs): Extracting IBIs from a PPG signal (left) using: (i) onsets determined applying the tangent intersection method; (ii) maximum slope points determined using the first derivative of the PPG; and (iii) systolic points determined as the maximum point of each individual pulse wave. The IBIs obtained from each approach are shown on the right.

3.6.3. Detecting atrial fibrillation

Atrial fibrillation (AF) is the most common arrhythmia, causing a fivefold increase in stroke risk [207]. Fortunately, the risk of stroke can be reduced through medication if it is diagnosed. AF is typically diagnosed through a short (≈ 30 second) ECG recording, or extended Holter ECG monitoring (over 1-14 days). However, AF can occur without symptoms, meaning an ECG assessment may not be conducted, and it can occur only intermittently, meaning a short ECG assessment may not capture all cases of AF. PPG-based wearables provide an alternative approach to identify AF, by assessing the variability in inter-beat-intervals. In this manner, wearables allow for frequent, unobtrusive rhythm assessments in daily life.

Techniques to identify AF from a PPG segment typically either analyse specified features of PPG pulse waves, or use deep learning without the need for any specified features [208]. These two approaches are now described.

Specified features of pulse waves, such as inter-beat-intervals or pulse amplitudes [209] can be used to classify a PPG segment as either AF or non-AF in three steps:

- 1) **Feature extraction:** One or more features is extracted from each pulse wave to produce a time series of feature measurements. Inter-beat-intervals are commonly used as shown in Figure 22 (I-III), as well as pulse amplitudes [209].
- 2) **Calculate summary statistics:** One or more summary statistics is calculated for each time series of features. The summary statistics can indicate the value of the time series (such as the mean value), or its variability (such as the standard deviation). They can be linear or nonlinear (such as entropy measures), and are often calculated using a Poincaré plot [210] as shown in Figure 22 (IV).
- 3) **Classification:** A classification technique is used to classify the summary statistics as either AF or non-AF. Either traditional statistical analysis techniques can be used, such as pre-specified thresholds or a logistic regression model, or machine learning techniques, such as k-nearest neighbours, a support vector machines, or decision trees [211].

Deep learning models can be used to classify a PPG segment as either AF or non-AF as follows. Often, the first step is to assess the quality of the segment to determine whether it is of sufficient quality to determine whether it exhibits AF. The second step is to use a deep learning model to classify the segment. The PPG signal can be used directly as an input to the model, and/or features extracted from it [208]. Additional signals or features can also be used, such as accelerometry data. The amount of labelled data required to train a deep learning model can be reduced by using transfer learning to fine-tune a pre-trained deep learning model [211].

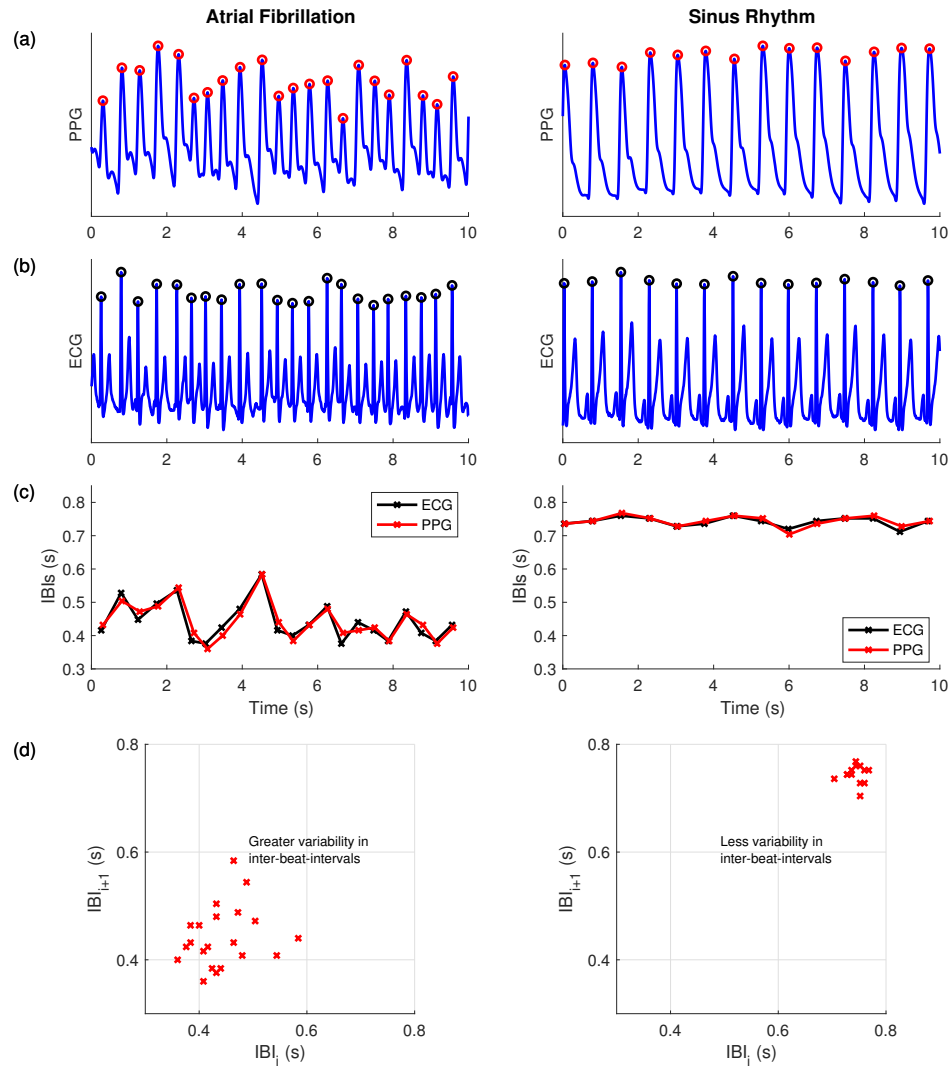


Fig. 22. Detecting atrial fibrillation (AF) from the PPG: (a) PPG signals acquired during a period of AF (left) and normal sinus rhythm (right); (b) corresponding ECG signals; (c) inter-beat intervals (IBIs) extracted from the ECG and PPG signals; and (d) Poincaré plots constructed using pairs of consecutive IBIs derived from the PPG.

Source: [212] under CC BY 4.0.

PPG-based techniques to identify AF have shown good performance, with many studies reporting values for sensitivity and specificity of over 90% [208], [211]. Recent studies have assessed the real-world performance of such techniques when incorporated into wrist-worn wearables, such as the Apple Heart Study [213] and the Huawei Heart Study [214]. The results of these studies demonstrate the potential of PPG-based wearables for AF detection in daily life: the Apple Heart Study, in which 419,297 participants were monitored for a median of 117 days, found a reassuringly low alert rate (0.52%), and a high positive predictive value of alerts (84%, verified against simultaneous ECG monitoring) [213]. Further work is required to fully understand the performance of these approaches, such as to understand their sensitivity in the target setting of monitoring older adults in daily life.

3.6.4. Pulse rate variability

Pulse rate variability (PRV) metrics assess the variability in inter-beat intervals (IBIs) derived from the PPG. PRV has been proposed as a potential surrogate of heart rate variability (HRV), which is measured from the electrocardiogram (ECG) [58]. HRV has been largely used for the assessment of cardiac autonomic activity. Both branches of the autonomic nervous system (ANS), sympathetic and parasympathetic nervous systems, control the

firing rate of the sinus node in the heart, and hence their behaviour determines heart rate [215]. By characterising the changes in heart rate over time, *i.e.*, measuring HRV, it is possible to assess the ANS using a non-invasive, indirect measure. HRV has been used for diagnostic and monitoring purposes of several cardiovascular, autonomic, and mental diseases [58].

The relationship between PRV and HRV is not straightforward. It has been proposed that PRV and HRV should not be considered equivalent, and that further research is needed to understand the additional processes that influence PRV beyond those that influence HRV [58], [216]–[218]. Nonetheless, PRV is now widely used in research, and it has been proposed as a useful tool for several applications, such as the detection, characterization, and monitorization of somatic diseases; the assessment of mental health; sleep studies; and pharmaceutical research [58].

PRV assessment is performed by analysing IBIs over time (see Section 3.6.2). As with HRV, the minimum recommended duration of PPG recordings for PRV analysis is 5 minutes, for short-term changes, while recordings with duration of up to 24 hours can be used to analyse long-term dynamics of pulse rate [137]. Several summary indices can be extracted from IBIs. The most commonly used indices are extracted in the time and frequency domains [137], [219]. Non-linear indices have also been used, including the analysis of Poincaré plots (see Figure 22 IV), different measures of entropy, detrended-fluctuation analysis and phase-related analysis [137], [220]–[225]. Table III describes the most commonly extracted indices for the analysis of PRV. When calculating PRV indices, it is important to identify and correct for the presence of outliers and ectopic beats. Most outlier removal methods are based on physiologically-based feasibility checks, mainly comparing consecutive IBIs and ensuring that their duration does not vary too greatly (see Section 3.2.5), allowing only ‘normal-to-normal’ (NN) intervals to be retained.

Guidelines have been published for the measurement, interpretation and clinical use of HRV [137]. However, no such guidelines have been established for PRV, and the different methodologies applied in PRV studies make it difficult to compare results. Key areas for consideration include: the selection of fiducial points for extracting IBIs; the minimum acceptable duration of PPG recordings for extraction of PRV indices; the PPG sampling frequency; the pre-processing methods for extracting PRV from PPG; the standardisation of frequency-domain analysis for assessing frequency-based indices; and the optimization of hyperparameters for the extraction of non-linear indices. This could help to further improve the technique and to better understand the physiological processes that affect PRV.

3.6.5. Respiratory rate

Respiratory rate (RR), the number of breaths taken in a minute, is used for diagnosis and prognosis in a range of clinical settings [226]. RR is a marker for clinical deteriorations in acutely-ill hospitalised patients, and an elevated RR is predictive of adverse events such as cardiac arrest [227] and death [228]. RR is also used in the identification of pneumonia [227] and sepsis [229]. Despite its importance, RR is usually measured through manual breath counting outside of intensive care. This process is time-consuming and inaccurate [230], [231]. Furthermore, existing methods for RR monitoring in wearables often require equipment such as chest-bands. Consequently, there is great potential for an unobtrusive method of RR monitoring using routine sensors such as a PPG sensor.

The PPG signal is subtly modulated by breathing, providing an opportunity to estimate RR from it. There are three main modulations, as shown in Figure 23(a): baseline wander (BW), amplitude modulation (AM) and frequency modulation (FM) [232], [233]. Most RR algorithms follow a standard structure consisting of three fundamental stages [139], as shown in Figure 23(b):

- 1) **Extraction of respiratory signals:** One or more respiratory signals are extracted from the PPG signal. This is beneficial as the extracted respiratory signals are dominated by a respiratory modulation, making it easier to estimate RR from them than from the original PPG signal. Broadly, there are two approaches for extracting respiratory signals: feature-based extraction and filter-based extraction [226]. In feature-based extraction, a feature is extracted from each pulse wave, such as the pulse wave amplitude (see Figure 23(b)). In filter-based extraction, filtering is used to extract a respiratory signal, such as a band-pass filter with a passband corresponding to the range of plausible respiratory frequencies.
- 2) **RR estimation:** RR is estimated from a respiratory signal typically using either a time- or frequency-domain technique (see Figure 23(b)). For instance, a time-domain technique could consist of identifying peaks in the signal (indicating breaths), and calculating RR from the number of peaks in a specified time. A frequency-domain technique could consist of calculating the frequency spectrum of the respiratory signal, and obtaining the RR as the frequency corresponding to the maximum power.

TABLE III
INDICES FOR ASSESSMENT OF PULSE RATE VARIABILITY

Abbreviation	Description
Time-domain indices	
AVNN	Average value of all normal-to-normal (NN) intervals
SDNN	Standard deviation of all normal-to-normal (NN) intervals
RMSSD	Root-mean-squared value of differences between adjacent intervals
SDSD	Standard deviation of differences between adjacent intervals
NN50	Number of pairs of adjacent NN intervals differing by more than 50 ms
pNN50	Proportion of number of pairs of adjacent NN intervals differing by more than 50 ms and the total number of pairs
Frequency-domain indices (5-min recordings)	
TP	Variance of NN intervals over the temporal segment
VLF	Power in the very-low frequency range ($f \leq 0.04$ Hz)
LF	Power in low frequency range ($0.04 < f \leq 0.15$ Hz)
nLF	Ratio between LF and TP minus VLF
HF	Power in high frequency range ($0.15 < f \leq 0.40$ Hz)
nHF	Ratio between HF and TP minus VLF
LF/HF	Ratio between LF and HF
Frequency-domain indices (24-h recordings)	
TP	Variance of all NN intervals
ULF	Power in the ultra-low frequency range ($f \leq 0.003$ Hz)
VLF	Power in the very-low frequency range ($0.003 < f \leq 0.04$ Hz)
LF	Power in low frequency range ($0.04 < f \leq 0.15$ Hz)
HF	Power in high frequency range ($0.15 < f \leq 0.40$ Hz)
Poincaré plot indices	
S	Area of the ellipse formed in the Poincaré plot
SD1	Short-term variability of the plot, determined as the minor axis of the ellipse
SD2	Long-term variability of the plot, determined as the major axis of the ellipse
SD1/SD2	Ratio between SD1 and SD2
Entropy analysis	
SampEn	Sample entropy of pulse rate variability
MSE	Multi-scale entropy of pulse rate variability, usually measured using SampEn in different scales of the signal
Detrended fluctuation analysis	
α_1	Short-range scaling exponent
α_2	Long-range scaling exponent

- 3) **Fusion of RR estimates:** Optionally, several RR estimates can be obtained from different respiratory signals and then fused to provide a single RR estimate. For instance, in [234] a RR estimate was calculated as the mean of estimates obtained from respiratory signals indicative of BW, AM and FM (see Figure 23(b)).

The techniques used in RR algorithms are described in further detail in [139], [226]. Recently, respiratory quality indices have been proposed to determine whether the respiratory modulations in a segment of PPG signal are sufficiently strong to accurately estimate RR [235].

The performance of algorithms to estimate RR from the PPG has been assessed in several studies. In studies of several algorithms from the literature, the best-performing algorithm was found to have limits of agreement of -5.1 to 7.2 breaths per minute when tested on healthy subjects in controlled conditions [139], and -9.2 to 8.8 breaths per minute when tested on critically-ill hospitalised patients [237]. The limits of agreement indicate the ranges in which 95% of errors are expected to lie. Future research may provide additional evidence on the performance of

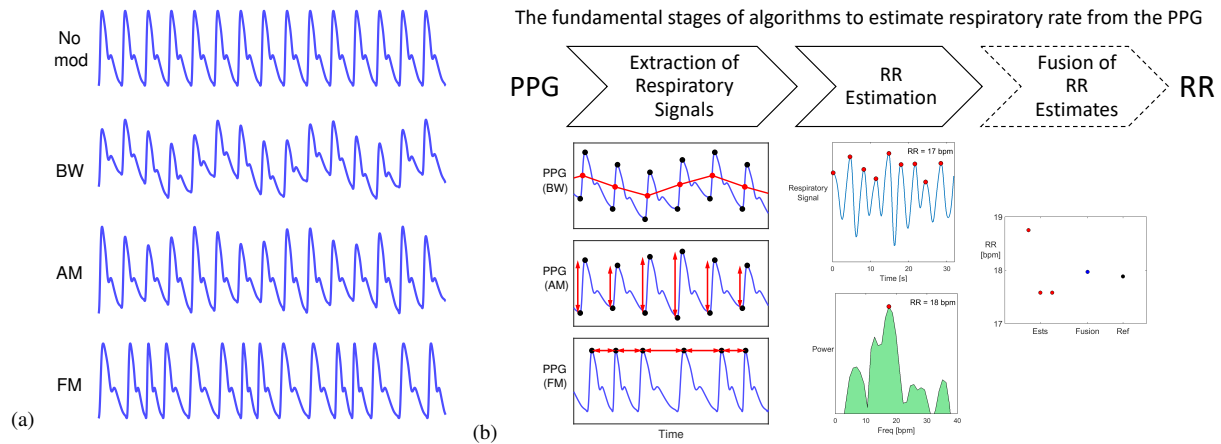


Fig. 23. Estimating respiratory rate (RR) from the PPG: (a) An idealised PPG signal (No mod) compared to idealised signals exhibiting three respiratory modulations: baseline wander (BW), amplitude modulation (AM) and frequency modulation (FM). (b) A typical algorithm to estimate RR from the PPG.

Sources: (a) and (b) adapted from [139] under [CC BY 3.0](#); (b) adapted from [226] under [CC BY 3.0](#); (b) adapted from [236] under [CC BY 4.0](#).

algorithms in target settings, such as when used with pulse oximeters or smartphones for spot-check assessments in home monitoring, or when used in wearables for continuous monitoring during daily living.

3.6.6. Blood pressure

Cardiovascular diseases (CVDs) are the most common cause of morbidity and mortality worldwide [238]. Blood pressure (BP) is widely measured to assess cardiovascular health. Abnormal BP incites several diseases that can lead to complications for vital organs such as the heart and brain [239]. Therefore, continuous BP monitoring could be useful for the early detection and treatment of abnormal BP. This in turn could assist in the early diagnosis, prevention and treatment of CVDs.

Despite its importance, there are several challenges to regular and continuous BP monitoring. The gold standard BP monitoring method is the direct invasive method [240]. It provides continuous BP measurement, although is only suitable for critically-ill hospital patients due to its invasive nature. The most widely used BP measurement technique in clinical practice is the sphygmomanometer [241]. Whilst it provides non-invasive BP measurements, it too has limitations, such as requiring an inflatable arm cuff which can be inconvenient and obtrusive, and only providing intermittent measurements.

An alternative approach is to assess BP from the speed of pulse wave propagation [242], which increases with BP. Two simultaneous signals are required, such as the electrocardiogram (ECG) and the PPG signal. BP can be estimated from parameters obtained from the two signals, such as pulse transit time (PTT) and pulse arrival time (PAT) (see Section 2.3.3) [23], [142], [243], [244]. This approach has been extensively reported in the literature [245]–[248]. However, it has several challenges such as requiring two sensors, synchronous signals, and difficulties in acquiring the ECG unobtrusively.

BP can also be assessed from PPG pulse wave shape [249]. This approach typically involves extracting handcrafted time-domain features (as described in Section 3.2.3) from the pulse wave and using a machine learning algorithm to estimate BP. In one representative study [111], twenty-one morphological features were extracted from PPG pulse waves. The systolic blood pressure (SBP) and diastolic blood pressure (DBP) were estimated by a two-layer feedforward neural network. This study reported a mean error (ME) \pm standard deviation (SD) of 3.80 ± 3.46 mmHg for SBP and 2.21 ± 2.09 mmHg for DBP. In another study, frequency domain features were extracted from PPG pulse waves [164]. These features were used as input for a one-layer feedforward neural network for estimating SBP and DBP. The reported ME \pm SD were 0.06 ± 7.08 mmHg and 0.01 ± 4.66 mmHg for SBP and DBP, respectively. In [189], a total of twenty-two features were extracted from the PPG waveform. The SBP and DBP values were estimated using a deep learning model that consists of one bidirectional gated recurrent unit (GRU) layer, followed two conventional GRU layers and an attention layer. The reported ME \pm SD were -0.52 ± 4.22 mmHg for SBP and -0.66 ± 2.07 mmHg for DBP. In addition, a ‘ResNet’ neural network has been used to estimate SBP and DBP from raw PPG signals without any feature extraction [250]. In this study, the deep neural network automatically

extracted features from the raw PPG including its first and second derivative. The mean absolute error (MAE) for the SBP and DBP were 15.41 mmHg and 12.38 mmHg, respectively.

BP estimation using machine learning and deep learning through a combination of signals such as ECG, PPG and ballistocardiograms (BCG) has also been investigated. For example, several features have been extracted from ECG and PPG signals, including PAT features, heart rate, augmentation index, large artery stiffness index and PPG pulse wave features [188]. In this study, several classical machine learning models were applied to estimate SBP and DBP, and the ME \pm SD for the best performing model (Random Forest) were -0.06 ± 9.88 mmHg for SBP and 0.36 ± 5.7 mmHg for the DBP. In [251], seven features were extracted from the ECG and PPG signals, and used as inputs to a Long Short-Term Memory (LSTM) recurrent neural network to estimate SBP and DBP, achieving root mean squared errors of 3.73 and 2.43 mmHg respectively. In [252], three signals (PPG, ECG and ballistocardiogram) were used to estimate BP. A neural network consisting of convolutional layers, a bidirectional GRU layer and an attention layer was used. This study reported a MAE \pm SD of 4.06 ± 4.04 mmHg for SBP and 3.33 ± 3.42 mmHg for DBP. [12] have recently published a comprehensive review paper covering the existing research for BP estimation using machine learning.

3.6.7. Arterial stiffness

Arteries tend to stiffen with age, becoming less compliant. Consequently, transmission of the pulse to the periphery (and its reflection back from the periphery) tends to get faster. Pulse wave propagation can also be affected by arterial calcification secondary to renal disease or diabetes, further speeding it up. Faster propagation resulting in earlier arrival of reflected waves from the periphery can augment the primary forward wave, thus changing pulse wave morphology. PPG pulse waves at the ear lobe, index finger and great toe tend to become more triangular in shape with advancing age [253] (Figure 24), pulse arrival time (PAT) decreases [133], and the risetime increases [131]. Linked to these examples of general age-related changes a whole host of PPG features which may be indicative of arterial stiffness have been explored (*e.g.*, in [11], [13]). Chapter 7 covers arterial stiffness and the PPG in more depth, so this section just aims to give a flavour of the potential of what can be done with PPG, in measurements and analysis, to study vascular ageing. Examples are given below for classic pulse wave timing, amplitude and shape features.

a) Pulse wave timing

In healthy subjects the pulse arrival time (PAT) decreases at ear, finger and toe sites with advancing age, and there is a tendency to bilateral similarity in such changes. Interestingly, the great toe site has appeared marginally more affected by age than finger and ear sites [133]. Pulse risetime increases with advancing age although high or low heart rates can have a significant impact on this measure [131]. Timing differences within a pulse can also include the Stiffness Index measure [108] - the subject height (in metres) divided by pulse timing difference between first systolic peak and early diastolic peak. PPG timing measures can include differences between body measurement sites, *e.g.*, between finger and toe sites, and these have been explored for: defining a normal range in children and contrasted to measurements in patients who have had a heart transplant [254]; and, peripheral arterial volume distensibility assessments using an external pressure cuff [255].

For whichever timing measure is extracted, the PPG signal(s) needs careful pre-processing using appropriate filtering to reduce noise and baseline wander, whilst not artificially distorting a PPG waveform with poor filter design. A range of methods exist to find fiducial points of the pulse foot and peaks (see Section 3.6.2). Furthermore, signal averaging should be used to account for physiological variability, based on beats that are of acceptable signal quality. However, there appears to be no standardization in such methods to date.

b) Pulse wave amplitude

Foot-to-peak PPG amplitude is not generally used to assess vascular ageing or arterial stiffness - it can be a highly variable measure in a subject in the space of just tens of seconds, for example, with changes in breathing or inspiratory gasp, or with cold or heat exposure. Relative amplitudes from derivatives of the PPG can however be used to form indices of ageing, such as the 'aging index' calculated from the second derivative (see Table II) [61], [256], [257]. The 'aging index' and 'b/a ratio' measures, for example, have been used to evaluate arterial stiffness. In addition, the augmentation index which is usually used for blood pressure pulses but can be applied to PPG, is defined as the ratio of the late systolic 'volume' inflection point to the early systolic 'volume' inflection point (often normalised to a specific heart rate, typically 75 beats per minute). Whichever feature is taken, careful denoising is needed prior to the use of signal differentiation to calculate the second derivative of the PPG. Averaging of indices over a number of beats should also be considered.

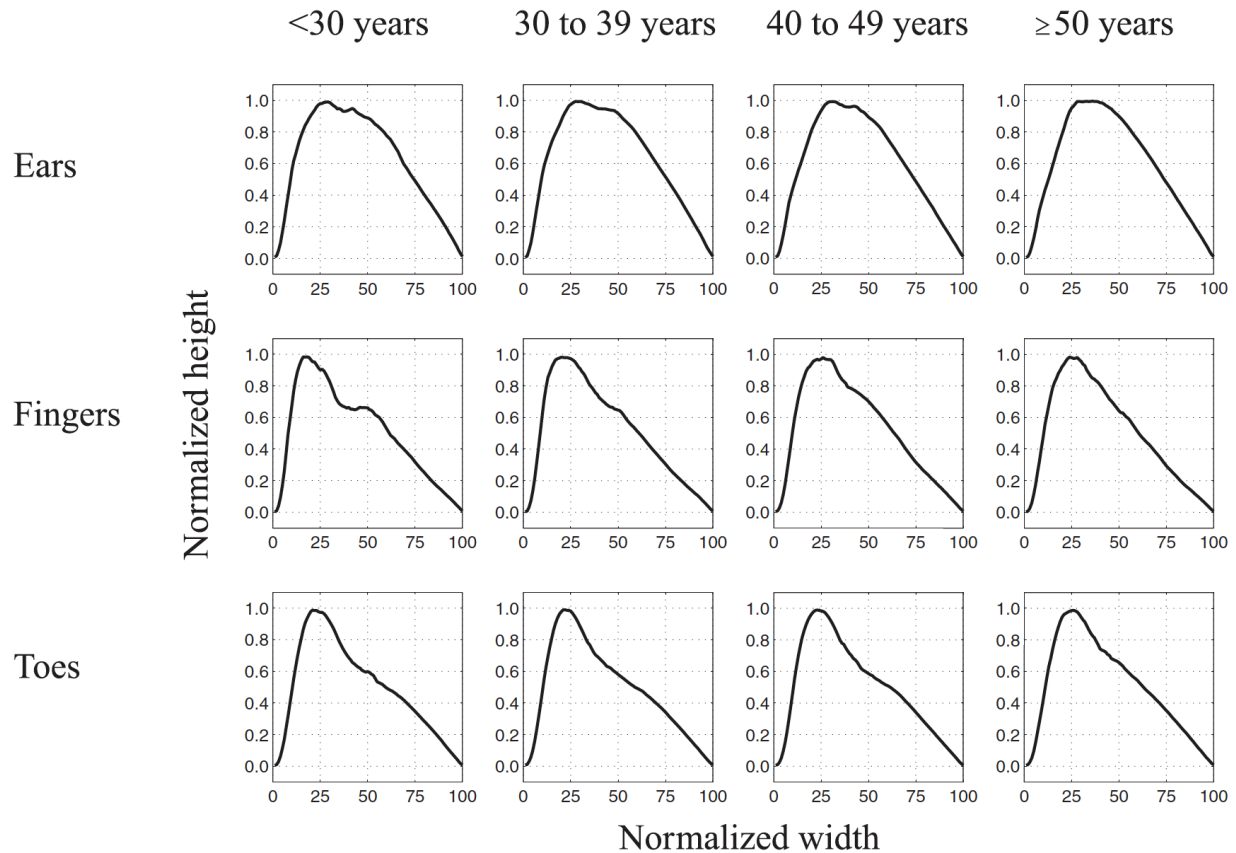


Fig. 24. Changes in the PPG pulse wave shape with ageing.

Source: [253], © Institute of Physics and Engineering in Medicine. Reproduced by permission of IOP Publishing. All rights reserved.

c) Pulse wave shape

Shape features can be extracted from the pulse wave normalised in amplitude or width, often by ‘ensemble averaging’ over a number of heart beats. It has already been noted that there is a tendency for increased triangularization of normalized peripheral PPG pulse shapes with age [253]. Careful pre-processing is required to reduce noise, for example, any beats showing clear motion artefact and/or significant baseline wander should be excluded. Since PPG signals at proximal sites can have a reflected peak that sometimes exceeds the primary peak (this can even alternate over the respiratory cycle), the amplitude from pulse foot to the first primary peak should be used for amplitude normalization. There is no standardization as yet to the number of beats that should be averaged for pulse morphology assessments, although a recent consensus survey of PPG experts did suggest a minimum of 51-60 beats [33].

d) Combinations of pulse wave features

As well as just a single pulse feature such as timing, amplitude or shape, a combination of features could be explored and linked to vascular age. This could include features derived using frequency analysis, transfer function analysis, and machine learning and deep learning techniques. This approach could offer value for establishing PPG-based indices linked to arterial stiffness and vascular ageing.

3.6.8. Left ventricular ejection time

Left ventricular ejection time (LVET, or the duration of systole) is the time for which blood is ejected from the left ventricle into the systemic circulation each heart beat. LVET has been found to be a predictor of future heart failure, and to be a useful risk factor for cardiovascular risk prediction [258]. LVET can be estimated from measurements of central arterial pulse waves obtained using techniques such as echocardiography, carotid tonometry and Doppler

flow measurements [259]. However, these techniques are time-consuming and require a specialist operator, so are not ideal for frequent assessments.

The PPG pulse wave is strongly influenced by the incident wave from the left ventricle, providing opportunity to estimate LVET from it. Techniques to estimate LVET consist of measuring the time interval between two points on the PPG indicating the beginning and end of ejection. Techniques to estimate LVET have used points on the original pulse wave and its first, second and third derivatives [259]–[262]. In addition, a pre-processing step of extracting the systolic portion of the PPG pulse wave (through Gaussian fitting) has been used prior to estimating LVET from the third derivative of the systolic portion [263]. Studies have found limits of agreement for between PPG-derived and reference LVETs of -24 to 17 ms [263], -41 to 13 ms [259], and (HR corrected LVET) -70 to 67 ms [262]. PPG-derived estimates of LVET have been found to change during blood loss [264], demonstrating their potential utility.

4. PHOTOPLETHYSMOGRAM SIGNAL SYNTHESIS

Photoplethysmogram signal synthesis, the generation of synthetic PPG signals, plays two important roles in the analysis of PPG signals. Firstly, it allows studies to be conducted using simulated signals where the equivalent *in vivo* signals are unavailable. For instance, it may be overly time-consuming or expensive to acquire PPG signals in a clinical study, it may be difficult to obtain simultaneous reference values of cardiovascular properties non-invasively (e.g., cardiac output), or it may be difficult to obtain PPG signals under a range of physiological conditions. In contrast, PPG signals can be simulated quickly and inexpensively, under known reference cardiovascular properties, and over a range of conditions [265]. This can facilitate early proof-of-concept studies to inform and justify future clinical studies. Secondly, PPG signal synthesis can be used for ‘analysis-by-synthesis’, in which PPG signals are parameterised for analysis [266]. For instance, a PPG pulse wave can be modelled as a sum of forward and reflected waves, each with known properties (magnitude, duration, and timing) which are more amenable to analysis than a time-series of points on a PPG pulse wave.

Most approaches to synthesising PPG signals consist of two steps: (i) simulating PPG pulse waves; and (ii) simulating a PPG signal as a train of pulse waves. This section provides an overview of these two fundamental steps, including techniques used to simulate PPG pulse waves based on mathematical and physical models (section 4.1), and techniques used to simulate PPG signals in normal sinus rhythm, irregular rhythms, and in the presence of noise (section 4.2). Research in this area is aided by publicly available resources, including a tool for synthesising PPG signals containing regular and irregular beats [267], and a database of simulated PPG pulse waves representative of a sample of healthy adults [265].

4.1. Simulating photoplethysmogram pulse waves

The first step in synthesising a PPG signal is to simulate individual PPG pulse waves. This has been primarily performed by using mathematical models to describe the pulse wave shape based on prior knowledge of the expected shape. More recently physical models have been used to generate a pulse wave based on physical principles of blood flow. These two approaches are now described.

4.1.1. Mathematical models

The PPG pulse wave is believed to be formed of an incident wave from the heart, and reflected waves from within the circulation [109]. Consequently, it has often been modelled as the sum of individual waves which together form the measured pulse wave. The PPG pulse wave has been modelled as the sum of: 2 Gaussian functions [47], [266], [267]; 4 Gaussians consisting of 2 in the systolic part, and 2 in the diastolic part [268]; 4-5 Gaussian functions [269]; and Gaussian and log-normal curves [270]. This approach involves finding the parameters of the Gaussians (or log-normal curves) which minimise the error between a reference pulse wave and the resulting modelled pulse wave. The parameters have often been optimised using nonlinear least squares fitting to minimise the squared differences between modelled and reference PPG pulse waves [270]. A variation on this is the use of a weighted least squares method, which weights specific fiducial points of interest on the PPG more heavily than other points, allocating more importance to those points which could inform clinical decision making [269]. The reference pulse wave can be a sample PPG pulse wave [271], one of five templates according to pulse wave morphologies typical of different ages [270]; or one of three templates according to quality (excellent, acceptable, and unfit, as described in Section 3.1.3) [47].

Some approaches to modelling the PPG pulse wave allow its amplitude to vary according to the neighbouring inter-beat intervals (IBIs). The rationale for this approach is that the left ventricle will fill with blood in the time prior to ejection (to a limit), and that the resulting stroke volume influences the amplitude of the PPG pulse wave. The amplitude of the pulse wave has been assumed to be proportional to the preceding IBI [270] (optionally capped at a maximum filling duration [271]). In the case of arrhythmias, if the beat is premature then the amplitude of the pulse wave has been assumed to increase exponentially with IBI duration [270]. This approach of simulating a pulse wave based on a reference IBI has the advantage that, if one is prepared to use an assumed pulse wave morphology, then the only information required to model PPG pulse waves is their duration. Pulse wave durations can be approximated from IBIs obtained from ECG recordings, which are more readily available in public databases than PPG recordings [270].

An alternative approach to simulate a PPG signal is to estimate it from a blood pressure (BP) pulse wave using a known transfer function. Generalised transfer functions relating the finger PPG to BP waves at the finger and wrist were proposed in [9]. This approach was subsequently used in [11] to simulate PPG pulse waves from reference BP pulse waves.

4.1.2. Physical models

Physical models can be used to generate PPG pulse waves at a range of locations around the body and under a range of cardiovascular conditions, as shown in Figure 25. This approach allows the pulse wave shape to be modelled in the absence of *in vivo* measurements. However, it is therefore, entirely reliant on the modelling assumptions being appropriate in order to produce realistic pulse waves. In [265], a computational model of blood flow through the circulation was used to simulate pulse wave propagation in the major arteries and into the microcirculation. The PPG pulse wave was then modelled as the volume of arterial blood contained within the microcirculation using a Windkessel model. This approach was used to simulate PPG pulse waves for subjects of a range of ages (25-75 years old), and with varying cardiovascular properties (normal ranges of heart rate, stroke volume, arterial stiffness and BP amongst others). The resulting database is publicly available [272]. It contains PPG pulse waves from 4,374 virtual subjects, and has been found to be useful for *in silico* analysis of pulse wave features and haemodynamic mechanisms [265].

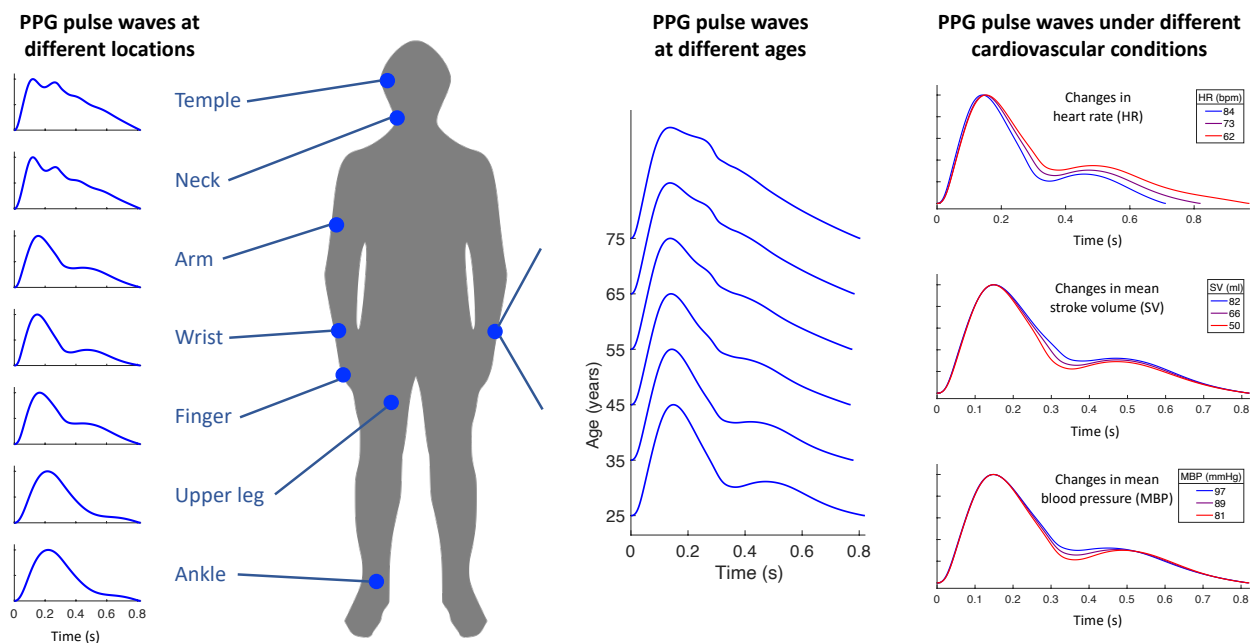


Fig. 25. Simulating PPG pulse waves: PPG pulse waves simulated using a physical model of blood flow: (i) at different locations around the body (representative of a healthy 25 year old); (ii) for healthy subjects of different ages (at the wrist); and (iii) under different cardiovascular conditions (representative of a healthy 25 year old).

Source: [273] under CC BY 4.0. Data are from the Pulse Wave Database [272]. The human outline is sourced from https://commons.wikimedia.org/wiki/File:Human_outline_generic.svg under CC0 1.0.

4.2. Simulating photoplethysmogram signals

The second step in synthesising a PPG signal is to concatenate a series of simulated pulse waves. Having simulated individual pulse waves, these can simply be concatenated by offsetting each pulse wave according to a reference set of IBIs. The resulting signal may need smoothing out at the joins of pulse waves to avoid discontinuities (such as by using cubic spline interpolation 0.05s either side of pulse onsets) [267]. Details are now provided on how different rhythms can be simulated, and how motion artefact and noise can be added.

4.2.1. Simulating different heart rhythms

The heart rhythm exhibited by a simulated PPG signal is determined by the reference set of IBIs used to construct the signal. Even in normal sinus rhythm, IBIs exhibit some natural variability. Consequently, one approach to simulate normal sinus rhythm is to use reference IBIs generated from a normal distribution with a specified mean and standard deviation [47]. More advanced techniques have been used to simulate ECG signals, which may have applications in this field [274].

Recently, there has been increased interest in simulating PPG signals containing irregular heart rhythms. PPG signals exhibiting atrial fibrillation (AF), extreme bradycardia and extreme ventricular tachycardia have been simulated using reference IBIs obtained from ECG signals recorded during AF [270], [271]. This was performed by simulating individual pulse waves based solely on IBIs and a template pulse wave shape. In addition, an approach to simulate PPG signals containing irregular beats has been proposed based on the modelling of individual pulse waves as the sum of Gaussians [47], [267]. Parameters were provided to construct PPG pulse waves as a sum of Gaussians in three types of irregular heartbeats [267]: (i) compensation beats: a short beat followed by a long beat, which together last the same duration as two normal beats; (ii) reset beats: a short beat followed by a long beat, which together last less than the duration of two normal beats; and (iii) interpolation beats: two beats which together last the duration of one normal beat. Synthetic PPG signals containing irregular heart rhythms may be particularly useful because of their potential utility for developing algorithms to detect AF from the PPG (see Section 3.6.3), and because arrhythmic PPG signals are not readily available in many public databases (although the IBIs required to simulate PPG signals can often be obtained from ECG recordings) [267].

4.2.2. Adding motion artefact and noise

PPG signals containing motion artefact and noise have been simulated by superimposing simulated noise or artefact on simulated PPG signals. Noise has been simulated at both low and high frequencies (such as ≤ 0.9 Hz and ≥ 50 Hz) as a sinusoid [47]. Motion artefact has simulated by filtering white noise using a filter designed based on the properties of PPG motion artefacts [270]. In addition, synthetic motion artefact has been created by subtracting a simulated clean PPG from the measured PPG, where artefacts were detected using a signal quality index (see Section 3.1.3), the clean PPG was simulated based on simultaneous RR intervals, and the measured PPG was high-pass filtered above 0.5 Hz [275].

5. CONCLUSION

Signal processing is a key step in using photoplethysmography to obtain physiological measurements. A wealth of research has been conducted into the development of PPG signal processing techniques, and the field is rapidly growing. A wide range of signal processing techniques have been used to analyse the PPG. These techniques have utilised different aspects of the signal, such as the pulse wave shape, inter-beat intervals, and low frequency variations. Signal processing techniques can be used to estimate several parameters, providing valuable insight into an individual's physiology.

The importance of PPG signal processing is increasing with the widespread use of photoplethysmography not only in clinical devices such as pulse oximeters, but also in consumer devices such as fitness trackers. PPG-based devices are now at a critical juncture: traditionally, they have been confined to use in clinical settings where measurements can be quality-controlled and interpreted by a clinician; in the future, they may be used by consumers in daily life, with measurements nonetheless being used to inform clinical decision making and lifestyle choices. This provides great incentive for further research into the field: PPG signal processing techniques could potentially be widely used with benefit to society. The field is highly accessible, aided by publicly available datasets, and minimal requirements of only a computer and open-source software in order to perform valuable research.

The evolving use of photoplethysmography presents several pressing directions for development of signal processing techniques. Signal processing techniques for consumer devices must be robust enough for unsupervised use in daily life. It is not yet clear whether signal processing techniques developed with clinical data, such as fingertip PPG signals acquired from stationary patients, can be translated to other settings such as wrist PPG signals acquired in daily life. The growing use of deep learning to develop pulse wave analysis algorithms provides opportunity to conduct hypothesis-free investigations where relevant PPG features are learnt from the data and extracted via neural networks, rather than pre-specified and extracted using pre-defined signal processing techniques. It is not yet clear whether one approach is superior, or whether a combination of approaches could be beneficial. There is a need to investigate how to reliably obtain pulse wave features from the PPG, considering the nature of recordings (duration and recording setting), signal quality assessment, and physiological variability. Finally, research should determine which physiological parameters can be estimated accurately enough to be useful in the intended setting. For instance, evidence is emerging for the utility of PPG-based smartwatches for detecting atrial fibrillation, whereas it is not yet clear whether respiratory rate can be accurately estimated from a wrist PPG signal in daily life.

Future research into PPG signal processing will be greatly aided by sharing research tools. Benchmark PPG datasets will greatly aid the development of signal processing algorithms, as has been the case in electrocardiogram (ECG) signal processing research [276]. Benchmark datasets should contain PPG signals alongside reference physiological measurements, and activity labels where appropriate. There is a role for benchmark datasets acquired in a range of settings, from hospital wards, to laboratory studies, to daily life. There is also benefit to acquiring both high-fidelity PPG signals using specialist recording equipment, as well as PPG signals representative of those measured by everyday devices. Benchmark PPG algorithms provide a foundation on which novel algorithms can be developed, and a standard against which novel algorithms can be compared. The sharing of datasets and code will enhance reproducibility, maintain the accessibility of the field, and aid translation of novel signal processing techniques into practice.

ACKNOWLEDGMENT

This work was supported by British Heart Foundation grant [FS/20/20/34626], and an EPSRC Impact Acceleration Award to PHC.

REFERENCES

- [1] J. Allen, "Photoplethysmography and its application in clinical physiological measurement," *Physiological Measurement*, vol. 28, no. 3, pp. R1–R39, 2007. <https://doi.org/10.1088/0967-3334/28/3/R01>
- [2] M. Shafique, P. A. Kyriacou, and S. K. Pal, "Investigation of photoplethysmographic signals and blood oxygen saturation values on healthy volunteers during cuff-induced hypoperfusion using a multimode PPG/SpO₂ sensor," *Medical and Biological Engineering and Computing*, vol. 50, no. 6, pp. 575–583, 2012. <https://doi.org/10.1007/s11517-012-0910-z>
- [3] K. Budidha and P. A. Kyriacou, "In vivo investigation of ear canal pulse oximetry during hypothermia," *Journal of Clinical Monitoring and Computing*, vol. 32, no. 1, pp. 97–107, 2018. <https://doi.org/10.1007/s10877-017-9975-4>
- [4] S. Chatterjee and P. A. Kyriacou, "Monte carlo analysis of optical interactions in reflectance and transmittance finger photoplethysmography," *Sensors*, vol. 19, no. 4, 2019. <https://doi.org/10.3390/s19040789>
- [5] S. Chatterjee, K. Budidha, and P. A. Kyriacou, "Investigating the origin of photoplethysmography using a multiwavelength Monte Carlo model," *Physiological Measurement*, vol. 41, no. 8, p. 084001, 2020. <https://doi.org/10.1088/1361-6579/aba008>
- [6] A. V. Moço, S. Stuijk, and G. De Haan, "New insights into the origin of remote PPG signals in visible light and infrared," *Scientific Reports*, vol. 8, no. 1, pp. 1–15, 2018. <https://doi.org/10.1038/s41598-018-26068-2>
- [7] A. A. Kamshilin and N. B. Margaryants, "Origin of photoplethysmographic waveform at green light," *Physics Procedia*, vol. 86, pp. 72–80, 2017. <https://doi.org/10.1016/j.phpro.2017.01.024>
- [8] P. Charlton, "Photoplethysmogram signal components.svg," 2021. https://commons.wikimedia.org/wiki/File:Photoplethysmogram_signal_components.svg
- [9] S. C. Millasseau *et al.*, "Noninvasive assessment of the digital volume pulse: comparison with the peripheral pressure pulse," *Hypertension*, vol. 36, no. 6, pp. 952–956, 2000. <https://doi.org/10.1161/01.HYP.36.6.952>
- [10] M. Elgendi, "On the analysis of fingertip photoplethysmogram signals," *Current Cardiology Reviews*, vol. 8, no. 1, pp. 14–25, 2012. <https://doi.org/10.2174/157340312801215782>
- [11] P. H. Charlton *et al.*, "Assessing mental stress from the photoplethysmogram: a numerical study," *Physiological Measurement*, vol. 39, no. 5, p. 054001, 2018. <https://doi.org/10.1088/1361-6579/aa6e6a>
- [12] C. El-Hajj and P. A. Kyriacou, "A review of machine learning techniques in photoplethysmography for the non-invasive cuff-less measurement of blood pressure," *Biomedical Signal Processing and Control*, vol. 58, p. 101870, 2020. <https://doi.org/10.1016/j.bspc.2020.101870>
- [13] S. C. Millasseau *et al.*, "Contour analysis of the photoplethysmographic pulse measured at the finger," *Journal of Hypertension*, vol. 24, no. 8, pp. 1449–1456, 2006. <https://doi.org/10.1097/01.hjh.0000239277.05068.87>
- [14] P. Charlton, "Photoplethysmogram (PPG) pulse wave.svg," 2021. [https://commons.wikimedia.org/wiki/File:Photoplethysmogram_\(PPG\)_pulse_wave.svg](https://commons.wikimedia.org/wiki/File:Photoplethysmogram_(PPG)_pulse_wave.svg)
- [15] T. R. Dawber, H. E. Thomas, and P. M. McNamara, "Characteristics of the dirotic notch of the arterial pulse wave in coronary heart disease," *Angiology*, vol. 24, no. 4, pp. 244–255, apr 1973. <https://doi.org/10.1177/000331977302400407>
- [16] P. H. Charlton, "Classes of photoplethysmogram (PPG) pulse wave shape.svg," 2021. [https://commons.wikimedia.org/wiki/File:Classes_of_photoplethysmogram_\(PPG\)_pulse_wave_shape.svg](https://commons.wikimedia.org/wiki/File:Classes_of_photoplethysmogram_(PPG)_pulse_wave_shape.svg)
- [17] M. Elgendi, *PPG signal analysis: An introduction using MATLAB*, 1st ed. CRC Press, 2020. <https://doi.org/10.1201/9780429449581>
- [18] J. G. Webster, Ed., *Design of Pulse Oximeters*. CRC Press, 1997. <https://doi.org/10.1201/9780367802592>
- [19] D. B. Wax, P. Rubin, and S. Neustein, "A comparison of transmittance and reflectance pulse oximetry during vascular surgery," *Anesthesia and Analgesia*, vol. 109, no. 6, pp. 1847–1849, 2009. <https://doi.org/10.1213/ANE.0b013e3181bbcc446>
- [20] Y. Sun and N. Thakor, "Photoplethysmography revisited: From contact to noncontact, from point to imaging," *IEEE Transactions on Biomedical Engineering*, vol. 63, no. 3, pp. 463–477, 2016. <https://doi.org/10.1109/TBME.2015.2476337>
- [21] A. Chandrasekhar *et al.*, "PPG Sensor Contact Pressure Should Be Taken Into Account for Cuff-Less Blood Pressure Measurement," *IEEE Transactions on Biomedical Engineering*, vol. 67, no. 11, pp. 3134–3140, 2020. <https://doi.org/10.1109/TBME.2020.2976989>
- [22] J. Allen, "Quantifying the delays between multi-site photoplethysmography pulse and electrocardiogram r-r interval changes under slow-paced breathing," *Frontiers in Physiology*, vol. 10, no. SEP, 2019. <https://doi.org/10.3389/fphys.2019.01190>
- [23] R. Mukkamala *et al.*, "Toward ubiquitous blood pressure monitoring via pulse transit time: theory and practice," *IEEE Transactions on Biomedical Engineering*, vol. 62, no. 8, pp. 1879–1901, 2015. <https://doi.org/10.1109/TBME.2015.2441951>
- [24] F. U. Mattace-Raso *et al.*, "Determinants of pulse wave velocity in healthy people and in the presence of cardiovascular risk factors: Establishing normal and reference values," *European Heart Journal*, vol. 31, no. 19, pp. 2338–2350, 2010.
- [25] F. Rundo *et al.*, "An advanced bio-inspired photoplethysmography (PPG) and ECG pattern recognition system for medical assessment," *Sensors*, vol. 18, no. 2, 2018. <https://doi.org/10.3390/s18020405>
- [26] A. Goshvarpour and A. Goshvarpour, "The potential of photoplethysmogram and galvanic skin response in emotion recognition using nonlinear features," *Australasian Physical and Engineering Sciences in Medicine*, vol. 43, no. 1, pp. 119–134, 2019. <https://doi.org/10.1007/s13246-019-00825-7>
- [27] M. Boloursaz Mashhadi *et al.*, "Heart rate tracking using wrist-type photoplethysmographic (PPG) signals during physical exercise with simultaneous accelerometry," *IEEE Signal Processing Letters*, vol. 23, no. 2, pp. 227–231, 2015. <https://doi.org/10.1109/lsp.2015.2509868>
- [28] A. J. Casson, A. Vazquez Galvez, and D. Jarchi, "Gyroscope vs. accelerometer measurements of motion from wrist PPG during physical exercise," *ICT Express*, vol. 2, no. 4, pp. 175–179, 2016. <https://doi.org/10.1016/j.ict.2016.11.003>
- [29] H. Lee, H. Chung, and J. Lee, "Motion artifact cancellation in wearable photoplethysmography using gyroscope," *IEEE Sensors Journal*, vol. 19, no. 3, pp. 1166–1175, 2019. <https://doi.org/10.1109/JSEN.2018.2879970>
- [30] C. Orphanidou, *Signal Quality Assessment in Physiological Monitoring*, 1st ed., ser. SpringerBriefs in Bioengineering. Cham: Springer International Publishing, 2018. <https://doi.org/10.1007/978-3-319-68415-4>

- [31] J. L. Semmlow and B. Griffel, *Biosignal and Medical Image Processing*, 3rd ed. CRC Press, 2014. <https://www.routledge.com/Biosignal-and-Medical-Image-Processing/Semmlow-Griffel/p/book/9781466567368>
- [32] Y. Liang *et al.*, “An optimal filter for short photoplethysmogram signals,” *Scientific Data*, vol. 5, pp. 1–12, 2018. <https://doi.org/10.1038/sdata.2018.76>
- [33] S. Huthart *et al.*, “Advancing PPG Signal Quality and Know-How Through Knowledge Translation From Experts to Student and Researcher,” *Frontiers in Digital Health*, vol. 2, p. 619692, 2020. <https://doi.org/10.3389/fgdh.2020.619692>
- [34] J. Allen and A. Murray, “Similarity in bilateral photoplethysmographic peripheral pulse wave characteristics at the ears, thumbs and toes,” *Physiological Measurement*, vol. 21, no. 3, pp. 369–377, 2000. <https://doi.org/10.1088/0967-3334/21/3/303>
- [35] J. Allen, “The measurement and analysis of multi-site photoplethysmographic pulse waveforms in health and arterial disease,” 2002.
- [36] W. Waugh *et al.*, “Novel Signal Noise Reduction Method through Cluster Analysis, Applied to Photoplethysmography,” *Computational and Mathematical Methods in Medicine*, vol. 2018, 2018. <https://doi.org/10.1155/2018/6812404>
- [37] B. S. Kim and S. K. Yoo, “Motion artifact reduction in photoplethysmography using independent component analysis,” *IEEE Transactions on Biomedical Engineering*, vol. 53, no. 3, pp. 566–568, 2006. <https://doi.org/10.1109/TBME.2005.869784>
- [38] S. M. Salehizadeh *et al.*, “Photoplethysmograph Signal Reconstruction based on a Novel Motion Artifact Detection-Reduction Approach. Part II: Motion and Noise Artifact Removal,” *Annals of Biomedical Engineering*, vol. 42, no. 11, pp. 2251–2263, 2014. <https://doi.org/10.1007/s10439-014-1030-8>
- [39] Z. Zhang, Z. Pi, and B. Liu, “TROIKA: A general framework for heart rate monitoring using wrist-type photoplethysmographic signals during intensive physical exercise,” *IEEE Transactions on Biomedical Engineering*, vol. 62, no. 2, pp. 522–531, 2015. <https://doi.org/10.1109/TBME.2014.2359372>
- [40] H. W. Lee *et al.*, “The periodic moving average filter for removing motion artifacts from PPG signals,” pp. 701–706, 2007.
- [41] P. Mullan *et al.*, “Unobtrusive heart rate estimation during physical exercise using photoplethysmographic and acceleration data,” in *Proc. IEEE EMBS*. IEEE, 2015, pp. 6114–6117. <https://doi.org/10.1109/EMBC.2015.7319787>
- [42] F. Peng, H. Liu, and W. Wang, “A comb filter based signal processing method to effectively reduce motion artifacts from photoplethysmographic signals,” *Physiological Measurement*, vol. 36, no. 10, pp. 2159–2170, 2015. <https://doi.org/10.1088/0967-3334/36/10/2159>
- [43] H. Han and J. Kim, “Artifacts in wearable photoplethysmographs during daily life motions and their reduction with least mean square based active noise cancellation method,” *Computers in Biology and Medicine*, vol. 42, no. 4, pp. 387–393, 2012. <https://doi.org/10.1016/j.combiomed.2011.12.005>
- [44] R. W. Wijshoff, M. Mischi, and R. M. Aarts, “Reduction of periodic motion artifacts in photoplethysmography,” *IEEE Transactions on Biomedical Engineering*, vol. 64, no. 1, pp. 196–207, 2017. <https://doi.org/10.1109/TBME.2016.2553060>
- [45] D. Jarchi and A. Casson, “Description of a database containing wrist PPG signals recorded during physical exercise with both accelerometer and gyroscope measures of motion,” *Data*, vol. 2, no. 1, p. 1, 2016. <https://doi.org/10.3390/data2010001>
- [46] P. H. Charlton *et al.*, “Acquiring wearable photoplethysmography data in daily life: The PPG Diary Pilot Study,” *Engineering Proceedings*, vol. 2, no. 1, p. 80, 2020. <https://doi.org/10.3390/ecsa-7-08233>
- [47] Q. Tang *et al.*, “Synthetic photoplethysmogram generation using two Gaussian functions,” *Scientific Reports*, vol. 10, no. 1, pp. 1–10, 2020. <https://doi.org/10.1038/s41598-020-69076-x>
- [48] Q. Li and G. D. Clifford, “Dynamic time warping and machine learning for signal quality assessment of pulsatile signals,” *Physiological Measurement*, vol. 33, no. 9, pp. 1491–501, 2012. <https://doi.org/10.1088/0967-3334/33/9/1491>
- [49] C. Fischer *et al.*, “An algorithm for real-time pulse waveform segmentation and artifact detection in photoplethysmograms,” *IEEE Journal of Biomedical and Health Informatics*, vol. 21, no. 2, pp. 372–381, 2017. <https://doi.org/10.1109/JBHI.2016.2518202>
- [50] J. A. Sukor, S. J. Redmond, and N. H. Lovell, “Signal quality measures for pulse oximetry through waveform morphology analysis,” *Physiological measurement*, vol. 32, no. 3, pp. 369–384, 2011. <https://doi.org/10.1088/0967-3334/32/3/008>
- [51] M. Elgendi, “Optimal signal quality index for photoplethysmogram signals,” *Bioengineering*, vol. 3, no. 4, pp. 1–15, 2016. <https://doi.org/10.3390/bioengineering3040021>
- [52] C. Orphanidou *et al.*, “Signal-quality indices for the electrocardiogram and photoplethysmogram: derivation and applications to wireless monitoring,” *IEEE Journal of Biomedical and Health Informatics*, vol. 19, no. 3, pp. 832–8, 2015. <https://doi.org/10.1109/JBHI.2014.2338351>
- [53] N. Selvaraj *et al.*, “Statistical approach for the detection of motion/noise artifacts in Photoplethysmogram,” in *Proc IEEE EMBS*. IEEE, 2011, pp. 4972–4975. <https://doi.org/10.1109/IEMBS.2011.6091232>
- [54] Xuxue Sun, Ping Yang, and Yuan-Ting Zhang, “Assessment of photoplethysmogram signal quality using morphology integrated with temporal information approach,” in *Proc. IEEE EMBS*, vol. 2012. IEEE, 2012, pp. 3456–3459. <https://doi.org/10.1109/EMBC.2012.6346709>
- [55] S. Vadrevu and M. Sabarimalai Manikandan, “Real-Time PPG Signal Quality Assessment System for Improving Battery Life and False Alarms,” *IEEE Transactions on Circuits and Systems II: Express Briefs*, vol. 66, no. 11, pp. 1910–1914, 2019. <https://doi.org/10.1109/TCSII.2019.2891636>
- [56] W. Karlen *et al.*, “Photoplethysmogram signal quality estimation using repeated Gaussian filters and cross-correlation,” *Physiological Measurement*, vol. 33, no. 10, pp. 1617–1629, 2012. <https://doi.org/10.1088/0967-3334/33/10/1617>
- [57] R. Krishnan, B. Natarajan, and S. Warren, “Motion artifact reduction in photoplethysmography using magnitude-based frequency domain independent component analysis,” *Proceedings - International Conference on Computer Communications and Networks, ICCCN*, pp. 309–313, 2008. <https://doi.org/10.1109/ICCCN.2008.ECP.71>
- [58] E. Mejía-Mejía *et al.*, “Heart Rate Variability (HRV) and Pulse Rate Variability (PRV) for the Assessment of Autonomic Responses,” *Frontiers in Physiology*, vol. 11, p. 779, 2020. <https://doi.org/10.3389/fphys.2020.00779>
- [59] T. Pereira *et al.*, “A Supervised Approach to Robust Photoplethysmography Quality Assessment,” *IEEE Journal of Biomedical and Health Informatics*, vol. 24, no. 3, pp. 649–657, 2020. <https://doi.org/10.1109/JBHI.2019.2909065>
- [60] T. Pereira *et al.*, “Deep learning approaches for plethysmography signal quality assessment in the presence of atrial fibrillation,”

- Physiological Measurement*, vol. 40, no. 12, 2019. <https://doi.org/10.1088/1361-6579/ab5b84>
- [61] K. Takazawa *et al.*, “Assessment of vasoactive agents and vascular aging by the second derivative of photoplethysmogram waveform,” *Hypertension*, vol. 32, no. 2, pp. 365–370, 1998. <https://doi.org/10.1161/01.HYP.32.2.365>
- [62] M. Elgendi *et al.*, “Detection of a and b waves in the acceleration photoplethysmogram,” *BioMedical Engineering OnLine*, vol. 13, no. 1, p. 139, 2014. <https://doi.org/10.1186/1475-925X-13-139>
- [63] M. Elgendi, “C, E and D Waves Detection in the Acceleration Photoplethysmogram,” *Computer Methods and Programs in Biomedicine*, vol. 117, no. 2, pp. 125–136, 2014. <https://doi.org/10.1016/j.cmpb.2014.08.001>
- [64] A. Savitzky and M. Golay, “Smoothing and differentiation of data by simplified least squares procedures,” *Analytical Chemistry*, vol. 36, no. 8, pp. 1627–1639, 1964. <https://doi.org/10.1021/ac60214a047>
- [65] P. A. Gorry, “General Least-Squares Smoothing and Differentiation by the Convolution (Savitzky-Golay) Method,” *Analytical Chemistry*, vol. 62, no. 6, pp. 570–573, 1990. <https://doi.org/10.1021/ac00205a007>
- [66] N. E. Huang *et al.*, “The empirical mode decomposition and the Hubert spectrum for nonlinear and non-stationary time series analysis,” *Proceedings of the Royal Society A: Mathematical, Physical and Engineering Sciences*, vol. 454, no. 1971, pp. 903–995, 1998. <https://doi.org/10.1098/rspa.1998.0193>
- [67] A. Garde *et al.*, “Empirical mode decomposition for respiratory and heart rate estimation from the photoplethysmogram,” in *Proc. CinC*. Zaragoza: IEEE, 2013, pp. 799–802. <https://ieeexplore.ieee.org/document/6713498>
- [68] G. Rilling, P. Flandrin, and P. Goncalves, “On empirical mode decomposition and its algorithms,” in *IEEE-EURASIP workshop on nonlinear signal and image processing*, vol. 3, 2003, pp. 8–11.
- [69] A. Stallone, A. Cicone, and M. Materassi, “New insights and best practices for the successful use of Empirical Mode Decomposition, Iterative Filtering and derived algorithms,” *Scientific Reports*, vol. 10, no. 1, pp. 1–15, 2020. <https://doi.org/10.1038/s41598-020-72193-2>
- [70] Y. Zhang, B. Liu, and Z. Zhang, “Combining ensemble empirical mode decomposition with spectrum subtraction technique for heart rate monitoring using wrist-type photoplethysmography,” *Biomedical Signal Processing and Control*, vol. 21, pp. 119–125, 2015. <https://doi.org/10.1016/j.bspc.2015.05.006>
- [71] B. Roy *et al.*, “I-PREXT: Photoplethysmography Derived Respiration Signal Extraction and Respiratory Rate Tracking Using Neural Networks,” *IEEE Transactions on Instrumentation and Measurement*, vol. 70, 2021. <https://doi.org/10.1109/TIM.2020.3043506>
- [72] S. Hadiyoso, E. M. Dewi, and I. Wijayanto, “Comparison of EMD, VMD and EEMD Methods in Respiration Wave Extraction Based on PPG Waves,” *Journal of Physics: Conference Series*, vol. 1577, no. 1, 2020. <https://doi.org/10.1088/1742-6596/1577/1/012040>
- [73] H. Sharma, “Extraction of respiratory rate from PPG using ensemble empirical mode decomposition with Kalman filter,” *Electronics Letters*, vol. 56, no. 13, pp. 650–653, 2020. <https://doi.org/10.1049/el.2020.0566>
- [74] M. A. Motin, C. K. Karmakar, and M. Palaniswami, “Selection of empirical mode decomposition techniques for extracting breathing rate from PPG,” *IEEE Signal Processing Letters*, vol. 26, no. 4, pp. 592–596, 2019. <https://doi.org/10.1109/LSP.2019.2900923>
- [75] M. A. Motin, C. K. Karmakar, and M. Palaniswami, “Ensemble empirical mode decomposition with principal component analysis: a novel approach for extracting respiratory rate and heart rate from photoplethysmographic signal,” *IEEE Journal of Biomedical and Health Informatics*, vol. 22, no. 3, pp. 766–774, 2018. <https://doi.org/10.1109/JBHI.2017.2679108>
- [76] R. N. Yin *et al.*, “Heart rate estimation based on face video under unstable illumination,” *Applied Intelligence*, 2021. <https://doi.org/10.1007/s10489-020-02167-4>
- [77] Y. Zhang *et al.*, “Illumination variation-resistant video-based heart rate monitoring using LAB color space,” *Optics and Lasers in Engineering*, vol. 136, p. 106328, 2021. <https://doi.org/10.1016/j.optlaseng.2020.106328>
- [78] R. Lei *et al.*, “Estimation of heart rate and respiratory rate from ppg signal using complementary ensemble empirical mode decomposition with both independent component analysis and non-negative matrix factorization,” *Sensors*, vol. 20, no. 11, pp. 1–13, 2020. <https://doi.org/10.3390/s20113238>
- [79] M. Pittara and C. Orphanidou, “Robust Estimation of Pulse Rate from a Wrist-type PPG During Intensive Exercise,” in *Proc IEEE EMBS*, 2018, pp. 5515–5518. <https://doi.org/10.1109/EMBC.2018.8513584>
- [80] B. Roy and R. Gupta, “MoDTRAP: Improved heart rate tracking and preprocessing of motion-corrupted photoplethysmographic data for personalized healthcare,” *Biomedical Signal Processing and Control*, vol. 56, p. 101676, 2020. <https://doi.org/10.1016/j.bspc.2019.101676>
- [81] G. Liu *et al.*, “SVR-EEMD: An Improved EEMD Method Based on Support Vector Regression Extension in PPG Signal Denoising,” *Computational and Mathematical Methods in Medicine*, vol. 2019, pp. 1–10, 2019. <https://doi.org/10.1155/2019/5363712>
- [82] Y. Zha *et al.*, “Non-invasive assessment of cerebral hemodynamics with CWNIRS-ICG and application of EEMD-SSE in PPG signal extraction,” *Optik*, vol. 156, pp. 22–30, 2018. <https://doi.org/10.1016/j.ijleo.2017.10.116>
- [83] J. Song *et al.*, “A robust dynamic heart-rate detection algorithm framework during intense physical activities using photoplethysmographic signals,” *Sensors*, vol. 17, no. 11, 2017. <https://doi.org/10.3390/s17112450>
- [84] M. U. Khan *et al.*, “Expert Hypertension Detection System Featuring Pulse Plethysmograph Signals and Hybrid Feature Selection and Reduction Scheme,” *Sensors*, vol. 21, no. 1, p. 247, 2021. <https://doi.org/10.3390/s21010247>
- [85] X. Sun *et al.*, “Blood pressure evaluation based on photoplethysmography using deep learning,” in *Proc AOPC*, Y. Wang *et al.*, Eds. SPIE, 2020, p. 45. <https://doi.org/10.1117/12.2576841>
- [86] H. C. Wei *et al.*, “Digital volume pulse measured at the fingertip as an indicator of diabetic peripheral neuropathy in the aged and diabetic,” *Entropy*, vol. 21, no. 12, 2019. <https://doi.org/10.3390/e21121229>
- [87] L. M. B. Alonzo and H. S. Co, “Ensemble Empirical Mode Decomposition of Photoplethysmogram Signals for Assessment of Ventricular Fibrillation,” in *2018 IEEE 10th International Conference on Humanoid, Nanotechnology, Information Technology, Communication and Control, Environment and Management (HNICEM)*. IEEE, 2018, pp. 1–4. <https://doi.org/10.1109/HNICEM.2018.8666241>
- [88] H.-C. Wei *et al.*, “Instantaneous frequency from Hilbert-Huang transformation of digital volume pulse as indicator of diabetes and arterial stiffness in upper-middle-aged subjects,” *Scientific Reports*, vol. 8, no. 1, p. 15771, 2018. <https://doi.org/10.1038/s41598-018-34091-6>

- [89] Ching-Shuen Chen *et al.*, “Ensemble Empirical Mode Decomposition for atherosclerosis in high-risk subjects,” in *2011 8th International Conference on Information, Communications and Signal Processing*. IEEE, 2011, pp. 1–4. <https://doi.org/10.1109/ICICS.2011.6173567>
- [90] H. T. Wu *et al.*, “Arterial waveforms measured at the wrist as indicators of diabetic endothelial dysfunction in the elderly,” *IEEE Transactions on Instrumentation and Measurement*, vol. 61, no. 1, pp. 162–169, 2012. <https://doi.org/10.1109/TIM.2011.2159416>
- [91] W. B. Murray and P. A. Foster, “The peripheral pulse wave: Information overlooked,” *Journal of Clinical Monitoring*, vol. 12, no. 5, pp. 365–377, 1996. <https://doi.org/10.1007/BF02077634>
- [92] E. J. Argüello Prada and R. D. Serna Maldonado, “A novel and low-complexity peak detection algorithm for heart rate estimation from low-amplitude photoplethysmographic (PPG) signals,” *Journal of Medical Engineering and Technology*, vol. 42, no. 8, pp. 569–577, 2018. <https://doi.org/10.1080/03091902.2019.1572237>
- [93] P. van Gent *et al.*, “HeartPy: A novel heart rate algorithm for the analysis of noisy signals,” *Transportation Research Part F: Traffic Psychology and Behaviour*, vol. 66, pp. 368–378, 2019. <https://doi.org/10.1016/j.trf.2019.09.015>
- [94] M. Aboy *et al.*, “An automatic beat detection algorithm for pressure signals,” *IEEE Transactions on Biomedical Engineering*, vol. 52, no. 10, pp. 1662–1670, 2005. <https://doi.org/10.1109/TBME.2005.855725>
- [95] S. Vadrevu and M. Sabarimalai Manikandan, “A robust pulse onset and peak detection method for automated PPG signal analysis system,” *IEEE Transactions on Instrumentation and Measurement*, vol. 68, no. 3, pp. 807–817, 2019. <https://doi.org/10.1109/TIM.2018.2857878>
- [96] M. Elgendi *et al.*, “Systolic peak detection in acceleration photoplethysmograms measured from emergency responders in tropical conditions,” *PLoS ONE*, vol. 8, no. 10, pp. 1–11, 2013. <https://doi.org/10.1371/journal.pone.0076585>
- [97] E. Billauer, “peakdet: Peak detection using MATLAB,” 2012. <http://billauer.co.il/peakdet.html>
- [98] B. N. Li, M. C. Dong, and M. I. Vai, “On an automatic delineator for arterial blood pressure waveforms,” *Biomedical Signal Processing and Control*, vol. 5, no. 1, pp. 76–81, 2010. <https://doi.org/10.1016/j.bspc.2009.06.002>
- [99] W. Zong *et al.*, “An open-source algorithm to detect onset of arterial blood pressure pulses,” in *Proc CinC*. IEEE, 2003, pp. 259–62. <https://doi.org/10.1109/CIC.2003.1291140>
- [100] N. J. Conn and D. A. Borkholder, “Wavelet based photoplethysmogram foot delineation for heart rate variability applications,” in *IEEE Signal Processing in Medicine and Biology Symposium*. IEEE, 2013. <https://doi.org/10.1109/SPMB.2013.6736782>
- [101] M. Singla, S. Azeemuddin, and P. Sistla, “Accurate Fiducial Point Detection Using Haar Wavelet for Beat-by-Beat Blood Pressure Estimation,” *IEEE Journal of Translational Engineering in Health and Medicine*, vol. 8, p. 1900711, 2020. <https://doi.org/10.1109/JTEHM.2020.3000327>
- [102] S. M. Bishop and A. Ercole, “Multi-scale peak and trough detection optimised for periodic and quasi-periodic neuroscience data,” in *Intracranial Pressure and Neuromonitoring XVI. Acta Neurochirurgica Supplement*, T. Heldt, Ed. Springer, 2018, vol. 126, pp. 189–195. https://doi.org/10.1007/978-3-319-65798-1_39
- [103] P. H. Charlton, “Photoplethysmogram (PPG) pulse wave indices.svg,” 2021. [https://commons.wikimedia.org/wiki/File:Photoplethysmogram_\(PPG\)_pulse_wave_indices.svg](https://commons.wikimedia.org/wiki/File:Photoplethysmogram_(PPG)_pulse_wave_indices.svg)
- [104] M. Elgendi, “Detection of c, d, and e waves in the acceleration photoplethysmogram,” *Computer Methods and Programs in Biomedicine*, vol. 117, no. 2, pp. 125–136, 2014. <https://doi.org/10.1016/j.cmpb.2014.08.001>
- [105] H. F. Posada-Quintero *et al.*, “Evaluation of pulse rate variability obtained by the pulse onsets of the photoplethysmographic signal,” *Physiological Measurement*, vol. 34, no. 2, pp. 179–87, feb 2013. <https://doi.org/10.1088/0967-3334/34/2/179>
- [106] M. C. Hemon and J. P. Phillips, “Comparison of foot finding methods for deriving instantaneous pulse rates from photoplethysmographic signals,” *Journal of Clinical Monitoring and Computing*, vol. 30, no. 2, pp. 157–168, 2016. <https://doi.org/10.1007/s10877-015-9695-6>
- [107] H. J. Baek *et al.*, “Reliability of the Parabola Approximation Method in Heart Rate Variability Analysis Using Low-Sampling-Rate Photoplethysmography,” *Journal of Medical Systems*, vol. 41, no. 12, 2017. <https://doi.org/10.1007/s10916-017-0842-0>
- [108] S. Millasseau *et al.*, “Determination of age-related increases in large artery stiffness by digital pulse contour analysis,” *Clinical Science*, vol. 103, no. 4, pp. 371–377, 2002. <https://doi.org/10.1042/cs1030371>
- [109] P. J. Chowieczyk *et al.*, “Photoplethysmographic assessment of pulse wave reflection: Blunted response to endothelium-dependent beta2-adrenergic vasodilation in type II diabetes mellitus,” *Journal of the American College of Cardiology*, vol. 34, no. 7, pp. 2007–2014, 1999. [https://doi.org/10.1016/S0735-1097\(99\)00441-6](https://doi.org/10.1016/S0735-1097(99)00441-6)
- [110] S. Alty *et al.*, “Cardiovascular disease prediction using support vector machines,” in *2003 46th Midwest Symposium on Circuits and Systems*. IEEE, 2003, pp. 376–379. <https://doi.org/10.1109/MWSCAS.2003.1562297>
- [111] Y. Kurylyak, F. Lamonaca, and D. Grimaldi, “A Neural Network-based method for continuous blood pressure estimation from a PPG signal,” in *Conference Record - IEEE Instrumentation and Measurement Technology Conference*. IEEE, 2013, pp. 280–283. <https://doi.org/10.1109/I2MTC.2013.6555424>
- [112] J. M. Ahn, “New aging index using signal features of both photoplethysmograms and acceleration plethysmograms,” *Healthcare Informatics Research*, vol. 23, no. 1, pp. 53–59, 2017. <https://doi.org/10.4258/hir.2017.23.1.53>
- [113] M. Peltokangas *et al.*, “Parameters extracted from arterial pulse waves as markers of atherosclerotic changes: performance and repeatability,” *IEEE Journal of Biomedical and Health Informatics*, vol. 22, no. 3, pp. 750–757, 2018. <https://doi.org/10.1109/JBHI.2017.2679904>
- [114] M. Lueken *et al.*, “Photoplethysmography-based in-ear sensor system for identification of increased stress arousal in everyday life,” *2017 IEEE 14th International Conference on Wearable and Implantable Body Sensor Networks, BSN 2017*, pp. 83–86, 2017.
- [115] C. P. Chua and C. Heneghan, “Continuous blood pressure monitoring using ECG and finger photoplethysmogram,” in *Proc IEEE EMBS*. IEEE, 2006, pp. 5117–5120. <https://doi.org/10.1109/IEMBS.2006.259612>
- [116] L. Wang *et al.*, “Noninvasive cardiac output estimation using a novel photoplethysmogram index,” in *Proc IEEE EMBS*, vol. 2009, 2009, pp. 1746–1749. <https://doi.org/10.1109/IEMBS.2009.5333091>
- [117] H. J. Baek *et al.*, “Second derivative of photoplethysmography for estimating vascular aging,” in *Proc. ITAB*. IEEE, 2007, pp. 70–72. <https://doi.org/10.1109/ITAB.2007.4407346>
- [118] T. Ushiroyama *et al.*, “Assessment of chilly sensation in Japanese women with laser Doppler fluxmetry and acceleration plethysmogram

- with respect to peripheral circulation,” *Bull. Osaka Med. Coll.*, vol. 51, pp. 76–84, 2005. <http://ci.nii.ac.jp/naid/80017503095/en/>
- [119] C. C. Wei, “Developing an effective arterial stiffness monitoring system using the spring constant method and photoplethysmography,” *IEEE Transactions on Biomedical Engineering*, vol. 60, no. 1, pp. 151–154, 2013. <https://doi.org/10.1109/TBME.2012.2207384>
- [120] A. A. Awad *et al.*, “The relationship between the photoplethysmographic waveform and systemic vascular resistance,” *Journal of Clinical Monitoring and Computing*, vol. 21, no. 6, pp. 365–372, 2007. <https://doi.org/10.1007/s10877-007-9097-5>
- [121] S. Alty *et al.*, “Predicting arterial stiffness from the digital volume pulse waveform,” *IEEE Transactions on Biomedical Engineering*, vol. 54, no. 12, pp. 2268–2275, 2007. <https://doi.org/10.1109/TBME.2007.897805>
- [122] X. F. Teng and Y. T. Zhang, “Continuous and Noninvasive Estimation of Arterial Blood Pressure Using a Photoplethysmographic Approach,” in *Proc IEEE EMBS*, 2003, pp. 3153–3156. <https://doi.org/10.1109/iembs.2003.1280811>
- [123] M. Liu, L.-M. Po, and H. Fu, “Cuffless Blood Pressure Estimation Based on Photoplethysmography Signal and Its Second Derivative,” *International Journal of Computer Theory and Engineering*, vol. 9, no. 3, pp. 202–206, 2017. <https://doi.org/10.7763/IJCTE.2017.V9.I138>
- [124] J. Padilla *et al.*, “Assessment of relationships between blood pressure, pulse wave velocity and digital volume pulse,” in *Proc CinC.*, 2006, pp. 893–896. <https://ieeexplore.ieee.org/document/4511996>
- [125] J. Simek *et al.*, “Second derivative of the finger arterial pressure waveform: an insight into dynamics of the peripheral arterial pressure pulse,” *Physiological Research*, vol. 54, no. 5, pp. 505–513, 2005. <https://pubmed.ncbi.nlm.nih.gov/15641931/>
- [126] I. Imanaga *et al.*, “Correlation between Wave Components of the Second Derivative of Plethysmogram and Arterial Distensibility,” *Japanese Heart Journal*, vol. 39, no. 6, pp. 775–784, 1998. <https://doi.org/10.1536/ihj.39.775>
- [127] S. Kontaxis *et al.*, “Photoplethysmographic Waveform Analysis for Autonomic Reactivity Assessment in Depression,” *IEEE Transactions on Biomedical Engineering*, vol. 68, no. 4, pp. 1273–1281, 2021. <https://doi.org/10.1109/TBME.2020.3025908>
- [128] S. Banerjee *et al.*, “A two step Gaussian modelling to assess ppg morphological variability induced by psychological stress,” in *Proc CinC.*, vol. 44, 2017. <https://doi.org/10.22489/CinC.2017.270-035>
- [129] J. Lazaro *et al.*, “Respiratory Rate Derived from Pulse Photoplethysmographic Signal by Pulse Decomposition Analysis,” in *Proc IEEE EMBS*. IEEE, 2018, pp. 5282–5285. <https://doi.org/10.1109/EMBC.2018.8513188>
- [130] J. Lázaro *et al.*, “Baroreflex sensitivity measured by pulse photoplethysmography,” *Frontiers in Neuroscience*, vol. 13, p. 339, 2019. <https://doi.org/10.3389/fnins.2019.00339>
- [131] J. Allen *et al.*, “Age-related changes in pulse risetime measured by multi-site photoplethysmography,” *Physiological Measurement*, vol. 41, no. 7, 2020. <https://doi.org/10.1088/1361-6579/ab9b67>
- [132] J. Allen and A. Murray, “Variability of photoplethysmography peripheral pulse measurements at the ears, thumbs and toes,” *IEE Proceedings - Science, Measurement and Technology*, vol. 147, no. 6, pp. 403–407, 2000. <https://doi.org/10.1049/ip-smt:20000846>
- [133] J. Allen and A. Murray, “Age-related changes in peripheral pulse timing characteristics at the ears, fingers and toes,” *Journal of Human Hypertension*, vol. 16, no. 10, pp. 711–717, 2002. <https://doi.org/10.1038/sj.jhh.1001478>
- [134] C. Orphanidou, “Quality assessment for the photoplethysmogram (PPG),” in *Signal quality assessment in physiological monitoring*. Cham: Springer, 2018, pp. 41–63. https://doi.org/10.1007/978-3-319-68415-4_3
- [135] R. Insall, “Pulse transit time measurements in peripheral vascular disease: a comparison of different pulse waveform features,” 1991.
- [136] J. Mateo and P. Laguna, “Analysis of heart rate variability in the presence of ectopic beats using the heart timing signal,” *IEEE Transactions on Biomedical Engineering*, vol. 50, no. 3, pp. 334–43, 2003. <https://doi.org/10.1109/TBME.2003.808831>
- [137] Task Force of the European Society of Cardiology and the North American Society of Pacing and Electrophysiology, “Heart Rate Variability,” *Circulation*, vol. 93, no. 5, pp. 1043–1065, 1996. <https://doi.org/10.1161/01.CIR.93.5.1043>
- [138] E. Gil *et al.*, “Photoplethysmography pulse rate variability as a surrogate measurement of heart rate variability during non-stationary conditions,” *Physiological Measurement*, vol. 31, no. 9, pp. 1271–1290, sep 2010. <https://doi.org/10.1088/0967-3334/31/9/015>
- [139] P. H. Charlton *et al.*, “An assessment of algorithms to estimate respiratory rate from the electrocardiogram and photoplethysmogram,” *Physiological Measurement*, vol. 37, no. 4, pp. 610–26, 2016. <https://doi.org/10.1088/0967-3334/37/4/610>
- [140] Y.-j. Wang *et al.*, “Estimation of blood pressure in the radial artery using strain-based pulse wave and photoplethysmography sensors,” *Micromachines*, vol. 9, no. 11, p. 556, 2018. <https://doi.org/10.3390/mi9110556>
- [141] H. Obeid *et al.*, “Evaluation of arterial stiffness by finger-toe pulse wave velocity: Optimization of signal processing and clinical validation,” *Journal of Hypertension*, vol. 35, no. 8, pp. 1618–1625, 2017. <https://doi.org/10.1097/HJH.0000000000001371>
- [142] K. Welykholowa *et al.*, “Multimodal photoplethysmography-based approaches for improved detection of hypertension,” *Journal of Clinical Medicine*, vol. 9, no. 4, p. 1203, 2020. <https://doi.org/10.3390/jcm9041203>
- [143] J. Balmer *et al.*, “Pre-ejection period, the reason why the electrocardiogram Q-wave is an unreliable indicator of pulse wave initialization,” *Physiological Measurement*, vol. 39, no. 9, p. 095005, 2018. <https://doi.org/10.1088/1361-6579/aada72>
- [144] M. Gao, N. B. Olivier, and R. Mukkamala, “Comparison of noninvasive pulse transit time estimates as markers of blood pressure using invasive pulse transit time measurements as a reference,” *Physiological Reports*, vol. 4, no. 10, pp. 1–7, 2016. <https://doi.org/10.14814/phy2.12768>
- [145] J. Allen *et al.*, “A prospective comparison of bilateral photoplethysmography versus the ankle-brachial pressure index for detecting and quantifying lower limb peripheral arterial disease,” *Journal of Vascular Surgery*, vol. 47, no. 4, pp. 794–802, 2008. <https://doi.org/10.1016/j.jvs.2007.11.057>
- [146] M. Bentham, G. Stansby, and J. Allen, “Innovative Multi-Site Photoplethysmography Analysis for Quantifying Pulse Amplitude and Timing Variability Characteristics in Peripheral Arterial Disease,” *Diseases*, vol. 6, no. 3, p. 81, 2018. <https://doi.org/10.3390/diseases6030081>
- [147] A. Buchs *et al.*, “Right-left correlation of the sympathetically induced fluctuations of photoplethysmographic signal in diabetic and non-diabetic subjects,” *Medical and Biological Engineering and Computing*, vol. 43, no. 2, pp. 252–7, 2005. <https://doi.org/10.1007/BF02345963>
- [148] N. D. McKay *et al.*, “Novel photoplethysmography cardiovascular assessments in patients with Raynaud’s phenomenon and systemic sclerosis: A pilot study,” *Rheumatology (United Kingdom)*, vol. 53, no. 10, pp. 1855–1863, 2014.

- <https://doi.org/10.1093/rheumatology/keu196>
- [149] M. J. Drinnan, J. Allen, and A. Murray, "Relation between heart rate and pulse transit time during paced respiration," *Physiological Measurement*, vol. 22, no. 3, pp. 425–432, 2001. <https://doi.org/10.1088/0967-3334/22/3/301>
- [150] M. Elgendi *et al.*, "Frequency analysis of photoplethysmogram and its derivatives," *Computer Methods and Programs in Biomedicine*, vol. 122, no. 3, pp. 503–512, 2015. <https://doi.org/10.1016/j.cmpb.2015.09.021>
- [151] K. Budidha and P. A. Kyriacou, "Photoplethysmography for quantitative assessment of sympathetic nerve activity (SNA) during cold stress," *Frontiers in Physiology*, vol. 10, no. JAN, pp. 1–10, 2019. <https://doi.org/10.3389/fphys.2018.01863>
- [152] J. Allen *et al.*, "Characterization of the Korotkoff sounds using joint time-frequency analysis," *Physiological Measurement*, vol. 25, no. 1, pp. 107–117, 2004. <https://doi.org/10.1088/0967-3334/25/1/010>
- [153] M. Misiti, G. Oppenheim, and J.-M. Poggi, "Get Started with Wavelet Toolbox," 2021. <https://www.mathworks.com/help/wavelet/getting-started-with-wavelet-toolbox.html>
- [154] R. Banerjee *et al.*, "Identifying coronary artery disease from photoplethysmogram," in *UbiComp 2016 Adjunct - Proceedings of the 2016 ACM International Joint Conference on Pervasive and Ubiquitous Computing*, 2016, pp. 1084–1088. <https://doi.org/10.1145/2968219.2972712>
- [155] N. Paradkar and S. Roy Chowdhury, "Coronary artery disease detection using photoplethysmography," in *Proc IEEE EMBS*. IEEE, 2017, pp. 100–103. <https://doi.org/10.1109/EMBC.2017.8036772>
- [156] R. Banerjee, S. Bhattacharya, and S. Alam, "Time series and morphological feature extraction for classifying coronary artery disease from photoplethysmogram," in *Proc IEEE ICASSP*. IEEE, 2018, pp. 950–954. <https://doi.org/10.1109/ICASSP.2018.8462604>
- [157] F. Fathieh *et al.*, "Predicting cardiac disease from interactions of simultaneously-acquired hemodynamic and cardiac signals," *Computer Methods and Programs in Biomedicine*, vol. 202, p. 105970, 2021. <https://doi.org/10.1016/j.cmpb.2021.105970>
- [158] S. P. Shashikumar *et al.*, "A deep learning approach to monitoring and detecting atrial fibrillation using wearable technology," in *2017 IEEE EMBS International Conference on Biomedical and Health Informatics, BHI 2017*. IEEE, 2017, pp. 141–144. <https://doi.org/10.1109/BHI.2017.7897225>
- [159] T. Schack *et al.*, "Computationally efficient algorithm for photoplethysmography-based atrial fibrillation detection using smartphones," in *Proc IEEE EMBS*, 2017, pp. 104–108. <https://doi.org/10.1109/EMBC.2017.8036773>
- [160] V. D. Corino *et al.*, "Detection of atrial fibrillation episodes using a wristband device," *Physiological Measurement*, vol. 38, no. 5, pp. 787–799, 2017. <https://doi.org/10.1088/1361-6579/aa5dd7>
- [161] I. Gotlibovych *et al.*, "End-to-end Deep Learning from Raw Sensor Data: Atrial Fibrillation Detection using Wearables," *arXiv preprint*, p. arXiv:1807.10707, 2018. <http://arxiv.org/abs/1807.10707>
- [162] S. Fallet *et al.*, "Can one detect atrial fibrillation using a wrist-type photoplethysmographic device?" *Medical and Biological Engineering and Computing*, vol. 57, no. 2, pp. 477–487, 2019. <https://doi.org/10.1007/s11517-018-1886-0>
- [163] S. Kwon *et al.*, "Deep Learning Approaches to Detect Atrial Fibrillation Using Photoplethysmographic Signals: Algorithms Development Study," *JMIR mHealth and uHealth*, vol. 7, no. 6, p. e12770, 2019. <https://doi.org/10.2196/12770>
- [164] X. Xing and M. Sun, "Optical blood pressure estimation with photoplethysmography and FFT-based neural networks," *Biomedical Optics Express*, vol. 7, no. 8, p. 3007, 2016. <https://doi.org/10.1364/BOE.7.003007>
- [165] S. G. Khalid *et al.*, "Blood Pressure Estimation Using Photoplethysmography Only: Comparison between Different Machine Learning Approaches," *Journal of Healthcare Engineering*, vol. 2018, pp. 1–13, 2018. <https://doi.org/10.1155/2018/1548647>
- [166] A. R. Kavsaoğlu, K. Polat, and M. Hariharan, "Non-invasive prediction of hemoglobin level using machine learning techniques with the PPG signal's characteristics features," *Applied Soft Computing Journal*, vol. 37, pp. 983–991, 2015. <https://doi.org/10.1016/j.asoc.2015.04.008>
- [167] S. Acharya *et al.*, "Non-Invasive Estimation of Hemoglobin Using a Multi-Model Stacking Regressor," *IEEE Journal of Biomedical and Health Informatics*, vol. 24, no. 6, pp. 1717–1726, 2020. <https://doi.org/10.1109/JBHI.2019.2954553>
- [168] M. Lakshmi, P. Manimegalai, and S. Bhavani, "Non-invasive haemoglobin measurement among pregnant women using photoplethysmography and machine learning," *Journal of Physics: Conference Series*, vol. 1432, p. 012089, 2020. <https://doi.org/10.1088/1742-6596/1432/1/012089>
- [169] H. Liu *et al.*, "Development and Validation of a Photoplethysmography System for Noninvasive Monitoring of Hemoglobin Concentration," *Journal of Electrical and Computer Engineering*, vol. 2020, p. 3034260, 2020. <https://doi.org/10.1155/2020/3034260>
- [170] E. Monte-Moreno, "Non-invasive estimate of blood glucose and blood pressure from a photoplethysmograph by means of machine learning techniques," *Artificial Intelligence in Medicine*, vol. 53, no. 2, pp. 127–138, 2011. <https://doi.org/10.1016/j.artmed.2011.05.001>
- [171] S. Ramasahayam, L. Arora, and S. R. Chowdhury, "FPGA Based Smart System for Non Invasive Blood Glucose Sensing Using Photoplethysmography and Online Correction of Motion Artifact," in *Sensors for Everyday Life. Smart Sensors, Measurement and Instrumentation*, O. Postolache *et al.*, Eds. Cham: Springer, 2017. https://doi.org/10.1007/978-3-319-47319-2_1
- [172] S. Habbu, M. Dale, and R. Ghongade, "Estimation of blood glucose by non-invasive method using photoplethysmography," *Sadhana - Academy Proceedings in Engineering Sciences*, vol. 44, no. 6, pp. 1–14, 2019. <https://doi.org/10.1007/s12046-019-1118-9>
- [173] A. Hina and W. Saadeh, "A Noninvasive Glucose Monitoring SoC Based on Single Wavelength Photoplethysmography," *IEEE Transactions on Biomedical Circuits and Systems*, vol. 14, no. 3, pp. 504–515, 2020. <https://doi.org/10.1109/TBCAS.2020.2979514>
- [174] S. K. Habbu *et al.*, "Comparison of Noninvasive Blood Glucose Estimation Using Various Regression Models," in *Proc SIRS 2019*, S. Thampi, Ed. Springer, Singapore, 2020, pp. 306–318. https://doi.org/10.1007/978-981-15-4828-4_25
- [175] S. Venkat *et al.*, "Machine Learning based SpO₂ Computation Using Reflectance Pulse Oximetry," in *Proc IEEE EMBS*. IEEE, 2019, pp. 482–485. <https://doi.org/10.1109/EMBC.2019.8856434>
- [176] G. Priem *et al.*, "Clinical grade SpO₂ prediction through semi-supervised learning," in *Proc IEEE BIBE*, 2020, pp. 914–921. <https://doi.org/10.1109/BIBE50027.2020.00155>
- [177] S. Vijayarangan *et al.*, "Robust Modelling of Reflectance Pulse Oximetry for SpO₂ Estimation," in *Proc IEEE EMBS*. IEEE, 2020, pp. 374–377. <https://doi.org/10.1109/EMBC44109.2020.9176410>
- [178] D. Cho *et al.*, "Detection of Stress Levels from Biosignals Measured in Virtual Reality Environments Using a Kernel-Based Extreme

- Learning Machine,” *Sensors*, vol. 17, no. 10, p. 2435, 2017. <https://doi.org/10.3390/s17102435>
- [179] O. M. Mozos *et al.*, “Stress Detection Using Wearable Physiological and Sociometric Sensors,” *International Journal of Neural Systems*, vol. 27, no. 02, p. 1650041, 2017. <https://doi.org/10.1142/S0129065716500416>
- [180] Y. Cho, S. J. Julier, and N. Bianchi-Berthouze, “Instant Stress: Detection of Perceived Mental Stress Through Smartphone Photoplethysmography and Thermal Imaging,” *JMIR Mental Health*, vol. 6, no. 4, p. e10140, 2019. <https://doi.org/10.2196/10140>
- [181] Y. S. Can *et al.*, “Continuous stress detection using wearable sensors in real life: Algorithmic programming contest case study,” *Sensors*, vol. 19, no. 8, 2019. <https://doi.org/10.3390/s19081849>
- [182] A. Arsalan *et al.*, “Classification of Perceived Human Stress using Physiological Signals,” in *Proc IEEE EMBS*. IEEE, 2019, pp. 1247–1250. <https://doi.org/10.1109/EMBC.2019.8856377>
- [183] J. B. Prinable *et al.*, “Using a recurrent neural network to derive tidal volume from a photoplethysmograph,” in *Proc IEEE LSC*, 2018, pp. 218–221. <https://doi.org/10.1109/LSC.2017.8268182>
- [184] V. Ravichandran *et al.*, “RespNet: A deep learning model for extraction of respiration from photoplethysmogram,” in *Proc IEEE EMBS*. IEEE, 2019, pp. 5556–5559. <https://doi.org/10.1109/EMBC.2019.8856301>
- [185] D. Bian, P. Mehta, and N. Selvaraj, “Respiratory Rate Estimation using PPG: A Deep Learning Approach,” in *Proc IEEE EMBS*, 2020, pp. 5948–5952. <https://doi.org/10.1109/EMBC44109.2020.9176231>
- [186] N. Pradhan, S. Rajan, and A. Adler, “Evaluation of the signal quality of wrist-based photoplethysmography,” *Physiological Measurement*, vol. 40, no. 6, pp. 0–11, 2019. <https://doi.org/10.1088/1361-6579/ab225a>
- [187] M. S. Roy, R. Gupta, and K. D. Sharma, “Photoplethysmogram Signal Quality Evaluation by Unsupervised Learning Approach,” in *Proc IEEE ASPCON*, 2020, pp. 6–10. <https://doi.org/10.1109/ASPCON49795.2020.9276733>
- [188] M. Kachuee *et al.*, “Cuffless Blood Pressure Estimation Algorithms for Continuous Health-Care Monitoring,” *IEEE Transactions on Biomedical Engineering*, vol. 64, no. 4, pp. 859–869, 2017. <https://doi.org/10.1109/TBME.2016.2580904>
- [189] C. El-Hajj and P. A. Kyriacou, “Deep learning models for cuffless blood pressure monitoring from PPG signals using attention mechanism,” *Biomedical Signal Processing and Control*, vol. 65, p. 102301, 2021. <https://doi.org/10.1016/j.bspc.2020.102301>
- [190] L. Breiman, “Random forests,” *Machine Learning*, vol. 45, pp. 5–32, 2001. <https://doi.org/10.1023/A:1010933404324>
- [191] N. Cristianini and J. Shawe-Taylor, *An Introduction to Support Vector Machines and Other Kernel-based Learning Methods*. Cambridge University Press, mar 2000. <https://doi.org/10.1017/CBO9780511801389>
- [192] N. Sviridova, “Towards Understanding of Photoplethysmogram Dynamics through Nonlinear Time Series Analysis,” *Seisan Kenkyu*, vol. 71, no. 2, pp. 141–145, 2019. <https://doi.org/10.11188/seisankenkyu.71.141>
- [193] M. Nandi, J. Venton, and P. J. Aston, “A novel method to quantify arterial pulse waveform morphology: Attractor reconstruction for physiologists and clinicians,” *Physiological Measurement*, vol. 39, no. 10, 2018. <https://doi.org/10.1088/1361-6579/aae46a>
- [194] P. H. Charlton, “Nonlinear analysis of the photoplethysmogram.svg,” 2021. https://commons.wikimedia.org/wiki/File:Nonlinear_analysis_of_the_photoplethysmogram.svg
- [195] F. Takens, “Detecting strange attractors in turbulence,” in *Dynamical Systems and Turbulence, Warwick 1980*, vol. 898 of *Springer Lecture Notes in Mathematics*, D. A. Rand and L.-S. Young, Eds. New York: Springer-Verlag, 1981, pp. 366–381. <https://doi.org/10.1007/bfb0091924>
- [196] P. H. Charlton *et al.*, “Measurement of cardiovascular state using attractor reconstruction analysis,” in *Proc. EUSIPCO*. Nice: IEEE, 2015, pp. 444–8. <https://doi.org/10.1109/EUSIPCO.2015.7362422>
- [197] N. Sviridova and K. Sakai, “Human photoplethysmogram: New insight into chaotic characteristics,” *Chaos, Solitons and Fractals*, vol. 77, pp. 53–63, 2015. <https://doi.org/10.1016/j.chaos.2015.05.005>
- [198] N. Sviridova *et al.*, “Photoplethysmogram at green light: Where does chaos arise from?” *Chaos, Solitons and Fractals*, vol. 116, pp. 157–165, 2018. <https://doi.org/10.1016/j.chaos.2018.09.016>
- [199] P. J. Aston *et al.*, “Beyond HRV: attractor reconstruction using the entire cardiovascular waveform data for novel feature extraction,” *Physiological Measurement*, vol. 39, no. 2, p. 024001, 2018. <https://doi.org/10.1088/1361-6579/aaa93d>
- [200] P. J. Aston *et al.*, “Comparison of Attractor Reconstruction and HRV Methods for Analysing Blood Pressure Data,” in *Proc CinC.*, vol. 41. IEEE, 2014, pp. 437–40. <https://ieeexplore.ieee.org/document/7043073>
- [201] D. Roh and H. Shin, “Recurrence plot and machine learning for signal quality assessment of photoplethysmogram in mobile environment,” *Sensors*, vol. 21, no. 6, pp. 1–12, 2021. <https://doi.org/10.3390/s21062188>
- [202] R. Sahni, “Noninvasive Monitoring by Photoplethysmography,” *Clinics in Perinatology*, vol. 39, no. 3, pp. 573–583, 2012. <https://doi.org/10.1016/j.clp.2012.06.012>
- [203] S. Ismail, U. Akram, and I. Siddiqi, “Heart rate tracking in photoplethysmography signals affected by motion artifacts: a review,” *Eurasip Journal on Advances in Signal Processing*, vol. 2021, no. 1, 2021. <https://doi.org/10.1186/s13634-020-00714-2>
- [204] D. Biswas *et al.*, “Heart rate estimation from wrist-worn photoplethysmography: A review,” *IEEE Sensors Journal*, vol. 19, no. 16, pp. 6560–6570, 2019. <https://doi.org/10.1109/jsen.2019.2914166>
- [205] S. Li *et al.*, “A Hybrid Wavelet-Based Method for the Peak Detection of Photoplethysmography Signals,” *Computational and Mathematical Methods in Medicine*, vol. 2017, 2017. <https://doi.org/10.1155/2017/9468503>
- [206] D. Li, H. Zhao, and S. Dou, “A new signal decomposition to estimate breathing rate and heart rate from photoplethysmography signal,” *Biomedical Signal Processing and Control*, vol. 19, pp. 89–95, 2015. <https://doi.org/10.1016/j.bspc.2015.03.008>
- [207] Wolf PA, Abbot RD, and Kannel WB, “Atrial fibrillation as an independent risk factor for stroke: the Framingham study,” *Stroke*, vol. 22, pp. 983–988, 1991. <https://doi.org/10.1161/01.str.22.8.983>
- [208] L. M. Erikäinen *et al.*, “Atrial fibrillation monitoring with wrist-worn photoplethysmography-based wearables: State-of-the-art review,” *Cardiovascular Digital Health Journal*, vol. 1, no. 1, pp. 45–51, 2020. <https://doi.org/10.1016/j.cvdhj.2020.03.001>
- [209] S.-C. Tang *et al.*, “Identification of atrial fibrillation by quantitative analyses of fingertip photoplethysmogram,” *Scientific Reports*, vol. 7, no. 1, p. 45644, 2017. <https://doi.org/10.1038/srep45644>
- [210] M. Brennan, M. Palaniswami, and P. Kamen, “Do existing measures of Poincare plot geometry reflect nonlinear features of heart rate

- variability?" *IEEE Transactions on Biomedical Engineering*, vol. 48, no. 11, pp. 1342–1347, 2001. <https://doi.org/10.1109/10.959330>
- [211] T. Pereira *et al.*, "Photoplethysmography based atrial fibrillation detection: a review," *npj Digital Medicine*, vol. 3, no. 1, p. 3, 2020. <https://doi.org/10.1038/s41746-019-0207-9>
- [212] P. H. Charlton, "Detecting atrial fibrillation from the photoplethysmogram." 2021. [https://commons.wikimedia.org/wiki/File:Detecting_atrial_fibrillation_\(AF\)_from_the_photoplethysmogram_\(PPG\).svg](https://commons.wikimedia.org/wiki/File:Detecting_atrial_fibrillation_(AF)_from_the_photoplethysmogram_(PPG).svg)
- [213] M. V. Perez *et al.*, "Large-scale assessment of a smartwatch to identify atrial fibrillation," *New England Journal of Medicine*, vol. 381, no. 20, pp. 1909–1917, 2019. <https://doi.org/10.1056/NEJMoa1901183>
- [214] Y. Guo *et al.*, "Mobile photoplethysmographic technology to detect atrial fibrillation," *Journal of the American College of Cardiology*, vol. 74, no. 19, pp. 2365–2375, 2019. <https://doi.org/10.1016/j.jacc.2019.08.019>
- [215] S. Fox, *Human Physiology*, 14th ed. New York, NY: McGraw Hill, 2016.
- [216] A. Schäfer and J. Vagedes, "How accurate is pulse rate variability as an estimate of heart rate variability?" *International Journal of Cardiology*, vol. 166, no. 1, pp. 15–29, 2013. <https://doi.org/10.1016/j.ijcard.2012.03.119>
- [217] E. Yuda *et al.*, "Pulse rate variability: A new biomarker, not a surrogate for heart rate variability," *Journal of Physiological Anthropology*, vol. 39, no. 1, pp. 1–4, 2020. <https://doi.org/10.1186/s40101-020-00233-x>
- [218] E. Mejía-Mejía *et al.*, "Differential effects of the blood pressure state on pulse rate variability and heart rate variability in critically ill patients," *npj Digital Medicine*, vol. 4, no. 1, p. 82, dec 2021. <https://doi.org/10.1038/s41746-021-00447-y>
- [219] F. Shaffer and J. P. Ginsberg, "An overview of heart rate variability metrics and norms," *Frontiers in Public Health*, vol. 5, p. 258, 2017. <https://doi.org/10.3389/fpubh.2017.00258>
- [220] S. Lu *et al.*, "Can photoplethysmography variability serve as an alternative approach to obtain heart rate variability information?" *Journal of clinical monitoring and computing*, vol. 22, no. 1, pp. 23–9, 2008. <https://doi.org/10.1007/s10877-007-9103-y>
- [221] J. Bolea *et al.*, "Pulse Rate and Transit Time Analysis to Predict Hypotension Events After Spinal Anesthesia During Programmed Cesarean Labor," *Annals of Biomedical Engineering*, vol. 45, no. 9, pp. 2253–2263, 2017. <https://doi.org/10.1007/s10439-017-1864-y>
- [222] R. Parasnis, A. Pawar, and M. Manivannan, "Multiscale entropy and poincaré plot-based analysis of pulse rate variability and heart rate variability of ICU patients," in *2015 International Conference on Intelligent Informatics and Biomedical Sciences (ICIIBMS)*. IEEE, 2015, pp. 290–295. <https://doi.org/10.1109/ICIIBMS.2015.7439531>
- [223] A. Mohan *et al.*, "Design and Development of a Heart Rate Variability Analyzer," *Journal of Medical Systems*, vol. 36, no. 3, pp. 1365–1371, 2012. <https://doi.org/10.1007/s10916-010-9597-6>
- [224] A. H. Khandoker *et al.*, *Poincaré Plot Methods for Heart Rate Variability Analysis*. Boston, MA: Springer US, 2013. <https://doi.org/10.1007/978-1-4614-7375-6>
- [225] P. Shi *et al.*, "Analysis of pulse rate variability derived from photoplethysmography with the combination of lagged Poincaré plots and spectral characteristics," *Medical Engineering and Physics*, vol. 31, no. 7, pp. 866–871, 2009. <https://doi.org/10.1016/j.medengphy.2009.05.001>
- [226] P. H. Charlton *et al.*, "Breathing rate estimation from the electrocardiogram and photoplethysmogram: a review," *IEEE Reviews in Biomedical Engineering*, vol. 11, pp. 2–20, 2018. <https://doi.org/10.1109/RBME.2017.2763681>
- [227] R. M. Schein *et al.*, "Clinical antecedents to in-hospital cardiopulmonary arrest," *Chest*, vol. 98, no. 6, pp. 1388–92, 1990. <https://doi.org/10.1378/chest.98.6.1388>
- [228] R. W. Duckitt *et al.*, "Worthing physiological scoring system: derivation and validation of a physiological early-warning system for medical admissions. An observational, population-based single-centre study." *British Journal of Anaesthesia*, vol. 98, no. 6, pp. 769–74, 2007. <https://doi.org/10.1093/bja/aem097>
- [229] C. W. Seymour *et al.*, "Assessment of clinical criteria for sepsis: for the third international consensus definitions for sepsis and septic shock (Sepsis-3)," *Journal of the American Medical Association*, vol. 315, no. 8, pp. 762–74, 2016. <https://doi.org/10.1001/jama.2016.0288>
- [230] P. B. Lovett *et al.*, "The vexatious vital: neither clinical measurements by nurses nor an electronic monitor provides accurate measurements of respiratory rate in triage," *Annals of Emergency Medicine*, vol. 45, no. 1, pp. 68–76, 2005. <https://doi.org/10.1016/j.annemergmed.2004.06.016>
- [231] K. E. J. Philip *et al.*, "The accuracy of respiratory rate assessment by doctors in a London teaching hospital: a cross-sectional study," *Journal of Clinical Monitoring and Computing*, vol. 29, no. 4, pp. 455–460, 2015. <https://doi.org/10.1007/s10877-014-9621-3>
- [232] P. H. Charlton *et al.*, "Extraction of respiratory signals from the electrocardiogram and photoplethysmogram: technical and physiological determinants," *Physiological Measurement*, vol. 38, no. 5, pp. 669–690, 2017. <https://doi.org/10.1088/1361-6579/aa670e>
- [233] H. Liu *et al.*, "Comparison of different modulations of photoplethysmography in extracting respiratory rate: From a physiological perspective," *Physiological Measurement*, vol. 41, no. 9, pp. 0–14, 2020. <https://doi.org/10.1088/1361-6579/abaaf0>
- [234] W. Karlen *et al.*, "Multiparameter respiratory rate estimation from the photoplethysmogram," *IEEE Transactions on Biomedical Engineering*, vol. 60, no. 7, pp. 1946–53, 2013. <https://doi.org/10.1109/TBME.2013.2246160>
- [235] D. A. Birrenkott *et al.*, "A robust fusion model for estimating respiratory rate from photoplethysmography and electrocardiography," *IEEE Transactions on Biomedical Engineering*, vol. 65, no. 9, pp. 2033–2041, 2018. <https://doi.org/10.1109/TBME.2017.2778265>
- [236] P. H. Charlton, "Presentation of: An assessment of algorithms to estimate respiratory rate from the electrocardiogram and photoplethysmogram." 2016. <https://doi.org/10.5281/zenodo.166525>
- [237] P. H. Charlton, "Continuous respiratory rate monitoring to detect clinical deteriorations using wearable sensors," 2017. <https://theses.eurasip.org/theses/829/continuous-respiratory-rate-monitoring-to-detect/>
- [238] World Health Organization, *World health statistics 2019: monitoring health for the SDGs sustainable development goals*. World Health Organisation, 2019, vol. 3, no. 2. <https://apps.who.int/iris/handle/10665/324835>
- [239] J. He and P. K. Whelton, "Elevated systolic blood pressure and risk of cardiovascular and renal disease: Overview of evidence from observational epidemiologic studies and randomized controlled trials," *American Heart Journal*, vol. 138, no. 3 II, pp. 12–17, 1999. [https://doi.org/10.1016/s0002-8703\(99\)70312-1](https://doi.org/10.1016/s0002-8703(99)70312-1)
- [240] L. A. Geddes, *Handbook of Blood Pressure Measurement*, 1st ed. Humana Press, 1991. <https://doi.org/10.1007/978-1-4684-7170-0>

- [241] Bonnafoux, "Auscultatory and oscillometric methods of ambulatory blood pressure monitoring, advantages and limits: a technical point of view." *Blood Pressure Monitoring*, vol. 1, no. 3, pp. 181–185, 1996. <http://www.ncbi.nlm.nih.gov/pubmed/10226223>
- [242] B. Gribbin, A. Steptoe, and P. Sleight, "Pulse Wave Velocity as a Measure of Blood Pressure Change," *Psychophysiology*, vol. 13, no. 1, pp. 86–90, jan 1976. <https://doi.org/10.1111/j.1469-8986.1976.tb03344.x>
- [243] Chan *et al.*, "Multi-site photoplethysmography technology for blood pressure assessment: Challenges and recommendations," *Journal of Clinical Medicine*, vol. 8, no. 11, p. 1827, 2019. <https://doi.org/10.3390/jcm8111827>
- [244] M. Sharma *et al.*, "Cuff-less and continuous blood pressure monitoring: A methodological review," *Technologies*, vol. 5, no. 2, p. 21, 2017. <https://doi.org/10.3390/technologies5020021>
- [245] H. Gesche *et al.*, "Continuous blood pressure measurement by using the pulse transit time: Comparison to a cuff-based method," *European Journal of Applied Physiology*, vol. 112, no. 1, pp. 309–315, 2012. <https://doi.org/10.1007/s00421-011-1983-3>
- [246] Y. Wang, Z. Liu, and S. Ma, "Cuff-less blood pressure measurement from dual-channel photoplethysmographic signals via peripheral pulse transit time with singular spectrum analysis," *Physiological Measurement*, vol. 39, no. 2, 2018. <https://doi.org/10.1088/1361-6579/aa996d>
- [247] W. Chen *et al.*, "Continuous estimation of systolic blood pressure using the pulse arrival time and intermittent calibration," *Medical and Biological Engineering and Computing*, vol. 38, no. 5, pp. 569–574, 2000. <https://doi.org/10.1007/BF02345755>
- [248] L. A. Geddes *et al.*, "Pulse arrival time as a method of obtaining systolic and diastolic blood pressure indirectly," *Medical and Biological Engineering and Computing*, vol. 19, no. 5, pp. 671–672, 1981. <https://doi.org/10.1007/BF02442787>
- [249] M. Hosanee *et al.*, "Cuffless single-site photoplethysmography for blood pressure monitoring," *Journal of Clinical Medicine*, vol. 9, no. 3, p. 723, 2020. <https://doi.org/10.3390/jcm9030723>
- [250] G. Slapničar, N. Mlakar, and M. Luštrek, "Blood pressure estimation from photoplethysmogram using a spectro-temporal deep neural network," *Sensors*, vol. 19, no. 15, p. 3420, 2019. <https://doi.org/10.3390/s19153420>
- [251] P. Su *et al.*, "Long-term blood pressure prediction with deep recurrent neural networks," in *Proc IEEE BHI*, 2018, pp. 323–328. <https://doi.org/10.1109/BHI.2018.8333434>
- [252] H. Eom *et al.*, "End-to-end deep learning architecture for continuous blood pressure estimation using attention mechanism," *Sensors*, vol. 20, no. 8, pp. 1–20, 2020. <https://doi.org/10.3390/s20082338>
- [253] J. Allen and A. Murray, "Age-related changes in the characteristics of the photoplethysmographic pulse shape at various body sites," *Physiological Measurement*, vol. 24, no. 2, pp. 297–307, 2003. <https://doi.org/10.1088/0967-3334/24/2/306>
- [254] E. J. Sharkey *et al.*, "Innovative multi-site photoplethysmography measurement and analysis demonstrating increased arterial stiffness in paediatric heart transplant recipients," *Physiological Measurement*, vol. 39, no. 7, 2018. <https://doi.org/10.1088/1361-6579/aac76a>
- [255] D. Zheng and A. Murray, "Peripheral arterial volume distensibility: Significant differences with age and blood pressure measured using an applied external pressure," *Physiological Measurement*, vol. 32, no. 5, pp. 499–512, 2011. <https://doi.org/10.1088/0967-3334/32/5/001>
- [256] L. A. Bortolotto *et al.*, "Assessment of vascular aging and atherosclerosis in hypertensive subjects: Second derivative of photoplethysmogram versus pulse wave velocity," *American Journal of Hypertension*, vol. 13, no. 2, pp. 165–171, 2000. [https://doi.org/10.1016/S0895-7061\(99\)00192-2](https://doi.org/10.1016/S0895-7061(99)00192-2)
- [257] N. Inoue *et al.*, "Second derivative of the finger photoplethysmogram and cardiovascular mortality in middle-aged and elderly Japanese women," *Hypertension Research*, vol. 40, no. 2, pp. 207–211, 2016. <https://doi.org/10.1038/hr.2016.123>
- [258] T. Biering-Sørensen *et al.*, "Left ventricular ejection time is an independent predictor of incident heart failure in a community-based cohort," *European Journal of Heart Failure*, vol. 20, no. 7, pp. 1106–1114, 2018. <https://doi.org/10.1002/ejhf.928>
- [259] G. S. H. Chan *et al.*, "Automatic detection of left ventricular ejection time from a finger photoplethysmographic pulse oximetry waveform: comparison with Doppler aortic measurement." *Physiological Measurement*, vol. 28, no. 4, pp. 439–52, 2007. <https://doi.org/10.1088/0967-3334/28/4/009>
- [260] M. R. Robinson and E. A. Allen, "Observational heart failure monitoring system (Patent WO 2017/100185 A1)," 2017.
- [261] A. Mathieu, P. H. Charlton, and J. Alastruey, "Using smart wearables to monitor cardiac ejection," *Proceedings*, vol. 4, no. 1, p. 48, 2019. <https://doi.org/10.3390/ecea-5-05744>
- [262] E. Von Wowern *et al.*, "Digital photoplethysmography for assessment of arterial stiffness: Repeatability and comparison with applanation tonometry," *PLoS ONE*, vol. 10, no. 8, pp. 1–19, 2015. <https://doi.org/10.1371/journal.pone.0135659>
- [263] R. Couceiro *et al.*, "Multi-Gaussian fitting for the assessment of left ventricular ejection time from the Photoplethysmogram," in *Proc. IEEE EMBS*. IEEE, 2012, pp. 3951–3954. <https://doi.org/10.1109/EMBC.2012.6346831>
- [264] P. M. Middleton *et al.*, "Changes in left ventricular ejection time and pulse transit time derived from finger photoplethysmogram and electrocardiogram during moderate haemorrhage," *Clinical Physiology and Functional Imaging*, vol. 29, no. 3, pp. 163–169, 2009. <https://doi.org/10.1111/j.1475-097X.2008.00843.x>
- [265] P. H. Charlton *et al.*, "Modeling arterial pulse waves in healthy aging: a database for in silico evaluation of hemodynamics and pulse wave indexes," *American Journal of Physiology-Heart and Circulatory Physiology*, vol. 317, no. 5, pp. H1062–H1085, 2019. <https://doi.org/10.1152/ajpheart.00218.2019>
- [266] D. Martin-Martinez *et al.*, "Stochastic modeling of the PPG signal: A synthesis-by-analysis approach with applications," *IEEE Transactions on Biomedical Engineering*, vol. 60, no. 9, pp. 2432–2441, 2013. <https://doi.org/10.1109/TBME.2013.2257770>
- [267] Q. Tang *et al.*, "PPGSynth: An Innovative Toolbox for Synthesizing Regular and Irregular Photoplethysmography Waveforms," *Frontiers in Medicine*, vol. 7, p. 597774, 2020. <https://doi.org/10.3389/fmed.2020.597774>
- [268] U. Rubins, "Finger and ear photoplethysmogram waveform analysis by fitting with Gaussians," *Medical and Biological Engineering and Computing*, vol. 46, no. 12, pp. 1271–1276, 2008. <https://doi.org/10.1007/s11517-008-0406-z>
- [269] L. Wang *et al.*, "Multi-Gaussian fitting for pulse waveform using Weighted Least Squares and multi-criteria decision making method," *Computers in Biology and Medicine*, vol. 43, no. 11, pp. 1661–1672, 2013. <http://dx.doi.org/10.1016/j.combiomed.2013.08.004>
- [270] A. Sološenko *et al.*, "Modeling of the photoplethysmogram during atrial fibrillation," *Computers in Biology and Medicine*, vol. 81, pp. 130–138, 2017. <https://doi.org/10.1016/j.combiomed.2016.12.016>
- [271] B. Paliakaite *et al.*, "Photoplethysmogram modeling of extreme bradycardia and ventricular tachycardia," in *IFMBE Proceedings*,

- vol. 76, 2020, pp. 1165–1174. https://doi.org/10.1007/978-3-030-31635-8_141
- [272] P. H. Charlton *et al.*, “Pulse Wave Database (PWDB): A database of arterial pulse waves representative of healthy adults,” 2019. <https://doi.org/10.5281/zenodo.2633175>
- [273] P. H. Charlton, “Simulated photoplethysmogram pulse waves.png,” 2021. https://commons.wikimedia.org/wiki/File:Simulated_photoplethysmogram_pulse_waves.png
- [274] P. McSharry *et al.*, “A dynamical model for generating synthetic electrocardiogram signals,” *IEEE Transactions on Biomedical Engineering*, vol. 50, no. 3, pp. 289–294, mar 2003. <http://ieeexplore.ieee.org/document/1186732/>
- [275] B. Paliakaite *et al.*, “Modeling of artifacts in the wrist photoplethysmogram: Application to the detection of life-threatening arrhythmias,” *Biomedical Signal Processing and Control*, vol. 66, p. 102421, 2021. <https://doi.org/10.1016/j.bspc.2021.102421>
- [276] G. B. Moody and R. G. Mark, “The impact of the MIT-BIH arrhythmia database,” *IEEE Engineering in Medicine and Biology Magazine*, vol. 20, no. 3, pp. 45–50, 2001. <https://doi.org/10.1109/51.932724>